Doctoral Dissertation.
Interuniversity Doctoral Program in
Urban and Regional Development (XXXVII Cycle)

Multiscale approach for the thermal-hydraulic analysis of heavy liquid metal pool systems

Pietro CIOLI PUVIANI

Supervisor(s):
Prof. R., Zanino
Dr. PhD. M., Tarantino

Doctoral Examination Committee:
Dr. PhD Marco Caramello, Referee, Ansaldo Energia SpA
Dr. PhD Paolo Ferroni, Referee, Westinghouse Electric Company LLC
Prof. Nicola Forgione, Member, Università di Pisa
Dr. PhD Ferry Roelofs, Member, Nuclear Research & Consultancy Group
Prof. Sandra Dulla, Member, Politecnico di Torino

Politecnico di Torino - Università degli Studi di Torino
February 27, 2025

This thesis is licensed under a Creative Commons License, Attribution - Non-commercial - NoDerivative Works 4.0 International: see www.creativecommons.org. The text may be reproduced for non-commercial purposes, provided that credit is given to the original author.

I hereby declare that the contents and organisation of this dissertation constitute my own original work and does not compromise in any way the rights of third parties, including those relating to the security of personal data.

Pietro Cioli Puviani Turin, February 27, 2025

Summary

This thesis describes the research work carried out within the framework of Generation IV Lead-cooled Fast Reactors (LFRs) development. Specifically, it presents an advancement in the modelling of LFR thermal-hydraulics (TH), achieved by coupling computer codes featuring different resolution and modelling scale, to improve design and analysis effectiveness of next-generation nuclear reactors.

The work benefits from the collaboration between Politecnico di Torino and the ENEA Brasimone research centre, combining an academic approach with practical, hands-on experience in the Heavy Liquid Metal (HLM) field. This partnership has facilitated access to state-of-the-art experimental facilities and data, promoting a research environment in which the development, verification, and validation of computational tools are tightly coupled with industrial and international project needs.

Firstly, an overview of the current status of TH) R&D is presented, setting the context for the TH modelling challenges that Generation IV LFRs face. Chapter 2 provides a literature review of existing TH tools applicable for the analysis of LFR systems. Traditional System Thermal-Hydraulics (STH) codes, initially developed for water reactors, have been foundational in the nuclear industry since the 1970s. However, these codes need to be further developed to effectively simulate LFR systems, especially due to the properties of lead coolant, analysing TH phenomena specific to the LFRs innovative pool reactor. This development involves incorporating advanced algorithms, models, and correlations specific to HLM, as well as expanding validation database of relevant experiments. Computational Fluid Dynamic (CFD) codes are becoming a valuable tool for component analysis, leveraging the increasing computational power available and adopting a three dimensional representation of the investigated domain. In recent decades, coupled CFD-STH tool are gaining attention as they allow to exploit the advantages of both families of codes, with a multiscale approach for system TH analysis of transient events. The motivations, current status, and classification of coupled CFD-STH

tools are discussed in Chapter 2, highlighting efforts made within international projects on the topic and reference applications available in the literature.

Chapter 3 describes a novel computational tool, focus of this thesis work, based of the coupling between the commercial CFD code Ansys CFX and the STH code RELAP5 Mod3.3. Furthermore, the chapter outlines the reasoning behind key design choices and the range of options available to users in terms of numerical schemes and domain discretization. The tool's integrates new developed software tools, such as Ansys CFX FORTRAN subroutine and in-house developed Python executables.

Chapter 4 presents the tool's verification and validation across multiple case studies with increasing complexity. Initial verification is conducted using a simple isothermal single-pipe model to test the tool's coupling strategy, ensuring that the Ansys CFX and RELAP5 components communicate and operate as intended. Subsequent validation is performed using experimental data from loop-type facilities, including the NACIE and NACIE-UP facilities at the ENEA Brasimone research centre and the TALL-3D facility at the Royal Institute of Technology in Sweden. Lessons learned are summarized at the end of the chapter, focusing on evaluating cases where the coupled approach proves valuable and assessing the impact of different coupling methodologies available within the tool.

The final section of Chapter 4 presents the application of the tool to ATHENA, a pool-type experimental facility designed to test full-scale ALFRED (Advanced Lead-cooled Fast Reactor European Demonstrator) components. The application of the developed tool to the ATHENA facility highlights the differences achieved by adopting a multiscale approach, where system analysis is enhanced through CFD component simulations. A code-to-code comparison is conducted, exploring the impact of using CFD models for three different ATHENA components: the Fitting Volume, the Main Pool, and the Core Simulator.

The thesis concludes with a summary of the achievements and limitations encountered throughout the development and validation process. The insights gained from this work address the field of CFD-STH coupled tool applications, highlighting their value and emphasizing the importance of expanding the experimental database, particularly from pool-type facilities designed for integral testing of reactor accident scenarios. Finally, further numerical optimizations of the presented tool are proposed.

Acknowledgment

My most sincere greetings go to ENEA, with particular mention of all the people who have been part of the Brasimone Centre during these years. My colleagues in Brasimone not only welcomed me but also supported me along the entire journey. I couldn't ask for a better environment to conduct my research.

Thanks to the NEMO group at the Politecnico di Torino: they taught me that research means sharing, even if my research topic is far from theirs, and that it is possible to find a home (not only physically) in a very short time if you have the luck to know the right people.

Thanks to the LFR community: I never returned from any conference or educational experience lacking enthusiasm. This community is made up of extremely well-prepared researchers who have always given me the opportunity to express my opinion.

Grazie a Mariano, vedere la tua incomprensibile capacità di parlare sempre con pertinenza e sicurezza nei tuoi 25 meeting giornalieri, accompagnata dall'umiltà di offrirti per pulire le tazzine di tutti in sala caffè, sono per me di ispirazione quotidiana. Grazie Ivan, Carlo, Daniele e Dario. Ognuno a suo modo, mi avete mostrato a cosa devo ambire per essere un lavoratore preparato e appassionato.

Grazie ai miei amici del Brasimone. Siete tanti, ma ognuno di voi ha condiviso con me un pezzo di questo percorso. Dai più grandi si impara, coi tuoi coetanei si cresce. Siete stati gioia e sostegno nelle mie giornate e serate insieme. Senza di voi non sarebbe stata la stessa cosa. Grazie Tommaso, tutto questo lo abbiamo vissuto fianco a fianco. Non avrei potuto chiedere persona migliore con cui camminare.

Grazie alla mia famiglia e ai miei amici, non avete mai mancato occasione di chiedermi come stesse andando questo percorso con l'interesse di coloro che ti stimano e che vogliono supportati qualora tu ne abbia bisogno. Grazie ad Annamaria, che durante questi anni è diventata la mia compagna di vita. A te dedico tutto quello che sono riuscito a raggiungere, perché senza di te non ce l'avrei mai fatta.

Grazie a Torino, al lago di Brasimone, alla mia Panda, alle bevande calde e ai contenitori per il cibo.

Dedication

To curiosity, and to those who never let it fade.

Contents

Summary IV
Acknowledgment VI
List of Figures X
List of Tables XVII
1 Introduction 1
1.1 Numerical tools for thermal-hydraulics analysis of nuclear reactors 2
1.2 Lead-cooled Fast Reactor Technology 5
1.2.1 General description of LFR design 5
1.2.2 Challenges in LFR thermal-hydraulics 8
2 Status of the available numerical tools 11
2.1 System Thermal-Hydraulics codes for LFR 11
2.1.1 RELAP5 Mod3.3 12
2.2 Computational Fluid Dynamics codes for LFR 14
2.2.1 Ansys CFX 16
2.3 Coupled STH and CFD tools 17
2.3.1 Classification 19
2.3.2 Scope of the tool 21
2.3.3 Original contribution of the thesis 22
3 Ansys CFX – RELAP5 Mod3.3 coupling tool 24
3.1 Description of the coupling strategy 24
3.2 Time advancing scheme 27
3.2.1 Explicit scheme 27
3.2.2 Semi-implicit scheme 30
3.3 Spatial discretization approach 33
3.3.1 Decomposition domain 34

3.3.2 Overlapping domain 35
4 Verification and validation of the tool 41
4.1 Isothermal pipe 42
4.2 Validation against loop type facility 48
4.2.1 NACIE 49
4.2.2 NACIE-UP (IAEA benchmark) 54
4.2.3 TALL-3D 80
4.2.4 Lesson learned from loop type facility test cases 106
4.3 Modelling of the ATHENA pool type facility 109
4.3.1 ATHENA facility 110
4.3.2 Fitting Volume transient 119
4.3.3 Pool thermal transient 126
4.3.4 Loss Of Flow Accident 134
5 Conclusions and future work 148
5.1 Conclusions 148
5.2 Future work 152
Acronyms 154
References 156

List of Figures

Figure 1.1 – Thermal-hydraulic code hierarchy [5]. 3

Figure 1.2 – Schematic of the ALFRED design [13]. 7

Figure 1.3 – Schematic of the LFR-AS-200 design. 8

Figure 2.1 – Velocity and temperature field of rectangular channel heated from top and bottom by NRG applying a fluid like air and water (Pr ~1) and a typical liquid metal (Pr<<1) [29]. 15

Figure 2.2 – Code coupling classification [50]. 21

Figure 3.1 – Time locations available during the Ansys CFX solver operation at which the junction box routine could be called [51]. 26

Figure 3.2 – Diagram describing the time-stepping process in an explicit scheme, highlighting the sequence of code execution and information exchange [52]. 28

Figure 3.3 – Coupling methodology between Ansys CFX and RELAP5 in the explicit scheme [52]. 30

Figure 3.4 – Diagram describing the time-stepping process in a semi-implicit scheme during a single coupling timestep, highlighting the sequence of code execution and the convergence check in the internal iteration [52]. 31

Figure 3.5 – Coupling methodology between Ansys CFX and RELAP5 in the semi-implicit scheme [52]. 33

Figure 3.6 – RELAP5 Mod3.3 schematization of the nodalization in the domain decomposition (a) and overlapping (b) approach [52]. 34

Figure 4.1 – Mass flow boundary condition for the test case transient [52]. 42

Figure 4.2 – Pipe test model: a) RELAP5 Mod3.3 standalone, b) Ansys CFX standalone, c) domain decomposition coupling, d) overlapping domain approach [52]. 43

Figure 4.3 – Difference between the theoretical and the numerical mass flow rate in the Ansys CFX standalone and decomposition model. 44

Figure 4.4 – Pipe pressure drops variation in time with the standalone and the decomposition models (entire transient). 45

Figure 4.5 – Pipe pressure drops variation in time with the standalone and the overlapping models (entire transient). 45

Figure 4.6 – Pipe pressure drops variation in time with the standalone and the decomposition models (start of the transient). 46

Figure 4.7 – Pipe pressure drops variation in time with the standalone and the overlapping models (start of the transient). 46

Figure 4.8 – Pipe pressure drops variation in time with the standalone and the decomposition models (end of the transient). 46

Figure 4.9 – Pipe pressure drops variation in time with the standalone and the overlapping models (end of the transient). 46

Figure 4.10 – Loop nodalization of the RELAP5 model of the NACIE loop, highlighting the components substituted by the Ansys CFX model in the coupled simulation [52]. 52

Figure 4.11 – Mesh of the Ansys CFX model of the NACIE Heating Structure [52]. 52

Figure 4.12 – Comparison of experimental vs modelled (RELAP5 standalone and coupled tool) flow rate in the NACIE loop [52]. 53

Figure 4.13 – Comparison of experimental vs modelled (RELAP5 standalone and coupled tool) inlet and outlet temperatures in the NACIE loop[52]. 53

Figure 4.14 – NACIE-UP FPBS layout (left) and cross section of the measuring plane view (right) [59]. 56

Figure 4.15 – Schematic drawing of the NACIE-UP primary loop [61]. 57

Figure 4.16 – NACIE-UP primary loop. 58

Figure 4.17 – Active pins (in red) during ADP10 (a) and ADP06 (b) tests [59]. 60

Figure 4.18 – Schematic of the pin materials [62]. 61

Figure 4.19 – Partition of the fluid region in bodies. 62

Figure 4.20 – Detail coarse improved mesh. 63

Figure 4.21 – Coarse improved mesh [62]. 63

Figure 4.22 – Thermocouples temperature comparison for the BOT steady state, ADP06 [62]. 65

Figure 4.23 – Thermocouples temperature comparison for the BOT steady state, ADP10 [62]. 65

Figure 4.24 – Thermocouples temperature comparison for the EOT steady state, ADP06. 65

Figure 4.25 – Thermocouples temperature comparison for the EOT steady state, ADP10. 66

Figure 4.26 – Ansys CFX BOT steady state, temperature comparison on Plane 3 (ADP06) [62]. 67

Figure 4.27 – Ansys CFX BOT steady state, temperature comparison on Plane 3 (ADP10) [62]. 67

Figure 4.28 – Ansys CFX EOT steady state, temperature comparison on Plane 3 (ADP06). 67

Figure 4.29 – Ansys CFX EOT steady state, temperature comparison on Plane 3 (ADP10). 67

Figure 4.30 – Nodalization of the RELAP5 model of the NACIE-UP loop [62]. 69

Figure 4.31 – Cheng and Todreas vs RELAP5 correlations for wire wrapped tube bundles [62]. 70

Figure 4.32 – Nodalization of the NACIE-UP open loop adopted for the coupled simulations. 73

Figure 4.33 – Exchanged parameters in the coupled NACIE-UP simulation [62]. 74

Figure 4.34 –Preliminary comparison between the explicit and semi-implicit decomposition coupling approach [70]. 75

Figure 4.35 – Experimental vs RELAP5 vs coupling mass flow rate comparison (ADP06) [62]. 78

Figure 4.36 – Experimental vs RELAP5 vs coupling mass flow rate comparison (ADP10)[62]. 78

Figure 4.37 – Experimental vs RELAP5 vs coupling FPBS temperature comparison (ADP06)[62]. 78

Figure 4.38 – Experimental vs RELAP5 vs coupling FPBS temperature comparison (ADP10)[62]. 78

Figure 4.39 – Experimental vs RELAP5 vs coupling mass flow rate comparison, beginning of the transient (ADP10). 79

Figure 4.40 – Experimental vs RELAP5 vs coupling FPBS temperature comparison, beginning of the transient (ADP10). 79

Figure 4.41 – Experimental vs RELAP5 vs coupling HX temperature comparison (ADP06) [62]. 79

Figure 4.42 – Experimental vs RELAP5 vs coupling HX temperature comparison (ADP10) [62]. 79

Figure 4.43 – Experiment vs coupling TC13 and TC44 temperature comparison (ADP06) [62]. 80

Figure 4.44 – Experiment vs coupling TC13 and TC44 temperature comparison (ADP10) [62]. 80

Figure 4.45 – TALL-3D facility main components [71]. 83

Figure 4.46 – Picture of the TALL-3D facility [71]. 84

Figure 4.47 – Design drawings of main loop components (main heater (left); heat exchanger (centre); LBE pump (right)) [71]. 84

Figure 4.48 – TALL-3D test section: components (a) and thermocouples position and nomenclature (b) [71]. 85

Figure 4.49 – Detail of the discretization in Mesh 2 [74]. 88

Figure 4.50 – Comparison with experimental data of the different modelling approaches of the 3D-Test Section during the initial steady state [74]. 90

Figure 4.51 – Comparison with experimental data of the different modelling approaches of the 3D-Test Section during the final steady state [74]. 90

Figure 4.52 – Temperature distribution inside the 3D-Test Section during the initial steady state with the 2D improved model [74]. 91

Figure 4.53 – Temperature distribution inside the 3D-Test Section during the final steady state with the 2D improved model [74]. 91

Figure 4.54 – Transient simulation with the Ansys CFX model and boundary conditions from experimental results [74]. 92

Figure 4.55 – RELAP5 nodalization of TALL-3D facility [74]. 94

Figure 4.56 – Coupled simulation with the decomposition domain approach at different coupling timestep with the explicit (top) and semi-implicit (bottom) time advancing schemes [74]. 97

Figure 4.57 – Coupled simulation with the overlapping domain approach at different coupling timestep with the explicit (top) and semi-implicit (bottom) time advancing scheme [74]. 100

Figure 4.58 – Overlay of the mass flow rate in the 3D test section leg for all presented coupling approaches with a timestep of 1e-1s [74]. 101

Figure 4.59 – Comparison between experiment, RELAP5 standalone and coupled simulation of the mass flow rate in the 3D test section leg [74]. 102

Figure 4.60 – Comparison between experiment, RELAP5 standalone and coupled simulation of the mass flow rate in the Main Heater leg [74]. 103

Figure 4.61 – Comparison between experiment, RELAP5 standalone and coupled simulation of the upper and lower surface temperature of the 3D test section [74]. 103

Figure 4.62 – Comparison between experiment, coupled decomposition simulation and CFX transient simulation of IPT thermocouples inside the 3D test section [74]. 105

Figure 4.63 – Comparison between experiment, coupled decomposition simulation and CFX transient simulation of CIP thermocouples inside the 3D test section [74]. 105

Figure 4.64 – ATHENA main vessel layout and primary coolant flow path [78]. 112

Figure 4.65 – ATHENA main vessel (top left), cover (bottom left) and internals (right). 113

Figure 4.66 – Schematic layout of the ATHENA fuel assemblies [78]. 115

Figure 4.67 –Design of the spacer grids for the internal and external FAs... 116

Figure 4.68 –Core Simulator and Dead Volume before the installation in the main vessel. 116

Figure 4.69 – Lateral view of the ATHENA Main Heat eXchanger. 118

Figure 4.70 – Cross section view of the tube bundle (left) and of the bayonet tube structure (right). 119

Figure 4.71 – Solid structures that define the ATHENA Fitting Volume CFD domain [52]. 121

Figure 4.72 – RELAP5 nodalization of the Fitting Volume test case, with highlighted the part of the domain that in the coupled simulation are simulated in Ansys CFX [52]. 122

Figure 4.73 – Mass flow rate during the first 150s of the transient in the three channels and the global one [52]. 124

Figure 4.74 – Temperature at the inlet of the Fitting Volume during the first 150s of the transient in the three channels [52]. 124

Figure 4.75 – Temperature at the outlet of the Fitting Volume [52]. 125

Figure 4.76 – Streamlines and temperature distribution in the symmetry plane, at the end of the transient (1000 s) [52]. 125

Figure 4.77 – Pool model domain. 127

Figure 4.78 – Pool azimuthal nodalization. 128

Figure 4.79 – Feeding Conduit temperature evolution during the pool thermal transient. 129

Figure 4.80 – Temperature distribution in the CFD model on a plan cutting the centres of the Main Heat eXchanger outlet and Feeding Conduit inlet at 500 s on the left and 3220 s on the right. 130

Figure 4.81 – Temperature at the Plane A location after 3220 s from the start of the transient. In the boxes, RELAP5 temperature of the corresponding volumes. 131

Figure 4.82 – Temperature at the Plane B location after 3220 s from the start of the transient. In the boxes, RELAP5 temperature of the corresponding volumes. 132

Figure 4.83 – Streamlines of the Ansys CFX model in the downcomer of the ATHENA facility at 3220 s. 133

Figure 4.84 – Layout of the domain definition in the Ansys CFX code: steel (grey), liquid lead (blue), central porous medium (orange) and external porous media (red) [78]. 135

Figure 4.85 – Axial view of the ATHENA Core Simulator with dimension in meters [79]. 136

Figure 4.86 – Pressure per unit length for different velocities in the ATHENA infinite lattice model [81]. 137

Figure 4.87 – Outlet temperature maps in detailed CFD model (on the left) and the porous media model (on the right) for the steady state condition studied in Ref. [81]. 138

Figure 4.88 – "1D" region of the primary side axial nodalization [78]. 140

Figure 4.89 – Secondary loop nodalization. 141

Figure 4.90 – Enthalpy inside the Main Heat eXchanger in function of the unmodified simulation time. 143

Figure 4.91 – Mass flow rate in the Core Simulator during the transient for the central Fuel Assembly and external Fuel Assemblies. 143

Figure 4.92 – Mass flow rate in the Core Simulator during the transient for the inter-wrapper channel. 144

Figure 4.93 – Outlet temperatures of the Core Simulator during the transient for the central Fuel Assembly, external Fuel Assemblies and the inter-wrapper channels and the global value. 144

Figure 4.94 – Outlet temperatures of the Core Simulator during the transient for the central Fuel Assembly, external Fuel Assemblies and the inter-wrapper channels and the global value, first 100 s. 145

Figure 4.95 – Power transferred to the inter-wrapper region during the transient. 145

List of Tables

Table 3.1: Characteristics of the Continuous Update and CAlculation overlapping methods. 40

Table 4.1: Total simulation time and time spent on the FORTRAN subroutine for the different spatial discretization approached and time advancing schemes. . 47

Table 4.2: NACIE Heat Source geometrical and operational parameters..... 50

Table 4.3: Experimental boundary conditions for ADP10 and ADP06 tests [59]. 59

Table 4.4: Diameters of the different parts of the pin in the active region [59]. 60

Table 4.5: Mesh size sensitivity study of the Fuel Pin Bundle Simulator CFD model [62]. 62

Table 4.6: Mean and maximum temperature difference between CFD and experiment. 66

Table 4.7: Thermal conductivity (k) of the thermal insulator [59]. 68

Table 4.8: Coefficients for the calibration of the Fuel Pin Bundle Simulator pressure drops in the RELAP5 model. 70

Table 4.9: Numerical pressure drops along the loop in the end of the transient steady state [62]. 71

Table 4.10: Experimental vs RELAP vs coupled results (ADP10 test). 76

Table 4.11: Experimental vs RELAP vs coupled results (ADP06 test). 76

Table 4.12: Experimental test initial and final steady state conditions [74]. .. 86

Table 4.13: Grid independence study of the 2D model of the 3D Test Section [74]. 88

Table 4.14: Information exchanged during the TALL-3D coupled simulation for the different approaches. 95

Table 4.15: Computational time with the decomposition domain approach at different timestep for the explicit and semi-implicit time advancing schemes [74]. 98

Table 4.16: Core Simulator geometry and operational parameters. 117
Table 4.17: Main Heat eXchange geometrical and operational parameters. 119
Table 4.18: Porous media parameters for the Core Simulator model [81]. .. 138

Chapter 1

1 Introduction

The present thesis contributes to the advancement in the nuclear field toward the development and licensing of Generation IV nuclear reactors, in particular Lead-cooled Fast Reactors. The work involves numerical studies, directly driven by past and planned experimental campaigns to address R&D needs in the thermal-hydraulic field.

Thanks to the collaboration between the Politecnico di Torino and the ENEA Brasimone research centre, the thesis benefits from both an academic perspective and the practical experience gained by ENEA through its participation in an international project and its collaboration with industrial partners. This framework has given the possibility to conduct activities related to the development, verification and validation of computational tool with the constant look at practical goals, with proximity of the facilities that allow the advancement of the research toward the design and development of new reactors.

In this introductory chapter, the motivation of the thesis is discussed, presenting the current scenario in terms of thermal-hydraulic R&D needs.

The second chapter discusses the status of the thermal-hydraulic codes investigated in this work, presenting a literature review on the state of the art and giving to the reader the framework and the instruments to fully understand the tool description presented in detail in the third chapter. Here the development choices and their advantages are discussed, while introducing the different options that a user of the tool could adopt.

The applications of the tool are presented in the third chapter where the verification and validation process are reported, from simple but significative cases towards the application to facilities more representative of reactor conditions.

1.1 Numerical tools for thermal-hydraulics analysis of nuclear reactors

Thermal-Hydraulics (TH), in the nuclear field, is a fundamental part in the process of designing and licensing nuclear power plants [1]. Their safe and efficient operation largely depends on the accurate prediction and control of TH phenomena within the reactor core and associated systems. Furthermore, TH performance of systems designed to handle the fuel after the core utilization, e.g. fuel storage, or systems managing the heat dissipation during normal and abnormal conditions, e.g. the containment cooling system, will benefit from codes that are able to reproduce accurately the processes involved.

A substantial aspect of the licensing procedure of a new reactor requires demonstrating the ability to operate the reactor safely in any scenario, by evaluating the likelihood of failure based on the uncertainties associated with the calculations. To this end, advanced numerical tools are required to simulate and forecast complex thermal-hydraulic phenomena, encompassing heat generation, heat transfer, phase change, and fluid flow.

The analysis of thermal-hydraulic systems in nuclear reactors is inherently complex due to the nonlinear, multiphase, and multiscale nature of the phenomena involved. Consider fuel rods deformation inside a fuel assembly of a water-cooled reactor:

- if the effect of the deformation determines an increase in power generation or a reduction in the cooling capability by water, undesired boiling could occur. This TH phenomenon involves a change of phase and occurs at local scale;
- an undesired dry-out in a fuel assembly subchannel could have an impact on adjacent fuel assemblies, determining an abnormal behaviour of the core. Thus, the problem could be studied also at component level.
- if the safety features of the reactor are not able to re-establish safe conditions, the accidental initiation event could have an impact at the system level, involving multiple or all systems of the reactor.

Conventional methods based on testing TH phenomena using experimental facilities remain an essential step for reactor safety demonstration. However, they they are expensive and time-consuming to perform, especially at full-scale, suggesting adoption of approaches that limit the number of tests while still ensuring

full understanding of the phenomena involved. As a result, numerical methods have become indispensable for analysing nuclear systems while reducing testing efforts [2].

The role of numerical tools is to solve the governing equations of fluid flow and heat transfer, such as the Navier-Stokes equations, the energy conservation equation, and the mass conservation equation, including the investigation of complex phenomena such as phase transitions and turbulent flow.

The analysis of various problems requires different numerical tools depending on the scale of the phenomena involved (Figure 1.1) [3]: moving from the smallest scale simulated with Direct Numerical Simulation (DNS), which numerically solves the Navier Stokes equations, to the system level, historically modelled by System Thermal-Hydraulic (STH) codes. The computational cost decreases as the scale increases; however, this is accompanied by decreasing resolution and by a growing need for approximations or empirical correlations [4].

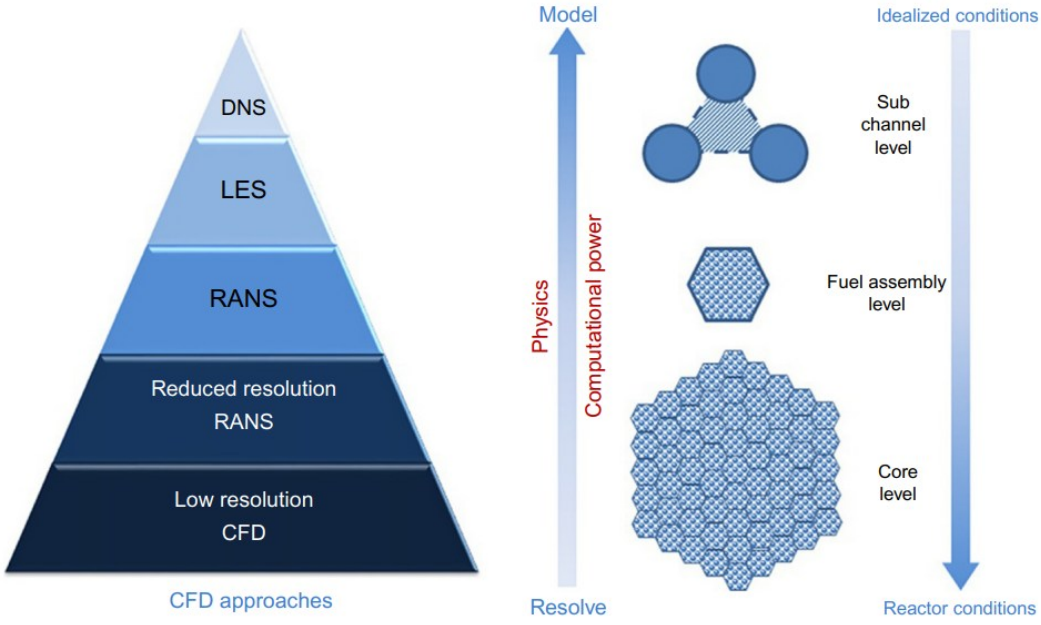


Figure 1.1 – Thermal-hydraulic code hierarchy [5].

In nuclear systems, the presence of phenomena occurring at different characteristic time and length scales is traditionally addressed by defining correlations based on experiments or general physical analysis. An example is the computation of local pressure drop coefficients. Nevertheless, it is not possible to have correlations and experiments that cover all the expected geometrical

configurations and flow regimes. When the data are not available, the user needs to consider analogies with those data, scaling methodologies, and/or making educated assumptions based on engineering practice or judgement [6].

Another situation in which approximation could lead to errors is the presence of complex 3D flow structures intrinsically dependent on the energy transfer phenomena. An example is represented by complex turbulent regimes in large region (plenum) in which local natural convection could affect the overall behaviour of the component [7].

The growing demand to analyse innovative, complex configurations, combined with advancements in highly accurate computational tools and the steadily increasing availability of computational resources, has driven the development of multiscale approaches in thermal-hydraulic analysis. These methods recognize that while improving accuracy is crucial, it is not always necessary to uniformly increase resolution. Nevertheless, if properly designed and exploited, the multiscale techniques enable selective refinement in critical regions, balancing high resolution and computational efficiency.

Traditionally, the licencing process of a water reactor leverages years of experience, large experimental databases, still updated with new campaigns, and large use of STH codes. The latter is also favoured by the configuration of the reactor primary circuit, mainly comprised by components (core, steam generator, pump, etc.) connected by pipes, constituting a single or more likely multiple loops. Within this configuration, the 1D approximation adopted by the STH codes (discussed in section 2.1) is sufficient for the majority of the cases. The fact that STH codes are able to deal with two phase flow with a satisfactory accuracy has also driven their application for safety assessment [6].

Conversely, nuclear technologies differing from water-based reactors in terms of materials (especially primary coolant) and geometric configuration cannot, or can only partly, leverage these tools and require development of ad-hoc experimental databases.

In section 1.2, the framework of Lead-cooled Fast Reactor (LFR) is presented. The use of molten lead as primary coolant promotes the adoption of a pool reactor configuration with single phase primary coolant. In addition, up to now, no power plants based on LFR technology has ever operated for civil applications, and the database of experimental data has certainly not reached the degree of maturity of

water technologies. These reasons underscore the urgent need for multiscale tools and pose the bases for the work presented in the thesis.

1.2 Lead-cooled Fast Reactor Technology

The LFRs are considered among the most promising technologies to meet the requirements introduced for GEN IV nuclear plants. Their main characteristics allow to fulfill the 4 pillars of GEN IV reactor designs [8]: *Sustainability, Safety and Reliability, Resistance to the Proliferation and Physical Protection, Economics.*

Worldwide, in recent years, various international actors have been promoting the development of this technology, leading to a race toward the commissioning of the first LFR. Examples could be found in the MYRRHA reactor designed by the Belgian Nuclear Research Centre SCK CEN, the Westinghouse LFR in USA, SEALER (Swedish Advanced Lead Reactor), CLEAR-I (China LEAd-based Research Reactor), or BREST-OD-300 in Russia which is currently being built and is therefore the most likely candidate to be the first LFR to start operation for civil purposes [9].

In this context, ENEA is supporting and contributing to the development of two relevant projects at the Italian and European levels, namely ALFRED [10] and LFR-AS-30 / LFR-AS-200 [11], driven respectively by Ansaldo Nucleare (within the FALCON consortium) and *new*cleo. The ENEA Brasimone centre is one of the main research infrastructures at the national and international level, dedicated to the study and development of technologies in the fields of GEN IV fission reactors and magnetic confinement nuclear fusion. Significant expertise is available in liquid metal technology, innovative materials for applications in harsh environments, and prototyping of systems and components for applications in energy systems.

1.2.1 General description of LFR design

The properties of lead coolant drive the design toward peculiar solutions that make the LFR archetype differ from the water-cooled reactors [12]. The most relevant pertaining to the TH field are:

- the very low neutron absorption cross section and poor moderating power allow operation in fast neutron spectrum with geometries

characterized by a high coolant/fuel ratio and Fuel Assemblies (FAs) with large pitch to diameter ratio. This fact allows reducing the pressure drops in the core and favour natural circulation inside the reactor during accidental conditions;

- the wide liquid temperature window and low vapor pressure allow the primary system to operate at atmospheric pressure and with sufficiently high margin from coolant boing, leading to the possibility to reach, in principle, very high temperature, thus high thermodynamic efficiency, conditional to materials' capability to withstand these conditions;
- high thermal conductivity and high thermal expansion coefficients make natural circulation effective for decay heat removal during accidents;
- the lack of exothermic reaction with air and water, together with operation at atmospheric pressure, eliminates the need for engineering provisions to address LOCA events, including pressure-resistant containment and intermediate loop that are instead required in other nuclear technologies. Since lead is prone to oxidation, a neutral cover gas is required to mitigate potential safety issues, but it does not present a fire hazard.

In addition, the favourable attributes above are often coupled, and some of them are conducive, to the adoption of a pool configuration for the reactor, i.e., all primary system's components are enclosed in the same reactor vessel, which is in turn enclosed in a Guard/Safety Vessel. In addition to increasing the system's thermal inertia, this configuration allows elimination of primary piping thus precluding LOCA events to occur, ultimately benefitting safety. Altogether, when combined with the elimination of the intermediate loop and high pressure containment, these design characteristics are supportive of a compact, high power density plant, which is a figure of merit conducive to promising economics.

In Figure 1.2, a schematic of the ALFRED reactor design is shown [13]. The primary system pool configuration was conceived in order to minimize thermal-hydraulic issues specific of liquid metal fast reactors (e.g., thermal stratification, thermal striping, free level fluctuations, gas entrainment) and their effects on immersed safety relevant mechanical components.

The hot fluid, exiting the core (designed with FA stem extended above the lead free level for favouring the handling during operation), is directed toward a hot pool by means of three pumps. Then it flows down in the plenum delimited by the

internal structure, while exchanging heat with the secondary loop in the Steam Generators (SGs). The coolant then flows upward toward the windows that feed the downcomer, eventually reaching the inlet of the core.

The reasons behind the definition of the described flow path are clearly presented in [13]. For the scope of this thesis, it is important to note the complexity of the flow path, which branches into three hot streams at the core's exit before reuniting inside the internal structure. Furthermore, Figure 1.2 reports the top view where the symmetric position of the SGs, pumps and the Dip-Cooler (DC) could be appreciated. The DCs play a fundamental role in the safety transients in removing passively the decay power in case the first line of defence in depth (the DHR1 connected to the SGs) fails: they are immersed in the pool and in certain accidental scenarios act as the heat sink for the transition from forced to natural circulation.

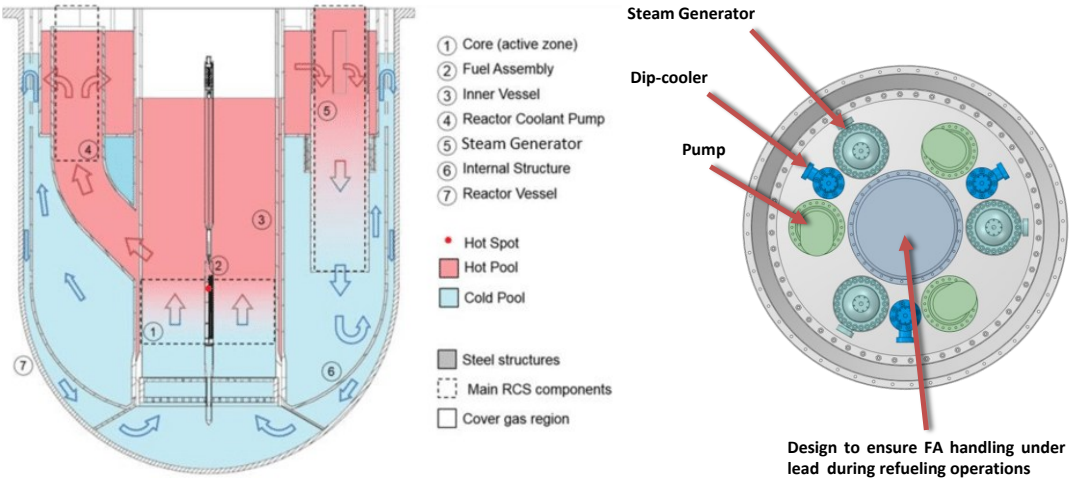


Figure 1.2 – Schematic of the ALFRED design [13].

In Figure 1.3, the schematic of LFR-AS-200, the *new*cleo's main design, is shown, where AS stands for Amphora-Shaped, referring to the shape of the inner vessel, and 200 indicates the electrical power in MW. The embodied innovations exploit the lead properties and enhance the potential for future deployment, owing to plant simplification and compactness, while ensuring passive safety. Key components are:

- core with fuel assemblies characterised by stem extended above the lead free level and hung by their heads;
- six innovative and compact Spiral-Tube Steam Generators (STSG);
- six recirculation pumps;

- three + three DCs of the Decay Heat Removal systems (DHR);
- the Amphora-Shaped Inner Vessel (ASIV).

Both the DCs and the ASIV could be respectively source and host peculiar TH phenomena, involving natural convection and circulation, thermal mixing and stratification and complex three-dimensional fluid streamlines that require to be studied in detail, especially in accidental conditions.

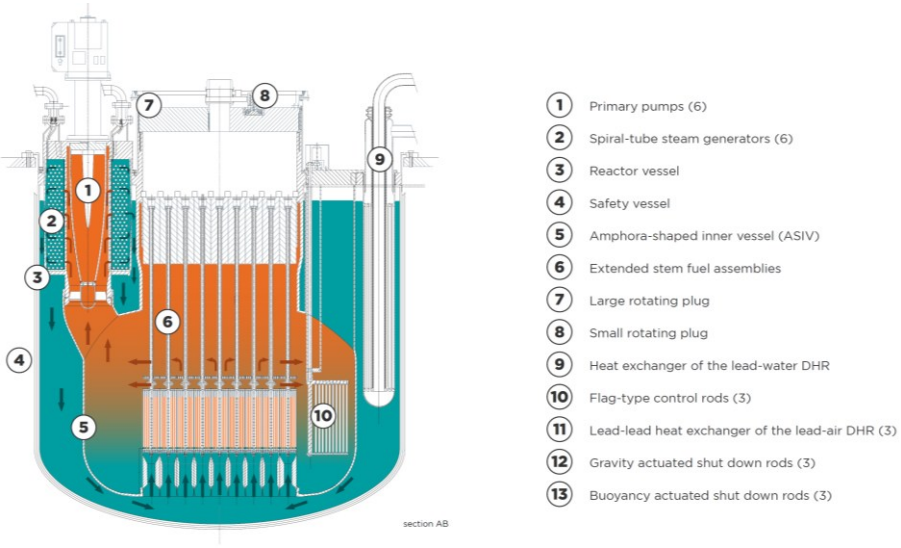


Figure 1.3 – Schematic of the LFR-AS-200 design.

1.2.2 Challenges in LFR thermal-hydraulics

Even though extensive research activities on lead technology development are ongoing, especially in the European context, some important R&D efforts are necessary toward demonstration of LFR technology to improve knowledge and experience in design, operations, maintenance and materials [14].

The most relevant technological challenges for LFRs in the TH field [15] concern the following topics:

- prediction and modelling of flow patterns in forced convection, including mixing;
- causes and impact of stratification, inducing thermal stresses;
- elimination of stagnant zones;
- impact of surface level oscillations;
- prediction of thermal fatigue issue;

- modelling of transition to buoyancy driven flow;
- modelling of natural convection flow;
- estimation of pressure drops of innovative components;
- prediction of fluid-structure interaction, including fluid induced vibration;
- prediction and modelling of sloshing due to seismic event.

The previous points need to be addressed by dedicated facilities and campaigns involving both experimental, modelling and validation efforts. The associated experimental efforts can be grouped into two main families of tests:

- HLM pool TH, which focuses on the study of forced convection flow (mixing, stratification, flow distribution, stagnant zones, surface level oscillations), natural convection flow (pressure drops, surface level oscillations), transition to buoyancy-driven flow, fluid-structure interaction, and system response to seismic events. This kind of test are usually performed in pool type facility.

- Component TH, in particular: Fuel Assembly (FA), with the main objective of defining assembly geometries to achieve optimal conditions for heat transfer between fuel rods and coolant in forced and natural circulation, demonstrating the capability to maintain geometrical features in abnormal scenarios; SG, with the focus to fully understand the heat transfer process between the primary and secondary fluid in all the possible conditions. Other areas requiring investigation include sub-channel flow distribution, cladding temperature profile and hot spots, pressure drops of innovative component, vibrations induced by flow, fluid-structure interaction at component level, and the consequences of hypothetical core damage (e.g. pin deformation or flow blockage). This kind of test are usually performed in loop type facility.

The HLM pool thermal-hydraulics experiments will be essential to investigate the behaviour of the different components that constitute the primary system and their mutual interaction (integral test facilities). Furthermore, in these campaigns, the effectiveness of safety procedures, e.g. the operation of the DHR system(s), will be tested.

The collection of experimental data aims to improve the knowledge of phenomena and processes and create a database for the validation of computer codes for the prediction of the system behaviour in relevant condition for design and safety.

An important aspect not covered by this thesis regards the requirement of suitable instrumentation for LFRs [16]: the measuring and monitoring techniques represent a significant challenge due to the high thermal loads, high temperatures, corrosive environment, fast neutron spectrum and non-transparency of the coolant. Research activities aim to develop instrumentation capable of withstanding the operational conditions of LFRs, maintaining the reliability of measurements over the long period. Ensuring high quality experimental data is propaedeutic to the understanding of the phenomena and the code validation.

Chapter 2

2 Status of the available numerical tools

This chapter gives a brief overview of System Thermal-Hydraulic (STH) codes (Section 2.1), Computational Fluid Dynamics (CFD) codes (Section 2.2) and their coupling (Section 2.3). The specific code used in the present work are described, i.e., RELAP5 for STH codes, and ANSYS CFX for CFD codes. In the last section, a brief overview of the state of the art of coupled CFD-STH code is provided.

2.1 System Thermal-Hydraulics codes for LFR

Within the context of safety assessment and design for nuclear reactors, system thermal-hydraulics (STH) codes are extensively employed to simulate the transient behaviour of entire systems, encompassing both primary and secondary circuits, as well as the balance of plant [17].

These STH codes have been under development since the early 1970s for pressurized water reactors (PWRs) and boiling water reactors (BWRs). Their validation has relied heavily on integral test facility and experimental data derived from the operation of prototypes and commercial nuclear reactors.

STH codes are built upon a foundation of six balance equations (three for steam and three for liquid) and are supplemented by various constitutive equations. These are integrated with models governing heat transfer and, in some cases, neutron kinetics. The two-phase flow domain is typically divided into interconnected control volumes, and the flow properties are averaged both spatially (1D component approximation) and temporally within these volumes. Consequently, phenomena occurring at small length and time scales, such as turbulence, are also averaged out.

To adapt these STH codes for application to LFR, it is imperative to incorporate algorithms, models, and correlations for HLM [18]. Furthermore, their validation must be expanded through the use of a comprehensive experimental database to ensure their suitability for safety analysis within the LFR context.

While these simulations have shown their effectiveness in modelling certain system behaviours, they have limitations resulting from three main contributions:

- their one-dimensional approach makes them less accurate for inherently multi-scale/multi-dimensional processes, like heat and mass transfer in pools;
- the fluid to fluid conduction is not usually considered in the STH code, an assumption reasonable for water or air, while for HLM this contribution acquires more importance due to the fluids properties and velocities involved;
- the experimental database is not able to fully cover, with sufficient accuracy all the possible TH conditions within a LFR design.

Various STH codes [18], primarily developed for other types of rectors, have been modified in the last decades to assess LFRs system, such as RELAP5, CATHARE, ATHLET, TRACE, SAS4, /SASSYS, SPECTRA. The efficiency of STH codes in solving multi-phase and multi-component problems, coupled with their low computational demands, makes them essential tools for advancing nuclear technology.

Of these STH codes, RELAP5 is briefly described in the next section as this code is selected for the CFD-STH coupled tool.

2.1.1 RELAP5 Mod3.3

RELAP5 [19] is a Fortran 77 code, established worldwide a reliable tool for nuclear system analysis. Extensive qualification projects, sensitivity analyses and uncertainty assessments of its physical models have been conducted by various international institution and documented in literature [20].

This STH code was developed at Idaho National Engineering Laboratory (INEL) for the U.S. Nuclear Regulatory Commission (NRC), conceived to simulate light water reactor (LWR) transient behaviour under both normal and accidental conditions.

RELAP5 is designed to analyse one-dimensional fluid dynamics and heat transfer problems. Its versatility extends to a wide variety of hydraulic and thermal transients, including those occurring in non-nuclear systems with mixtures of steam, water, non-condensable gases, and solutes [21].

A semi-implicit numerical method is employed to solve the governing equations within interconnected control volumes. Mass and energy balance equations are solved at the centre of each volume for both liquid and gaseous phases, resulting in scalar quantities (pressure, energy, density, and void fraction) being evaluated at these points. Momentum balance equations are solved at the junctions between volumes, where vector quantities (velocities) are computed. The code's two-phase flow model necessitates the identification of the flow regime to accurately determine interface friction forces and wall friction forces for each phase.

The RELAP5 models' primary components include:

- Pipe: represents one-dimensional flow channels where the conservation equations (mass, momentum, and energy) are solved. It captures the geometry and hydraulic connectivity of the system, allowing detailed analysis of fluid dynamics along each segment;
- Junction: acts as a zero-dimensional node that connects multiple fluid volumes or flow channels. Junctions enforce conservation laws (mass and energy) at the interconnection points, ensuring proper coupling between different system components;
- Time-Dependent Junction/Volume: models nodes or volumes whose properties evolve with time. These components account for transient mass and energy accumulations, capturing dynamic behaviours and non-steady state phenomena at critical points within the system;
- Heat Structures: represents the solid components (such as walls or structural elements) that interact thermally with the fluid. They model one-dimensional heat conduction and the thermal inertia (heat capacity) of the materials, enabling accurate simulation of fluid-structure heat exchange.

A cooperative effort between ENEA and Italian universities led to the development and validation of a modified version of RELAP5 Mod3.3 in which the HLMs thermo-physical properties are implemented [22]. The code has been adopted to analyse various facility both of the loop type (like NACIE [23]) and the

pool type (CIRCE [24]) and used in support of the ALFRED [25][26] reactor design and components performance evaluation.

2.2 Computational Fluid Dynamics codes for LFR

Advancements in computer technology have led to a surge in the application of CFD methodologies for addressing complex flow and heat transfer challenges. CFD methods are commonly classified based on how they model or resolve turbulence [27]. Within the LFR TH field, a diverse array of CFD approaches have been successfully implemented, including Direct Numerical Simulation (DNS), Large-Eddy Simulation (LES), and Reynolds-averaged Navier-Stokes (RANS) methods [28]. All these CFD methods necessitate the solution of the governing conservation equations for mass, momentum, and energy, albeit with varying degrees of closure models and simplifications.

The RANS approach, characterized by its computational efficiency, remains the most practical option for numerically modelling turbulent heat transfer in complex industrial flow configurations. RANS employs time averaging to reduce the range of scales within turbulent flows, necessitating the modelling of both turbulent momentum flux and turbulent heat flux terms.

Low Prandtl number (Pr) fluids, like liquid metal, are characterized by large thermal layer compared to the boundary layer, which is typically of the same size as the momentum boundary layer for fluids like air and water, in which the Pr is close to unity (Figure 2.1) [29].

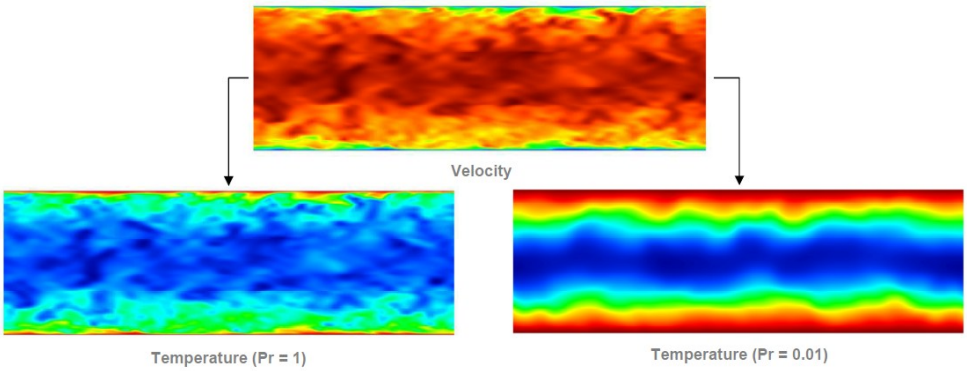


Figure 2.1 – Velocity and temperature field of rectangular channel heated from top and bottom by NRG applying a fluid like air and water (Pr ~1) and a typical liquid metal (Pr<<1) [29].

Given this unique characteristic, research has focused on evaluating the suitability of existing models for representing turbulent momentum and heat fluxes in liquid metals. This has led to investigations into the potential need for developing new and dedicated solutions. Relevant steps in this process have been carried out within EU projects as THINS (Thermal-Hydraulics of Innovative Nuclear Systems) [30] and SESAME (Simulations and Experiments for the Safety Assessment of MEtal cooled reactors) [31]. Based on the findings of THINS and SESAME, it is recommended to concentrate efforts on generating a robust reference database for validating and assessing different turbulent models. This database should encompass all flow regimes (forced, mixed, and natural convection) and reactor conditions, including both normal and off-normal scenarios.

Even if the maturity of the application of CFD to LFR applications still need some efforts to be considered fully achieved, in the last decade, various validation works [32] proposed a comparison between experimental data and simulation with good results. Furthermore, international projects like ANSELMUS (Advanced Nuclear Safety Evaluation of Liquid Metal Using Systems) [33] or the IAEA Coordinate Research Project (CRP)-I31038, named “Benchmark of Transition from Forced to Natural Circulation Experiment with Heavy Liquid Metal Loop”, will further favour cooperation and knowledge sharing on the best practices in the field of CFD applied to liquid metal systems.

Among the various CFD code, Ansys CFX is briefly described in the next section as this code is selected for the CFD-STH coupled tool.

2.2.1 Ansys CFX

Ansys CFX [34] is among the industry leading CFD software. In spite of being initially developed for turbomachinery applications, it was demonstrated to be reliable and robust for a variety of applications. It allows 3D steady-state and unsteady simulations in areas of complex geometry using multiple processors. The code is capable of modelling various physical phenomena, such as heat and mass transfer, radiation, turbulence, thermal convection etc. [35].

The solver utilizes a cell-vertex mixed finite volume/finite element approach to discretize the domain. In vertex-based schemes, flow variables are stored at the mesh element vertices. The code employs a coupled technique, simultaneously solving all transport equations across the entire domain through a false time-step algorithm. To expedite convergence, the linearized system of equations is preconditioned to reduce eigenvalue disparities.

The multi-grid approach effectively addresses low-frequency errors by converting them into high-frequency errors on the finest grid level, significantly accelerating convergence. While a single iteration in this method might be slower than a classical decoupled (segregated) SIMPLE approach, the overall number of iterations required for steady-state convergence is typically on the order of 10^2, compared to 10^3 for decoupled algorithms [36].

This CFD code is used in liquid metal research to analyze various phenomena and their impact on several components, such as:

- the normal and accidental behaviour of FA [36];
- performance of the pump [37];
- pool stratification and mixing [38];
- heat transfer in heat exchanger [39].

A commercial code like Ansys CFX consists of less customizable set of equations with respect to open source CFD codes, e.g. OpenFOAM. While this characteristic reduces the user's possibility to intervene in the solution process, it generally results in higher reliability and robustness. In the CFX code, in particular, it is possible to call Fortran subroutine [40] through a source code interface to implement customized physical models not already present in the code and manage data to be exchanged with external tools. For the purpose of the work presented in

this thesis, the Fortran subroutines demonstrated to be a successful instrument for the development of the Ansys CFX - RELAP5 Mod3.3 tool.

2.3 Coupled STH and CFD tools

Coupling different numerical codes is a methodology widely adopted in the nuclear field. The basic need for coupling comes from multi-physics problems (e.g. fluid/structure interaction, neutronics/thermal-hydraulic coupling, thermal/structure interaction) [41]. When the mutual interactions between two or more physical fields are so strongly interconnected that separate simulations of each field's effects cannot accurately predict a phenomenon with the desired level of accuracy, the coupling between codes allows improving such accuracy. On the other hand, code coupling is often (although not always) associated with an increase in computational resources and/or computational time, and thus the decision on whether to adopt coupling methodologies should be made on a case-by-case basis..

Effective coupling between codes depends on different characteristics, some of which are here reported:

- The level of maturity of the coupled tool depends on the maturity of the codes, coupling an established code with a new code will gives results with the same maturity of the least mature code.
- The simulation time required for the runs will be longer than that of the slowest code plus the time for information management. If the application of the tool has limitation on the simulation time that an average problem should take (e.g. tool for system or component design), it is important to select the coupled codes in such a way to ensure that both the codes can satisfy the requirement.
- The mass, momentum and energy conservation laws msut be verified through the coupling information exchange. The error introduced by the coupling methodology should be negligible with respect to the accuracy of the least accurate code.

In a physical field, coupling methods are required to analyze different system scales due to the limitations of large-scale codes in accurately capturing small-scale phenomena within a subsystem using the same approach and level of approximation as the rest of the domain.

At the Politecnico di Torino, broad experience on multiphysics/multiscale problem brought to the development of dedicated tools for fusion and fission applications. Two relevant examples are:

- FRENETIC, the Fast REactor NEutronics/ThermalhydraulICs (FRENETIC) code for the multiphysics analysis of liquid-metal cooled cores [42];
- 4C, the Cryogenic Circuit Conductor and Coil code to allow the TH modelling of transients in the whole magnet system of fusion devices exploiting both 1D and 2D approximation together with the object-oriented equations based modelling language Modelica [43].

To leverage the strengths of both STH and CFD codes, coupling them has been proposed to address specific multiscale problems. Over the past decade, CFD and STH coupled tools have been developed using various STH codes, such as RELAP5, ATHLET, TRACE, and CFD codes like Ansys Fluent, Ansys CFX, and STAR-CCM+. These tools have been applied to both GEN-III and GEN-IV technologies.

Examples of previous research include a proof-of-concept coupling between RELAP5-3D© and Ansys CFX for a blowdown problem [44].Additionally, TRACE was coupled with Ansys CFX and tested against experimental data for a double T-junction [45]. Other studies have explored the coupling of TRACE and STAR-CCM+, comparing domain overlapping and decomposition approaches [46]. Furthermore, a MATLAB© interface was used to couple Fluent and RELAP5 for analysing a pool-type facility [47].

These techniques were initially designed for analysing LWRs. An example of pioneering effort, conducted at the Korean Atomic Energy Research Institute (KAERI), involved coupling the three-dimensional code COBRA-TF with the STH code RELAP5/MOD3 [48]. The aim was to create a more accurate LWR simulation tool by combining the detailed 3D vessel hydrodynamics of COBRA-TF with the capabilities of RELAP5/MOD3. The effectiveness of this new tool was evaluated using the LOFT L2-3 large-break loss-of-coolant experiment.

In recent years, the same multiscale approach has been developed to enhance the modelling of coolant flow patterns in pool-type liquid metal-cooled reactors, especially for analysing three-dimensional effects in large reactor vessels. These efforts are part of a broader goal to improve the accuracy of predictions for the behaviour of SFRs and LFRs during accidents like loss of flow events.

2.3.1 Classification

This thesis discusses a coupling methodology between the STH code RELAP5/Mod3.3 and the CFD code Ansys CFX. The classification of the discussed resulting tool could be described with the criteria outlined by Toti et al., 2018 [49], considering six distinct characteristics (Figure 2.2) which are discussed below whereas the choice made for each is discussed later in Chapter 3.

- Code Integration

This refers to whether a single solver handles all subsystems ("Monolithic") for a stronger coupling, or if dedicated solvers are used for each subsystem ("Partitioned"). The main benefit of a Monolithic approach is its ability to be highly specialized for particular problems through careful adjustments and optimization. However, these highly specialized algorithms may not be adaptable or suitable for a variety of operating conditions. The Partitioned approach, instead, relies on a master-slave relationship between codes or an interface software, avoiding the need for an integrated solver, resulting easier to be implemented and more flexible, with the drawback of a more limited level of optimization for specific applications.

- Coupling Execution

This describes whether information flows only from one code to the other ("Off-line" or "One-way"), or if there's a two-way exchange ("In-line" or "Two-way"). The choice of the coupling execution defines if the connection will be weak or strong and should be selected depending on the impact of one code results to the other.

- Synchronization

This involves defining the time points for information transfer, which can be based on "Identical Timesteps" or "Sub-cycling approaches". For a coupled tool it is fundamental to address the problem of synchronization, verifying that the two codes are able to exchange information maintaining a proper coordination of the temporal coordinates. The possibility to adopt a Syb-cycling approach requires more development since checks should be defined, but it is a useful tool especially in cases where the computational cost of the two code differs.

- Information Exchange Type

This indicates whether the codes run simultaneously ("Parallel") or sequentially ("Sequential"). A Parallel coupling method necessitates all codes to operate concurrently and is particularly beneficial when dealing with calculations that demand comparable processing times, as it can help minimize idle periods.

However, it requires careful attention during the information exchange process. For these reasons, in CFD-STH tools the sequential approach is usually adopted.

- Numerical Scheme

This refers to the time-discretization method used by the solver, which can be "explicit," "semi-implicit," or "fully implicit". Fully implicit methods necessitate solving all the relevant transport equations simultaneously. This approach creates a very tight coupling that is maintained at each timestep and internal iteration. It can only be implemented if the monolithic approach is chosen as the underlying code structure and is practically impossible with a Partitioned integration. The explicit and semi-implicit approaches will be discussed in detailed in section 3.2.

- Spatial Domain:

This determines if the domain is partially simulated by the STH code and partially by the CFD code ("Decomposition"), or if the STH code covers the entire domain with partial overlap by the CFD domain ("Overlapping"). The decomposition approach is the most intuitive and requires less development, however it requires checking on conservation of mass, momentum and energy during information exchange. The overlapping has the potential to be more robust but could require complex implementation and code modification. The two approaches are presented in section 3.3.

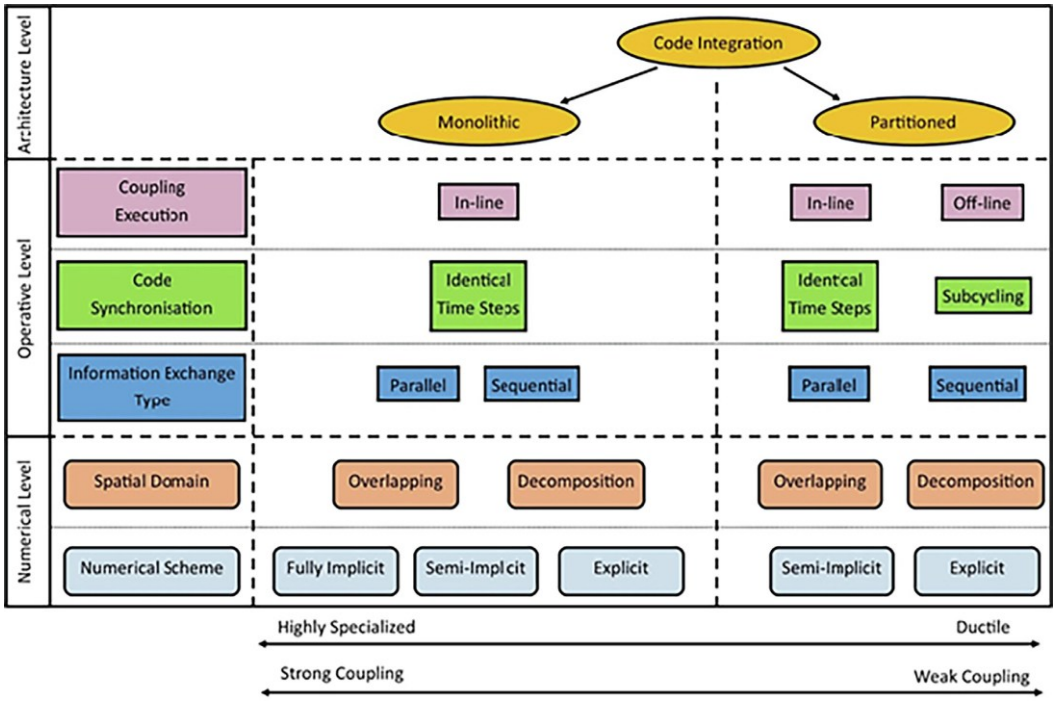


Figure 2.2 – Code coupling classification [50].

2.3.2 Scope of the tool

In the field of Light Water Reactors (LWRs), coupled Computational Fluid Dynamics (CFD)-System Thermal Hydraulics (STH) tools have been applied to various configurations and for diverse purposes. The ultimate objective is to develop a system TH analysis tool for use in the design and safety assessment of nuclear reactors. While coupled simulations require more computational time than standalone STH simulations, they can be justified by their improved representation of phenomena, when such improved representation is either necessary or required.

An effective CFD-STH code relies on the stability and robustness of its constituent codes, necessitating significant experience in the field. Therefore, its development encompasses the challenges associated with both codes and benefits from advancements in state-of-the-art coupling techniques. The CFD code should be implemented for single or multiple subsystems where the accuracy of the STH code does not meet requirements imposed by either the designer, or the regulator, or both. It is crucial to consider the resolution and scale of the problem being analysed. The CFD model will always provide a higher resolution representation of the subsystem due to its inherent higher fidelity. However, a coupled CFD-STH tool is truly necessary only under the following conditions:

1) the CFD model of a component is more accurate than the STH model;
2) the improved CFD representation pertains to quantities relevant at the system scale;
3) the quantities identified in point 2 impact the calculation of quantities relevant for safety assessment and/or design optimization, to a level that is deemed necessary by either the designer or the regulator (or both).

Consequently, a thorough understanding of the problem and an evaluation of the CFD model's performance are essential before implementing a coupled tool for system analysis.

A typical scenario where a coupled approach might not be necessary is the simulation of internal TH behaviour in a FA. The CFD model can provide a detailed representation of the FA, including hot spots and local gradients. However, if the CFD model's results for system-level relevant quantities (e.g., temperature outlet, heat losses of the FA, pressure drops) are consistent with the STH code results, a coupled tool can be avoided. In such cases, a standalone STH simulation can be initially conducted to compute boundary conditions, which can then be applied to the CFD model in a separate simulation.

Conversely, for example, if a plenum above the core is considered during a transient involving a change in mass flow rate, such as a Loss of Flow Accident (LOFA), the thermal hydraulic behaviour of that region may transition from mixed zone to thermal stratification due to reduced coolant velocity. Traditionally, this phenomenon could not be accurately represented by STH codes. By employing a CFD code to describe the plenum within the reactor model, it is possible to improve the representation of coolant temperature at the pump suction and heat losses from the hot pool to the cold pool. These quantities affect, for instance, the power exchanged in the SG or the inlet temperature of the core, ultimately impacting the overall system behaviour.

2.3.3 Original contribution of the thesis

To advance the research activities carried out to support LFR development, the need for a new coupled tool involving the widely adopted Ansys CFX and RELAP5/Mod3.3 codes emerged. The motivations include the opportunity to envelope the innovations available in the literature on coupled CFD-STH tools and to exploit the research work carried out in the HLM community on the two family of codes.

The tool is intended to be developed using a robust and organized program, with validation against experimental data in relevant environment, to be adopted to support the design of upcoming experimental facilities, the operation of which will further favour the validation of the tool.

Despite significant advancements in this field, establishing best practices for coupled simulations in HLM environments and identifying the scenarios where the coupled approach offers substantial benefits compared to standalone simulations remain ongoing challenges [50]. The thesis aims to contribute to solving these challenges by:

- discussing methodologies to setup coupled simulations involving Ansys CFX and RELAP5/Mod3.3 codes: domain definition, time advancing scheme and spatial discretization approach selection, interface boundary conditions definition, etc.;
- presenting in-house developed scripts for the data post processing and exchange, completely managed by the master code (Ansys CFX), thus avoiding tertiary platform or interface for this purpose, offering greater flexibility and customization;
- investigating a series of test cases that show the implications of the adoption of CFD-STH coupled tools for transient events in conditions relevant to LFRs;
- validating the tool against available experimental database.

Finally, the work intends to increase maturity and confidence in adopting CFD-STH coupling for LFR design and safety assessment.

Chapter 3

3 Ansys CFX – RELAP5 Mod3.3 coupling tool

The third chapter of the thesis presents in detail the coupling strategy developed. Different options are available within the Ansys CFX - RELAP5 Mod3.3 coupled tool, which foresee the adoption of common tools as FORTRAN 77 subroutines and Python written executables. The reasoning behind the adopted choices in the tool development is here highlighted with the goal of presenting an organic work: the Ansys CFX - RELAP5 Mod3.3 coupled tool aims to be a robust and usable tool readily available for use including both direct analysis applications and further development.

After a general description of the coupling strategy (Section 3.1), specific key features available in the developed coupling method are described: the time advancing schemes (Section 3.2) and spatial discretization approaches (Section 3.3).

3.1 Description of the coupling strategy

The Ansys CFX (CFX) and RELAP5 Mod3.3 (R5) are well-established codes that demonstrated to be valuable options in nuclear TH analysis. Consequently, referring to the coupling characteristics discussed in Section 2.3.1, a partitioned coupling is selected to preserve the robustness of the codes, without modification on governing equations and solvers.

The coupling methodology employs two-way communication to fully leverage the benefits of coupling, even though the possibility to choose a one-way data exchange is left to the user. In some cases, an off-line coupling could be sufficient, if the feedback of one code to the other is negligible or beyond the scope of the analysis. However, the user must verify the advantages of running the coupled tool,

rather than two separate simulations where the boundary conditions of one code come from the result of the other code.

Given the substantial difference in simulation times between CFD and STH codes, sequential execution is adopted. The synchronization between the code is achieved through sub-cycling: the cycling of the two codes is separate, thus two different timesteps could be implemented.

The coupling timestep is defined as the time between two consecutive data exchanges between the CFD and STH codes. In the tool, the coupling timestep always coincides with the CFX timestep. However, the R5 timestep can be either equal to or a fraction of the coupling timestep and not vice versa: R5 has a lower computational cost and the possibility to carry out more internal timesteps before exchanging information increases the robustness of the tool, with negligible impact on the overall simulation time. To ensure synchronization, the tool verifies that both codes have reached the same time point before initiating a new coupling timestep. The possibility to have an adaptive coupling/CFX timestep is available, based on the implementation offered in the CFX code. Nevertheless, the ratio between the coupling and the R5 timestep is constant throughout the simulation.

CFX is designated as the master code, and the need for an intermediary tool for data exchange is eliminated by developing Fortran 77 routines, named "Junction Box Routines." These routines are called at specific points within the CFX simulation (Figure 3.1). The timing of these calls should be optimized to minimize memory usage and computational overhead while ensuring CFX's ability to distribute calculations across multiple processors. The master processor will handle information exchange between the codes. In CFX, the only “time locations” where the master CPU's memory is replicated on all other processors are those beginning with "User Input" (e.g., "User Input (master only)," "User Input Start of the Timestep") [51]. Therefore, the scripts responsible for reading and writing boundary conditions are inserted at these points to facilitate proper Message Passing Interface (MPI) operation.

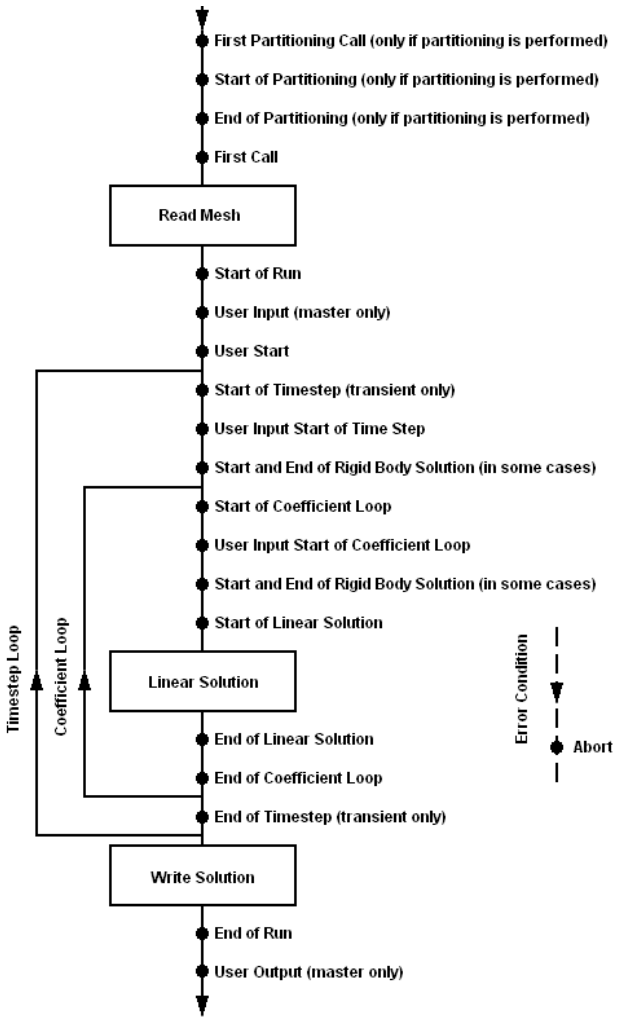


Figure 3.1 – Time locations available during the Ansys CFX solver operation at which the junction box routine could be called [51].

The Fortran routines' quantity and function are heavily influenced by the numerical time advancement scheme. Nonetheless, standardized tools are necessary for handling R5 files. The R5 restart file (*.rst*) is a prerequisite for launching the coupled calculation. It contains the initial condition of the variables describing the domain simulated in R5 and it will subsequently store the results relative to the STH domain of each timestep. The boundary conditions exchanged from the CFD code to R5 at the beginning of each timestep are stored in the memory and transferred to an input file (*.inp*) in which the corresponding data contained in the restart file are overwritten. In the coupling procedure, two Python-written in-house developed executables are used [52]:

1. *Modify_input_R5*, the executable that updates the input file with R5 boundary conditions and sets the timestep and termination time for the R5 run;
2. *Read_R5,* the executable responsible for analysing the binary restart file, extracting plot data, saving it to a plot file (*.plt*), identifying and isolating the restart block required for the next R5 timestep, and generating a .csv file containing the CFX boundary conditions. The user determines the plot frequency of the solution.

Since the current version of the coupling tool is not equipped by a graphic user interface, the tool takes advantage of a simple text file (*.dat*) in which all the variables to be exchanged and part of the coupled calculation setups are inserted by the user. The text file is formatted in such a way that the FORTRAN routines can properly read it. The text file is not modified during the run and comprises a collection of instructions for the coupling procedure.

3.2 Time advancing scheme

Decisions regarding time-discretization are inherently made at the numerical level, reflecting the strategy adopted to achieve stability and accuracy in the simulation process. Specifically, in the context of coupling CFD and STH codes, the choice of the numerical scheme for data transfer at the domain boundaries is fundamental, as it directly influences both computational efficiency and the robustness of the coupled tool.

3.2.1 Explicit scheme

The explicit method is the most straightforward and rapid approach for advancing time. In this method, the results from the current timestep of one code are directly used as boundary conditions for the next timestep of the other code. Figure 3.2 illustrates this communication process between the codes. The drawback of this approach is, in general, a limitation on the timestep dimension and a less frequent communication between codes per single timestep [53].

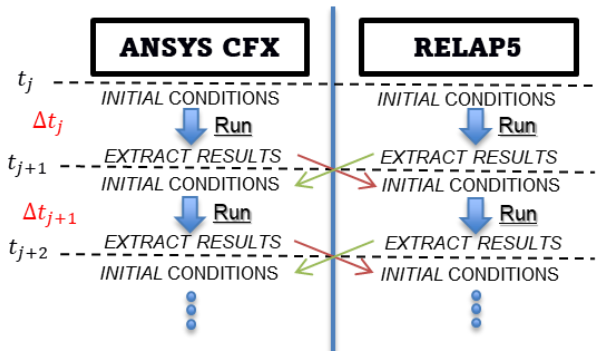


Figure 3.2 – Diagram describing the time-stepping process in an explicit scheme, highlighting the sequence of code execution and information exchange [52].

The definition of the boundary conditions in the CFX and R5 code is carried out following two different procedures. The CFX run is continuously proceeding, adopts a semi-implicit resolution of the equations in the solver and always perform a single timestep. For this reason, when a new boundary condition is imposed, the code internally takes into account the variation in time, requiring a single value to be imposed.

R5, on the other hand, performs multiple timestep and its contribution is represented by successive restarts of the simulation. To distribute the contributions of the terms with the time derivative within the solved equations for the entire coupling timestep, the variation of the boundary conditions is imposed as a linear variation between two values.

Practically, in the implementation of the explicit scheme, to CFX, the boundary conditions resulting from the R5 run of the previous coupling timestep are imposed; to R5, the boundary conditions consist of the linear interpolation between the value obtained from the CFX run of the previous coupling timestep and the one before.

In this work the following nomenclature is adopted. X^j and Y^j are defined as the boundary conditions of CFX and R5 at the j-th time instant, respectively, and $F(X)$ and $G(Y)$ as the results of the codes run.

It is possible to state that, in an explicit time advancing scheme:

$$\begin{aligned} Y^j &= F(X^{j-1}) \\ X^j &= G\left(Y^{j-1}\right) \end{aligned} \tag{1}$$

The fact that the code adopts a boundary condition coming from the other code at the previous timestep is the limiting approximation for this scheme, and does not introduce relevant error if the physical dynamics is sufficiently slow compared to the time step.

The FORTRAN routines adopted in the explicit scheme are divided in one User CEL (CFX Expression Language) Function and three Junction Box Routines (JBR) [51], the latter described as follows:

- *jbr_userinput*: this initialization function is executed before the simulation begins. It extracts essential information from the *.dat* file, including the names and locations of R5 files, as well as the number and names of CFX variables that will be exchanged with R5;
- *jbr_userinput_sott*: this function is called at the start of each timestep. This routine reads the R5 results to be transferred to CFX;
- *jbr_endofthetimestep*: this function is called at the end of each timestep. It is responsible for:
    - modifying the R5 input file by inserting the results of the CFX timestep (*Modify_input_R5)*;
    - running the R5 timestep(s);
    - post-processing the resulting restart file (*Read_R5)*;
    - extracting the variables to be passed to CFX (*Read_R5)*;
    - appending the last results to a *.plt* file while reducing the dimension of the *.rst* file to avoid the manipulation of big files (*Read_R5)*.

The User CEL Function sets the variables coming from RELAP5 as boundary conditions of the CFX timestep, and it is called autonomously by the code.

A schematic representation of the time locations of the routines is shown in Figure 3.3.

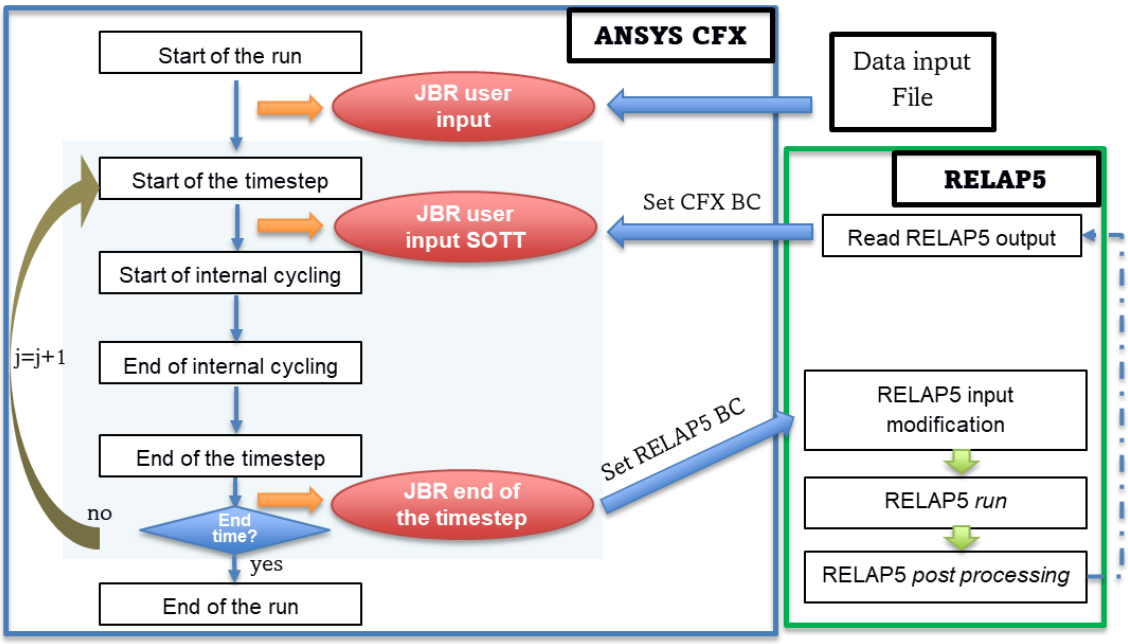


Figure 3.3 – Coupling methodology between Ansys CFX and RELAP5 in the explicit scheme [52].

3.2.2 Semi-implicit scheme

The semi-implicit method differs from the explicit method by considering the results of the other code during its internal iterations. However, it's not fully implicit because the two solvers remain separate, and the equations aren't solved simultaneously. Consequently, the semi-implicit method is often considered the most advanced approach for coupling codes like CFX and R5.

With the semi-implicit scheme, the tool iterates the same timestep until the difference between the boundary conditions obtained by two consecutive iterations (i and $i-1$) is smaller than a tolerance:

$$|X_i^j - X_{i-1}^j| < tol \qquad (1)$$

or the user-defined maximum number of internal cycles is reached. The check on the boundary condition assumes that from equal boundary conditions the codes will give the same solution (Figure 3.4).

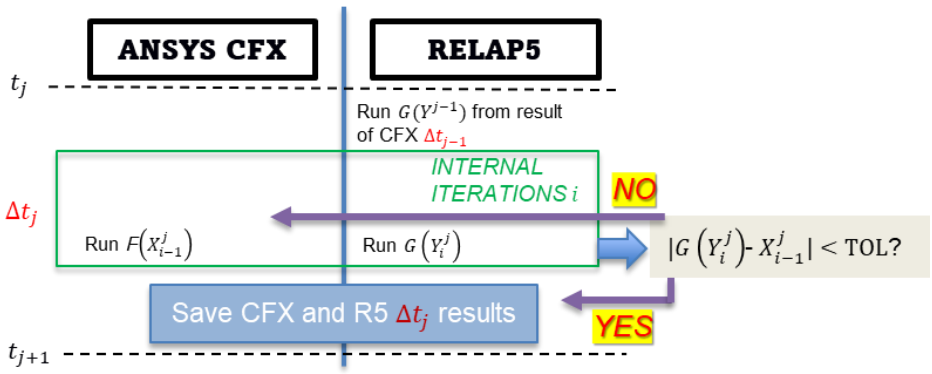


Figure 3.4 – Diagram describing the time-stepping process in a semi-implicit scheme during a single coupling timestep, highlighting the sequence of code execution and the convergence check in the internal iteration [52].

Throughout the internal iterations of a timestep, the codes exchange information, meaning that boundary conditions are not static. Instead, the latest results from the other code are incorporated into the calculations. For RELAP5, boundary conditions are adjusted linearly from the values of the previous timestep and to the current intermediate results from CFX (Y^{j-1} and $F(X_{i-1}^j) = Y_i^j$).

For CFX, in which a single timestep is run, the boundary conditions are taken from the RELAP5 current results ($G(Y_{i-1}^j) = X_i^j$).

The new coupled timestep starts with the run of the STH timestep, instead of the slower CFD one, assuming constant boundary condition coming from the results of the previous timestep ($G(Y^{j-1}) = X_0^j$). In this way, the semi-implicit effect on the boundary conditions is provided to CFX from the very first iteration. The convergence check is performed on the CFX boundary conditions received from RELAP5. This means that the tolerance level can be achieved even after the first internal iteration of the CFD solver, following the new RELAP5 run (if $|X_1^j - X_0^j| < tol$). In theory, this could allow the code to operate with just one CFD internal iteration, with the purpose of reducing as much as possible the computational time required by CFX.

In the tool, a user-defined underrelaxation factor w is implemented to smooth the variation of the CFX boundary conditions at the next internal iteration within the current timestep in the following way:

$$X_i^j = X_{i-1}^j + w\left[G\left(Y_i^j\right) - X_{i-1}^j\right] \quad (2)$$

where i is the internal iteration counter. The underrelaxation factor should be in the range 0 to 1 to dump potential oscillations of the solution. The default setting for w is 1, meaning that the updated boundary condition is not affected by the previous iteration.

The routines are divided in one User CEL Function and five JBRs. The following summarizes the functions of the JBRs:

- *jbr_userinput*: performs the same initialization tasks as in the explicit scheme;
- *jbr_userinput_sott*: executed at the beginning of each timestep, this routine retrieves the previous timestep's CFX results from memory, defines the coupling timestep, saves the *.rst* file from the previous run as *old.rst*, and starts the R5 code with boundary conditions coming from the previous timestep. The R5 results are processed, and the semi-implicit CFX boundary conditions are obtained;
- *jbr_userinput_socl*: called at the start of each coefficient loop, i.e., CFX internal iterations, except the first loop, this routine reads the R5 results from the previous coefficient loop and stores them in memory for CFX;
- *jbr_endofthecoefficientloop*: executed at the end of each coefficient loop, this routine deletes the last R5 results from the current time step, restarts the simulation from the *old.rst* file with updated semi-implicit boundary conditions, processes the R5 results, and compares the new CFX boundary conditions with the previous ones to check for convergence. If convergence is reached for all boundary conditions or the maximum number of internal iterations is reached, the simulation proceeds to the end of the time step; otherwise, another iteration begins;
- *jbr_endofthetimestep*: called at the end of the each timestep, this routine saves the final information, appends the last result to the *.plt* file, and reduces the size of the *.rst* file to avoid working with large files.

The semi-implicit coupled timestep is schematically shown in Figure 3.5.

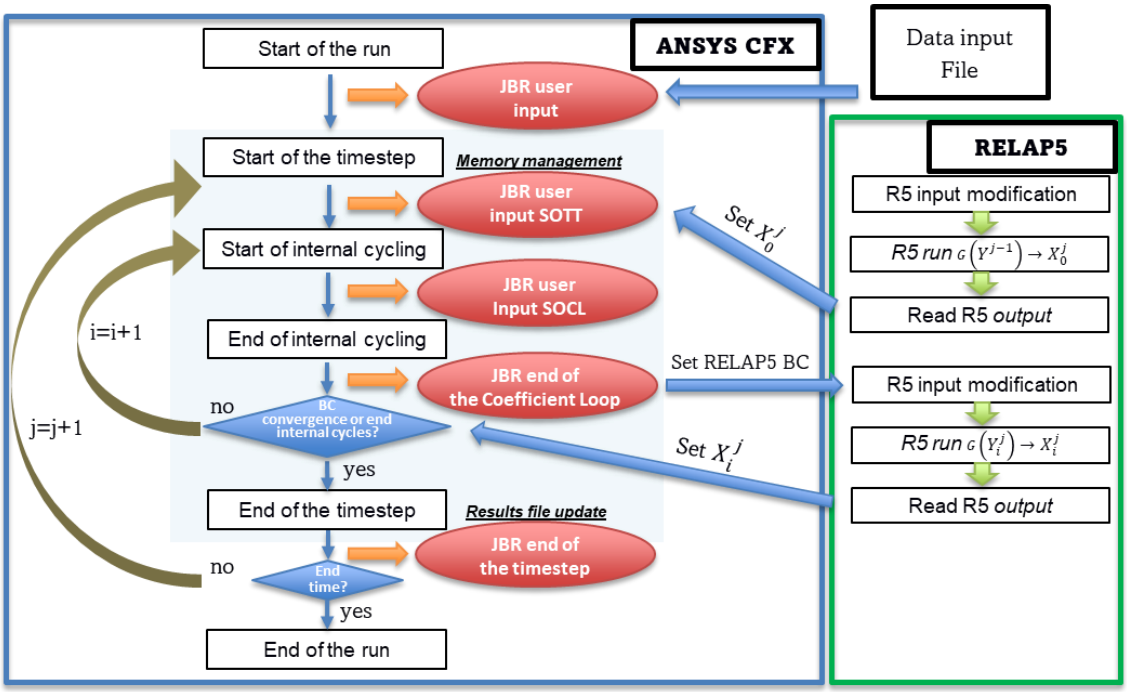


Figure 3.5 – Coupling methodology between Ansys CFX and RELAP5 in the semi-implicit scheme [52].

3.3 Spatial discretization approach

The discretization of the simulation domain in space could be realized following two approaches: the domain decomposition and overlapping. Both of them are available within the Ansys CFX – RELAP5 Mod3.3 coupled tool.

The domain decomposition approach is easier to be implemented since it consists of the direct exchange of the boundary conditions values, avoiding any manipulation of the quantities. With this approach, the primary objective of its development is to establish and maintain consistency between the information exchanged. Good correspondence on the section(s) at which the values are evaluated, and verification of the conservation of mass, momentum and energy are fundamental requirements (Figure 3.6a).

In the overlapping domain approach, the conservation of the variables is ensured by the STH code. The complexity in the approach is introduced by the information exchange method: the coupling is made by adjusting of some STH parameters in order to match the CFD results (Figure 3.6b). In this thesis, two

different overlapping approaches are presented, highlighting the differences between the two.

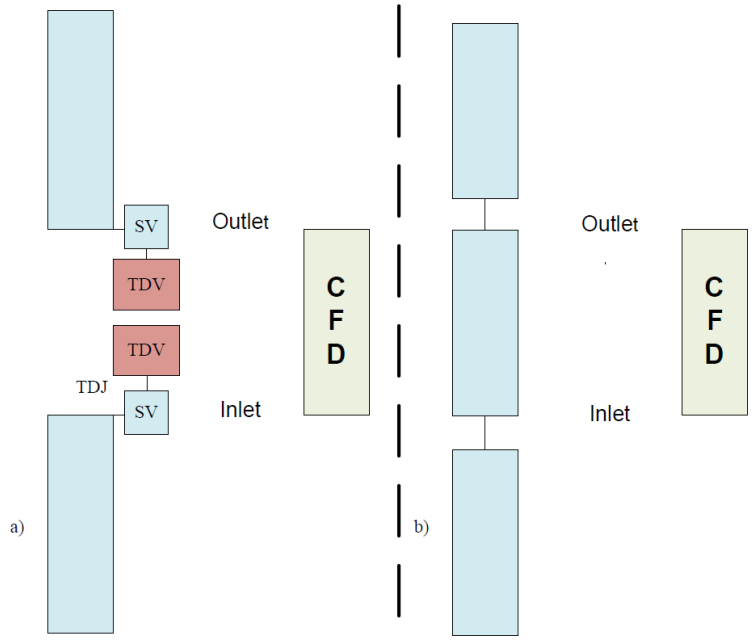


Figure 3.6 – RELAP5 Mod3.3 schematization of the nodalization in the domain decomposition (a) and overlapping (b) approach [52].

3.3.1 Decomposition domain

To implement the domain decomposition approach in the Ansys CFX – RELAP5 Mod3.3 coupled tool, the CFX domain should be carefully defined. *Opening* boundary conditions are generally more flexible, allowing for the consideration of reverse flow phenomena at both the CFD inlet and outlet. At one of the boundaries, a uniform constant velocity (or mass flow rate) can be imposed if pressure losses due to flow development are negligible. Otherwise, a non-dimensional map, assumed constant throughout the simulation, can be used. With the latter approach, it is crucial to verify that the mass flow rate calculated from the STH velocity and the velocity map align with the desired value. At the other boundary, relative pressure is set to zero. Within the CFD domain, both inlet and outlet temperatures can be specified as uniform or using non-dimensional maps.

The STH code receives from the CFD code velocity, fluid temperatures, and other thermal boundaries like heat flux or wall surface temperature, if required for the specific application.

Challenges associated with STH boundary conditions arise from the characteristic of R5 to store pressure and temperature at the centre of elemental volumes that constitute the domain, and not at the volume boundaries. This is particularly significant for vertical domains, especially with HLM, due to importance of gravitational term with respect to the overall pressure variation. A recommended approach involves positioning the information exchange surface at the boundary of an R5 volume and connecting it to a relatively small horizontal volume (Figure 3.6a). In R5, the friction pressure drop can be reduced to zero using a code flag, ensuring that the pressure calculated in the horizontal volume accurately represents the boundary surface pressure. Temperature is also obtained from the horizontal volume, albeit with a slight time delay due to the time required to traverse the horizontal volume. However, this delay is minimal due to the small axial dimension of the fluid volume.

R5 boundary conditions are imposed using two time-dependent volumes connected to the two small horizontal volumes. In a vertical domain with the outlet higher than the inlet, pressures are defined as follows:

$$\begin{aligned} p_{in}^{k} &= p_{out}^{k-1} + \Delta p_{CFX}^{k} \\ p_{out}^{k} &= p_{in}^{k-1} - \Delta p_{CFX}^{k} \end{aligned} \tag{3}$$

where p is the static pressure and the index $k-1$ corresponds to the last RELAP5 run (that corresponds to the previous timestep *j-1* in an explicit scheme or the one of the last internal iteration *i-1* for the semi-implicit approach). The Δp_{CFX} takes in account the gravitational forces as follow:

$$\Delta p_{CFX} = Relative\ Pressure_{in} - Relative\ Pressure_{out} + rho_{ref}\ g\ h \tag{4}$$

The temperatures imposed in the time dependent volume are the mass flow averaged temperatures on the corresponding CFX surfaces. The CFX mass flow rate or velocity is imposed through a time dependent junction connected to one of the time dependent volumes.

3.3.2 Overlapping domain

For the overlapping domain approach, CFX boundary conditions remain the same as described in section 3.3.1 for the decomposition domain approach, as the requirements are consistent across both cases.

Regarding R5 boundary conditions, the domain is closed, and feedback from the CFD code is achieved by adjusting model parameters rather than directly transferring variable values. While the conceptual approach is similar for all CFD-STH couplings, the practical implementation depends on the available parameters in the STH code.

To align R5 pressure drops with those from CFX, two primary solutions are possible: adjusting the friction factor in volumes or modifying local pressure loss coefficients in junctions. These modifications can be applied across the entire corresponding CFD domain or concentrated in one or more junctions or volumes.

The following solution is proposed:

- condense all the overlapped domain in a single volume (Main Volume) with the same height and volume of the fluid CFD domain;
- interpose between both the extremities of the Main Volume and the rest of the system two small horizontal volumes, in which the flag for avoiding pressure losses due to friction is active. It is important to preserve the domain boundary flow area in the components connecting the Main Volume to system;
- connect to the Main Volume and the two horizontal domain a heat structure each.

With this procedure, the user can choose to modify either the pressure loss coefficient at a single junction (upstream and or downstream to the Main Volume) or the friction factor of the Main Volume equivalent to the CFD domain. If the junction pressure loss coefficient is selected, also in the Main Volume the flag to avoid the calculation of friction pressure losses should be activated. If the friction factor method is selected, all the junction pressure loss coefficients should be set to zero. In this way, the equivalence between pressure drops in the STH and CFD models is handled by a single parameter.

The CFD code takes into account also the conduction in the fluid, the three-dimensionality of the heat exchange, including of the heat losses, and the axial conduction in the solids: for these reasons, it could be assumed that the CFD boundaries temperature are more accurate. The horizontal volumes are adopted to impose the temperatures computed at the boundaries of the CFD domain in the STH code. This is done by means of the fictitious heat structures. The heat structures should have large conductivity and small heat capacity in order to minimize the

temperature gradient and the time delay of the heat transfer to the fluid due to the conduction inside the solid. Moreover, imposing a very high convective heat transfer coefficient with the wall, the temperature imposed on the external surface of the heat structure corresponds to the one in the connected fluid volume.

The same typology of fictitious heat structure is also used to match the temperature in the single volume, with the average temperature in the CFD domain. Passing from a 3D volume to the STH 1D approximation, the most appropriate density value would be the integral along the flow direction in the domain. However, in the CFX code, this operation is not implemented, thus the volume averaged is considered a good approximation and selected because of its simplicity.

In this thesis two overlapping approaches are considered:

- the Continuous Update (CU) method;
- the CAlculation (CA) method.

The CU method consist in the continuous adjustment of a junction local pressure drop coefficient (K) to follow the variation of the CFD pressure drops. It is based on the following formulation:

$$K^k = K^{k-1} + s \cdot \frac{\left(\Delta p_{CFX}^{k-1} - \Delta p_{RELAP5}^{k-1}\right) + \left(\Delta p_{CFX}^{k-2} - \Delta p_{RELAP5}^{k-2}\right)}{2} \cdot \Delta t \cdot sign(v_{inlet}) \qquad (5)$$

The terms involved in the correlation are the following:

- a multiplication user-defined scaling factor (*s*) to give the possibility to relax the *K* variation: higher values of scaling factor tend to speed up the convergence of the two pressure drop values. However, if a too large value is selected, it could determine an unstable solution (oscillatory or divergent). This value is not known a priori, and the user should select it by practice and experience;
- the dimension of the timestep (*Δt*), because at lower timestep, sudden changes of the local pressure drop coefficient are not expected to occur;
- the *Δp* values evaluated at the last and second last step (indicted by the superscript *k*) and *K* values evaluated at the last step, where step indicate:
    - timesteps, in the explicit scheme;
    - or CFX internal iterations if the semi-implicit scheme is adopted;

- the sign of the area averaged velocity on the inlet section($sign(v_{inlet})$), since the relative pressure drops in the domain should invert its sign if reversed flow condition occurs. In this way, the local pressure drops coefficient increases its value if RELAP5 has underestimated the pressure variation in the previous timesteps, and vice versa.

It could be noticed that the formulation does not directly depend on the velocity or the mass flow rate inside the CFD domain, apart for its direction. The *K* value evaluated at the last value is modified accordingly to the discrepancies between the results obtained in the CFD and STH domain.

In general, this formulation is simple to be implemented since it requires only to read and store CFD quantities of previous timesteps or iterations. On the other hand, two main disadvantages could be noticed:

- fast variations of *K* are limited by the user-defined factor and by the formulation itself;
- the user-defined scaling factor is problem dependent and need to be selected for each application.

For all the cases in which the variation of the junction pressure loss coefficient *K)* associated to the pressure drops in the system is expected to be limited, the CU method could be a valuable option.

The CA method is developed based on the solution adopted by Huxford et al. in [54] but applied to Ansys CFX and RELAP5 Mod3.3 codes. It is based on the calculation, at each timestep of the friction factor of the Main Volume representing the overlapped domain (f_{RELAP5}).

The correlation between the f_{RELAP5} and Δp_{CFX} comes from the momentum conservation equation of the two codes:

RELAP5 Mod3.3
$$\rho\frac{\partial U}{\partial t}+\frac{1}{2}\rho\frac{\partial U^2}{\partial x}=-\frac{\partial p}{\partial x}-\frac{1}{2}\frac{f_{RELAP5}}{D_h}\rho U|U| - \rho g \tag{6}$$

Ansys CFX
$$\rho\frac{\partial \boldsymbol{U}}{\partial t}+\rho\boldsymbol{U}\cdot\nabla\boldsymbol{U}=-\nabla p+\nabla\cdot\boldsymbol{\tau}-\rho\boldsymbol{g} \tag{7}$$

In order to match the pressure gradients in equation 6 and 7, the friction term of the R5 formulation should be directly correlated with the pressure gradient correcting for the other terms, from left to right: local acceleration, convective acceleration and gravitational terms.

Especially with an explicit coupling scheme, it is not straightforward to correct for the local acceleration term in the STH code, since this term results from velocity updates at each time step. However, since the application of the tool regards incompressible flow, it is reasonable to assume that the difference between the local acceleration as computed by CFX and R5 for the overlapped domain is negligible as long as fluid velocities are consistent. Therefore, only the convective acceleration and gravitational terms need to be corrected [46].

Since the overall CFD pressure drop must be matched by the RELAP5 calculation, the sum of the pressure gradient and the local acceleration is substituted in equation 6, and the R5 friction factor could be computed as:

$$f_{RELAP5} = \frac{2D_h}{\rho U|U|}\left(\left[-\frac{1}{V}\int_V \left(\nabla p + \rho\frac{\partial \boldsymbol{U}}{\partial t}\right)\cdot \hat{n}\, dV\right]_{CFX} - \frac{\rho}{2}\frac{\partial U^2}{\partial x} - \rho g\right) \qquad (8)$$

The scalar product between the CFD terms ("3D" terms) and the versor $\hat{n}$ parallel to the flow direction is performed to convert them in "1D" elements, making them consistent with the RELAP5 1D formulation of the momentum equation. Therefore, only the projection of such vectors along the RELAP5 flow path is considered. The CFD informed term ($[\dots]_{CFD}$) is evaluated explicitly in the following way:

- $\frac{1}{V}\int_V(\nabla p\cdot\hat{n})dV = \Delta p_{CFX}/L = (p_{outlet} - p_{inlet})/L$. It is the pressure difference across the boundaries divided by their distance, i.e., their difference in absolute height;
- $\frac{1}{V}\int_V\left(\rho\frac{\partial \boldsymbol{U}}{\partial t}\cdot\hat{n}\right)dV = \frac{1}{V}\int_V\rho\frac{\partial U_x}{\partial t}dV$. It is the volume average of the time derivative of the velocity along to the flow direction.

From the formulation presented in equation 8, accurately computing all the terms within the parentheses is crucial. In the current version of RELAP5 Mod3.3, it is not possible to internally set the friction factor using control variables or equations. Future developments in this capability could enhance the accessibility of the CA method.

When the velocities approach zero, thus when there is a stagnant flow or a flow inversion, this approach could lead to numerical inaccuracy. The presence of the square of the velocity in the friction factor definition, the importance of gravity term with respect to the other terms (especially true with HLMs) and the approximation of the average density in the CFD domain are possible sources of discrepancies between pressure drop computed from the CFD model and the one obtained in the

STH domain. The CA method could be difficult to implement if "closed" codes are coupled, in which the accessibility and malleability of the codes are limited.

In Table 3.1, the main characteristics of the CU and CA methods are summarized. In general, the CA method could be considered a more accurate and advanced method, however, in cases where the velocity is foreseen to approach the zero, or cases in which the coupled code's structure hinders the possibility to accurately compute the momentum source terms, the CU method could be a valuable alternative.

Table 3.1: Characteristics of the Continuous Update and CAlculation overlapping methods.

CU method	**CA method**
• Continuous update of junction pressure loss coefficient • Based on a user-defined *s* factor that is case dependent • Capability to follow fast variation of the pressure loss coefficient could be limited	• Continuous calculation of the friction factor • Possible instabilities when the velocity goes to 0 (stagnant flow or flow inversion) • Need to compute accurately the momentum source terms in both the codes

Chapter 4

4 Verification and validation of the tool

In this chapter, the numerical activities for the verification and validation of the Ansys CFX - RELAP5 Mod3.3 coupled tool are presented. The chapter is divided in three main subsections that collect different applications with an increasing level of complexity and representativeness of the LFR geometry.

In section 4.1, the first test case is reported. An isothermal single pipe is modelled with CFX and R5 standalone models and the results compared with coupled simulation testing, testing all the approaches described in Chapter 3. This simple application is purposely selected to concentrate the analysis on the verification of the coupling strategy.

In section 4.2, the tool is validated against experimental data from loop-type facilities. The first two cases focus on the NACIE facility and its upgraded version, NACIE-UP, which have been widely used over the past two decades for testing components and relevant phenomena at the ENEA Brasimone research centre. The third application aims to validate the tool against experiments conducted on the TALL-3D facility, a loop-type facility located at the Royal Institute of Technology in Stockholm (Sweden). TALL-3D was designed for coupled and standalone code calibration, benchmarking, and validation. The lessons learned from applying the tool to loop-type facilities are summarized at the end of the section.

Finally, in Section 4.3, the coupled tool is applied to the pool-type ATHENA facility, which is described in detail. The tool has been tested with various discretisation of the entire system between the CFD and STH domains, involving different components and conditions. This final section represents the closest application to the tool's ultimate purpose: analysis of LFR systems to inform design and assess safety performance.

4.1 Isothermal pipe

To verify the consistency of the coupling tool, a first test case with simple geometry and boundary conditions has been identified and simulated: an adiabatic, 20 mm diameter horizontal pipe filled with liquid lead at 400°C, is simulated imposing a mass flow variation over time (Figure 4.1) to verify the capability of the code to reproduce a basic transient [52].

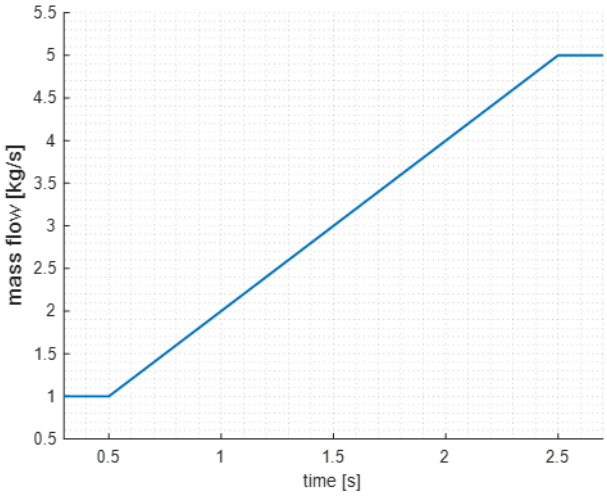


Figure 4.1 – Mass flow boundary condition for the test case transient [52].

For the test, four models represented in Figure 4.2 are setup: the RELAP5 standalone model (a), the CFX standalone model (b), the coupled models with the domain decomposition (c) and overlapping (d) approaches. For both the spatial discretization approaches, the explicit and semi-implicit time advancing schemes are considered as previously described. For what concern the overlapping approach both the CU and CA method are tested. The CFD domain simulated in the coupled simulations is half of the length of the entire pipe and it corresponds to the central part of the pipe.

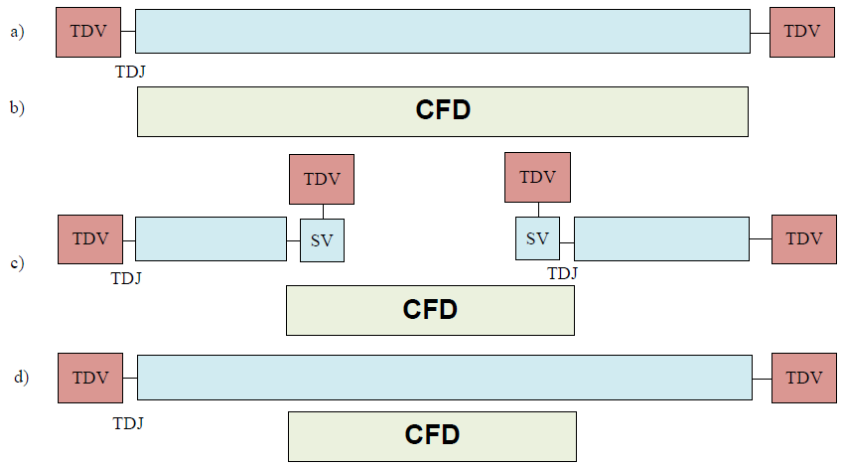


Figure 4.2 – Pipe test model: a) RELAP5 Mod3.3 standalone, b) Ansys CFX standalone, c) domain decomposition coupling, d) overlapping domain approach [52].

A similar configuration is chosen for the CFD domains in both the standalone and coupled cases. The mesh consists of 632 K cells for the standalone case and 319 K cells for the coupled simulations, and it is generated using the same meshing parameters on the face, extruded in the axial direction. The properties of lead are sourced from the liquid metals' handbook [55]. The SST k-ω turbulence model [56] is applied, along with the High Resolution CFX advection scheme and the Second Order Backward Euler Transient Scheme.

A fully developed flow profile is imposed at the inlet section in both the standalone and coupled CFD domains. This profile is described by three maps: velocity, turbulent kinetic energy (k), and specific dissipation rate (ω). These maps are derived from two separate steady-state CFD simulations representing the highest and lowest expected mass flow rates. The imposed maps are averages of these two cases, weighted according to the mass flow rate at the current time.

The timestep for both standalone and coupled simulations is 5×10^{-3} seconds, with a ratio of 5 set between the CFD and STH timesteps in the coupled simulation. The scaling factor (s), required for the overlapping CU approach for updating the K value is set to 5×10^{-3} and 2.5×10^{-2} (refer to equation 5) for the explicit and semi-implicit cases, respectively.

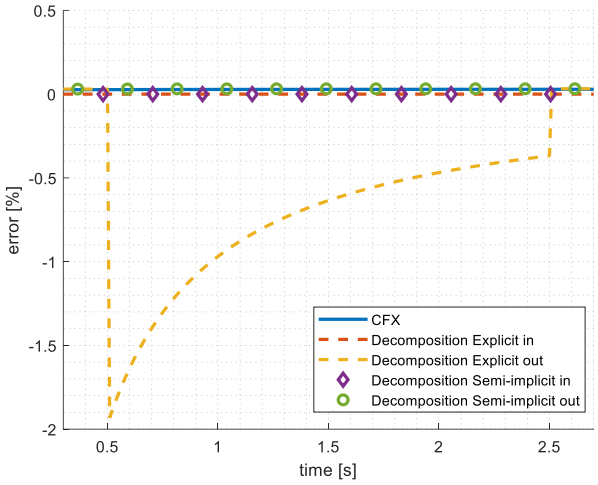


Figure 4.3 – Difference between the theoretical and the numerical mass flow rate in the Ansys CFX standalone and decomposition model.

Figure 4.3 illustrates the relative error of the mass flow rate compared to the theoretical value, i.e., the boundary condition shown in Figure 4.1 for the CFX and decomposition approach coupled model. The reported values from the decomposition approach coupled model are taken from the R5 domain at the segments upstream (in) and downstream (out) of the domain simulated in CFX. The results show that applying the velocity map at the inlet section in CFX introduces a small error in the mass flow rate, around 0.03%. This error is likely due to the interpolation scheme and is observed in the standalone simulation and downstream of the CFX domain when using the decomposition domain approach with the semi-implicit advection scheme. The decomposition method with an explicit scheme, however, shows a maximum error of just under 2% in the outlet mass flow rate at the start of the transient, caused by the time advancement method. Despite this, the tool is considered capable of tracking boundary condition variations with the selected timestep. The domain overlapping approach introduces no error in mass conservation and, therefore, is not shown in the plot.

The pressure variation in the pipe during the transient is reported for the decomposition and overlapping domain in Figure 4.4 and Figure 4.5 respectively. A zoomed-in view of the beginning and end of the transient is shown in Figure 4.6/Figure 4.7 and Figure 4.8/Figure 4.9.

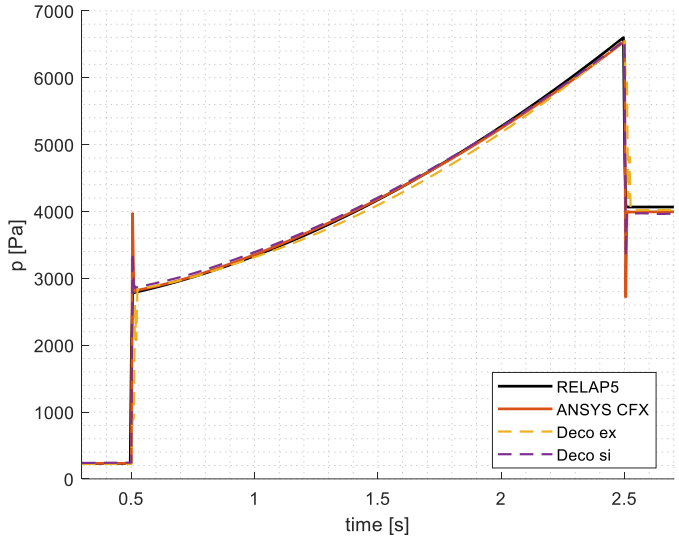


Figure 4.4 – Pipe pressure drops variation in time with the standalone and the decomposition models (entire transient).

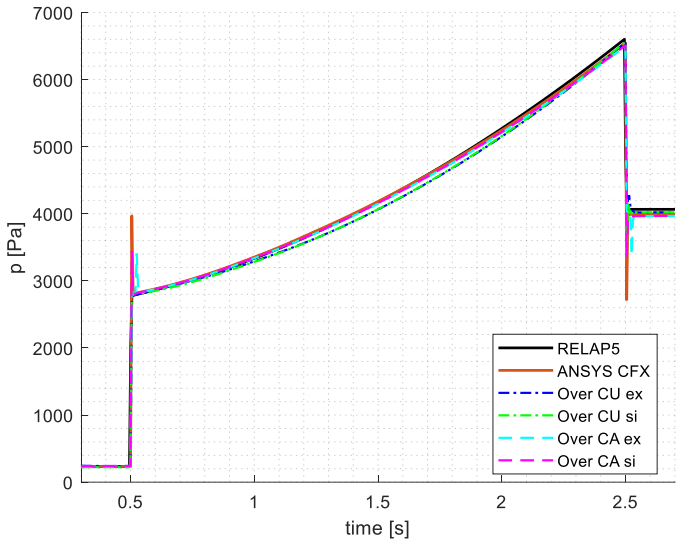


Figure 4.5 – Pipe pressure drops variation in time with the standalone and the overlapping models (entire transient).

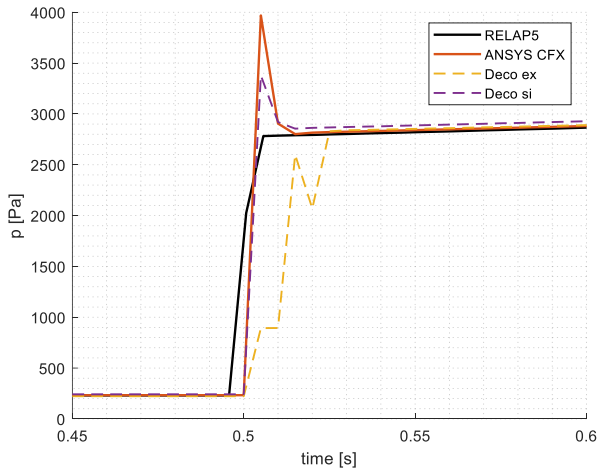


Figure 4.6 – Pipe pressure drops variation in time with the standalone and the decomposition models (start of the transient).

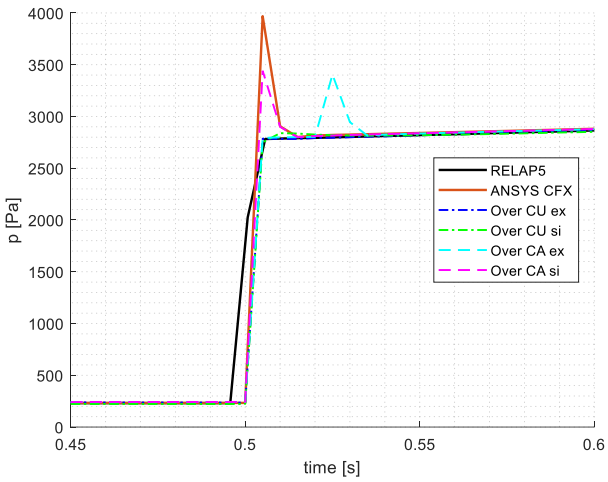


Figure 4.7 – Pipe pressure drops variation in time with the standalone and the overlapping models (start of the transient).

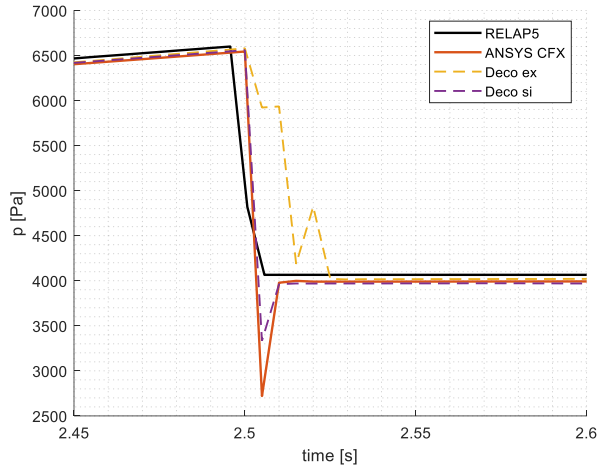


Figure 4.8 – Pipe pressure drops variation in time with the standalone and the decomposition models (end of the transient).

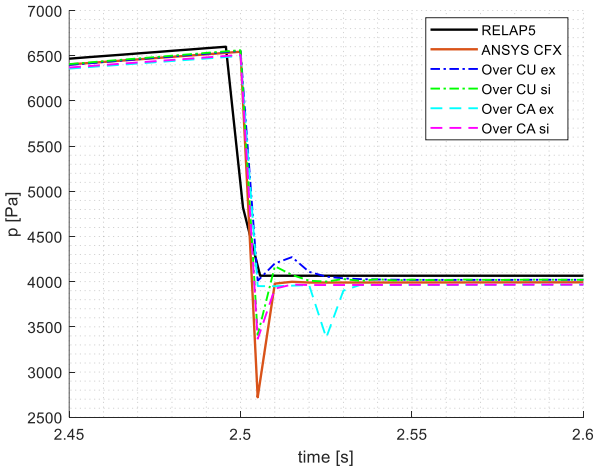


Figure 4.9 – Pipe pressure drops variation in time with the standalone and the overlapping models (end of the transient).

The obtained results are in very good agreement for all the models considered. The coupled approaches lay almost for the entire transient between the two standalone curves and the discrepancies between the simulations are negligible. The coupling tool is able to exchange the pressure information including both the static and dynamic contributions.

From the focus on the beginning and end of the mass flow transition, it could be noticed that:

- with the CFX standalone model the discontinuity of the mass flow derivative determines a spike in the pressure drops;
- the spike is visible also for the coupled decomposition and overlapping CA approaches that adopt a semi-implicit time advancing scheme. In the explicit overlapping CA approach, the spike is shifted in time;
- in general, the cases with an explicit scheme present some oscillations, which could be caused by the time delay in the imposed boundary conditions, which is intrinsic of the adopted numerical scheme.

Table 4.1: Total simulation time and time spent on the FORTRAN subroutine for the different spatial discretization approached and time advancing schemes.

Model	Time in FORTRAN	Tot simulation time
RELAP5 Mod3.3	/	1.3 s
Ansys CFX	/	7 h 13 min 12 s
Decomposition Explicit	9 min 42 s	3 h 46 min 9 s
Decomposition Semi-implicit	42 min 3 s	4 h 15 min 13 s
Overlapping CU Explicit	11 min 38 s	3 h 46 min 47 s
Overlapping CU Semi-implicit	41 min 14 s	4 h 12 min 47 s
Overlapping CA Explicit	10 min 44 s	3 h 39 min 35 s
Overlapping CA Semi-implicit	40 min 54 s	4 h 17 min 39 s

The simulation time obtained running the cases with 2 CPU is reported in Table 4.1, together with the time spent in the FORTRAN subroutine in the coupled simulation.

The time-saving benefit of the coupled approach relative to the standalone Ansys CFX run for this specific case is limited due to the nature of the problem analysed. However, the time saving is approximately proportional to the ratio between the CFD volume and the total domain volume, which is 2. As shown in

Table 4.1, it can be noticed that the explicit scheme spends around 4 times less time in executing the coupling methodology. The longer simulation time required by the semi-implicit schemes is due to the need for multiple iterations per timestep, where information is exchanged during internal iterations.

This case emphasizes the faster execution speed of the explicit scheme and the superior ability of the overlapping approach to maintain conservation of quantities within the system. While the semi-implicit scheme improves the tool's robustness, it comes at the cost of slower computation for a given timestep.

It is important to assess the pros and cons of all the proposed methods in more realistic scenarios. This analysis is reported in chapter 4.2.3.

4.2 Validation against loop type facility

Loop type facilities are largely adopted within LFR R&D programs for separate effect experimental studies. The versatility of this kind of facilities comes from the possibility to substitute a single test section or component with minimum modification of the overall layout. The TH studies carried out on loop facilities includes fundamental investigation on the heat transfer inside components like FAs, often at reduced scale (smaller number of pins, same pin geometries), or SGs. The experiments also encompass the analysis of accidental conditions like FA flow blockage, pin deformation, together with devoted component vibration induced tests. Furthermore, the loop facilities could include ad-hoc sections for assessing specific phenomena (e.g. lead freezing) or to increase the technological readiness of the coolant chemistry control and purification systems.

Even if the component level is usually the most relevant scale analysed within a loop facility experimental campaign, the mono-dimensionality of the flow path gives the possibility to easily design forced to natural convection experiments. The main parameters in play are the power, the pressure losses in the system and the relative height between the barycentres of the heat source and the heat sink. This type of transients is used to study the behaviour of components exposed to lead flows, ranging from velocities typical of normal operations to those seen during incidental events, involving pump shutdown.

The system-level behaviour of a loop-type facility provides essential experimental data for validating STH codes, along with correlations to accurately

characterize the heat exchange and pressure losses in the reactor components. A coupled CFD–STH tool, when applied to a loop-type facility, needs to perform similarly to the standalone STH code, while offering detailed insights into the domain simulated by the CFD code. If the thermal-hydraulic phenomena occurring within that domain provide significant feedback to the system that STH codes cannot reproduce, in such cases, the coupled approach could prove to be more reliable and effective.

In chapter 4.2, the coupled tool is validated comparing the simulation results with experimental data coming from three different campaign. The level of complexity of the loop gradually increases. Although CFD is not the primary focus, the subsequent discussion includes a detailed analysis of CFD simulations, with comparisons to experimental local temperature measurements.

At the end of the section, the lessons learned while carrying out the analysis of the loop type facilities are collected.

4.2.1 NACIE

The second test case deals with the onset of natural circulation in the NACIE facility. NACIE was an LBE-cooled loop located at the ENEA Brasimone Research Centre realized to accomplish different goals, among which the study of the circulation enhancement by means of gas injection in the hot leg and the study of the transition from forced to natural circulation [57]. The main components of the loop are the Heat eXchanger (HX) and the electrical Heating Structure (HS), the latter comprising two pins, whose geometrical properties and nominal power are shonw in Table 4.2.



Figure 4.8 – Isometric view of NACIE primary loop.

Table 4.2: NACIE Heat Source geometrical and operational parameters.

N° of active pins	2
Outer diameter	8.2 mm
Total length	1400 mm
Active length	890 mm
Heat flux	100 W/cm^2
Thermal power	21.5 kW

The primary LBE side is coupled to the water secondary side by means of "tube in tube" counter flow type HX essentially made of three coaxial tubes and fed by water at low pressure (about 1.5 bar). The loop is insulated with 70 mm of rock wool. The heat losses has not been considered in the calculation since considered beyond the scope of the application and the impact could be considered overall negligible for the investigated phenomena and relatively constant during the transient.

The transient under consideration represents the initiation of natural circulation from static conditions, driven by buoyancy forces resulting from the heat supplied and removed by the HS and HX, respectively, with a power of 21.5 kW. The height difference between the thermal barycenter of the heat source and the sink is approximately 5.7 meters. The power of both components is increased linearly over time by adjusting the electric power input and the secondary water flow rate, reaching the nominal value within 262 seconds. A detailed description of the test, referred to as "Test 301," and the facility can be found in [58].

The transient simulation is carried out using both the R5 standalone code and the coupled tool, with the results compared against experimental data. The system nodalization is identical for both cases and includes three fluids: LBE in the loop, water on the secondary side of the HX, and argon in the cover gas of the expansion vessel. The only distinction is in the modelling of the active length of the heat source HS, which in the coupled simulations is handled by the CFD code. For this transient, an explicit numerical scheme is chosen, and both the domain decomposition and overlapping approaches were tested, for the latter the CU method is implemented. In the HS, the fluid region is simulated along with the stainless steel solid components, which include the external 2 ½" sch. 40 tube, the pin cladding, and the support rod, modelled as solid. A spacer grid is located within the active length near the outlet, modelled as a porous region with a local pressure loss coefficient of 0.5.

Figure 4.10 shows the RELAP5 standalone nodalization, while Figure 4.11 reports the CFD domain, meshed with 805 K cells, which replaces components 101 and 103 in the coupled simulation. The CFX simulation setup is similar to the one described in the first test case excepts for the fact that uniform velocity at the inlet section is adopted. The power is imposed as a uniform heat flux on the pin cladding internal surfaces and symmetric conditions are exploited simulating only half of the domain. The CFD code receives temperature and mass flow rate. The STH code receives pressure, temperature and mass flow rate in the decomposition case (section 3.3.1), while temperature, power and local pressure drop coefficient in the overlapping case (section 3.3.2).

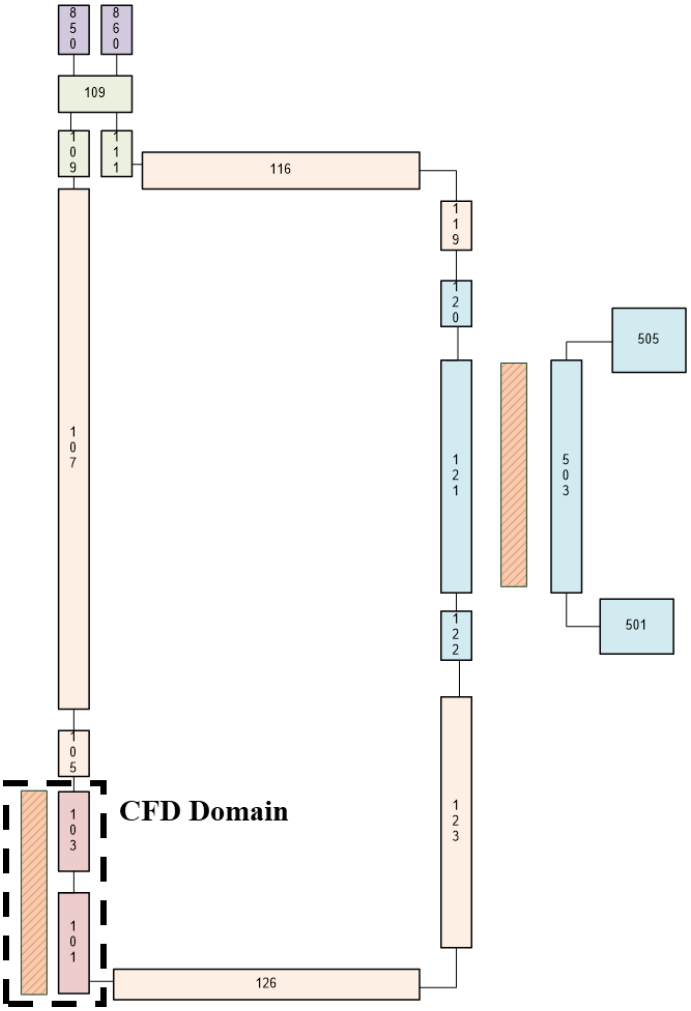


Figure 4.10 – Loop nodalization of the RELAP5 model of the NACIE loop, highlighting the components substituted by the Ansys CFX model in the coupled simulation [52].



Figure 4.11 – Mesh of the Ansys CFX model of the NACIE Heating Structure [52].

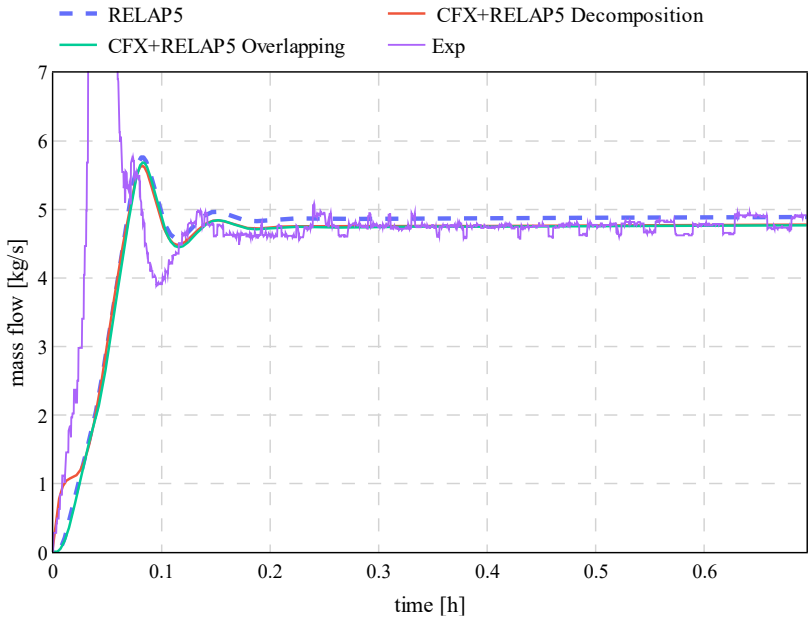


Figure 4.12 – Comparison of experimental vs modelled (RELAP5 standalone and coupled tool) flow rate in the NACIE loop [52].

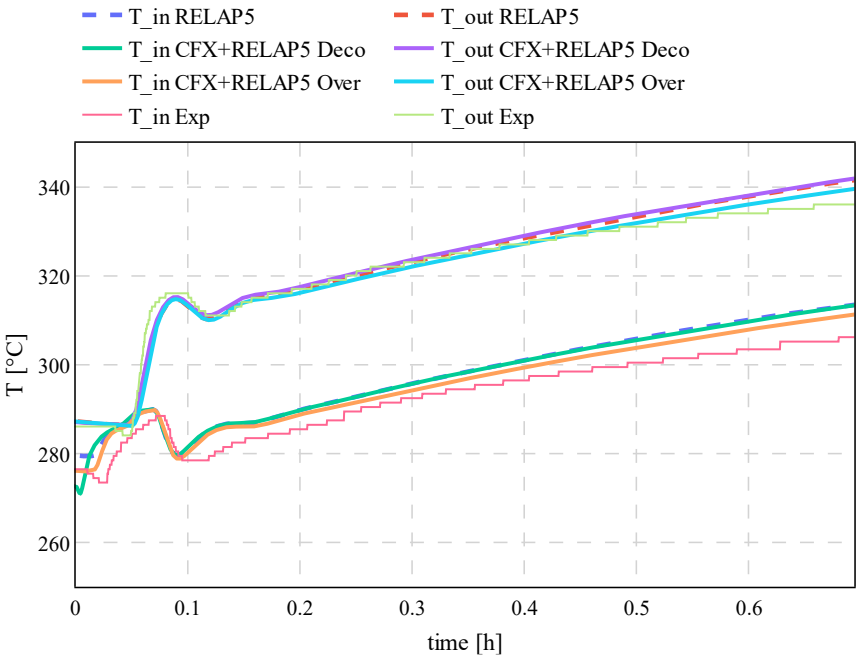


Figure 4.13 – Comparison of experimental vs modelled (RELAP5 standalone and coupled tool) inlet and outlet temperatures in the NACIE loop[52].

The simulation results show good agreement in reproducing the experimental results and limited differences could be noticed between the STH standalone calculation and the coupled one for both the mass flow rate (Figure 4.12 where the maximum divergence in steady state is around 5% of the mass flow) and the HS inlet temperature and outlet temperature (Figure 4.13 where the maximum difference is around 8°C toward the end of the transient at the inlet temperature). The discrepancies with experiment in Figure 4.12 at the start of the transient are closely related to the method used to measure the mass flow rate, which is calculated from a thermal balance in the HS. This method is not reliable during the initial phase of the test, when both the mass flow rate and power are low. Despite this, the temperature trends indicate that the TH simulation is able to accurately capture the early stages of the test.

As expected, the HS is accurately modelled by the one-dimensional RELAP5 simulation, which aligns well with the CFD results. While the coupled tool offers more detailed insights into the domain simulated with CFX, the STH code still successfully captures the overall behaviour of the component.

4.2.2 NACIE-UP (IAEA benchmark)

The second application to loop facilities aims to validate the developed coupling tool against experimental data from the NACIE-UP facility, the upgraded version of the NACIE facility studied in the previous section (4.2.1). Even in this case the CFD code is adopted to simulate the heat source of the facility and improve its representation.

Facility description

With respect to the NACIE facility, NACIE-UP has a new heat source represented by a Fuel Pin Bundle Simulator (FPBS), located at the bottom of the riser section, upstream of the gas lift (injection of argon in the riser to enhance the natural circulation) and the expansion vessel.

The FPBS, shown in Figure 4.14, is composed of 19 wire-spaced electrical rods, arranged in a triangular lattice with a pitch-to diameter ratio of about 1.28. The pin diameter is equal to 6.55 mm, while the wire diameter is 1.75 mm, and it is helicoidally twisted around the pin with a helical pitch of 262 mm. Each pin is 2000 mm long with an active length of 600 mm. In the “pre-active” length about ~8-10% of the overall power is provided to the fluid because of the combined effect of axial conduction along the pin and the joule effect, having this region a lower electric

resistance than the active one but still non null. The pins are kept in position by a grid downstream the FPBS. The bundle is contained in a hexagonal wrapper. Thermo-Couples (TCs) in the FPBS are located on Plane 1, Plane 2 and Plane 3, respectively at 38, 300 and 532 mm from the beginning of the active length. A selected pin, i.e., Pin 3, is equipped with more wall-embedded TCs, one every 43.7 mm after the Plane 1 [59]. The drawing is reported in Figure 4.14, where the active and the non-active length of the pins are highlighted, along with the instrumented planes position in the active region (left) and the numbering of pins and subchannels together with the TCs position in the measuring planes (right).

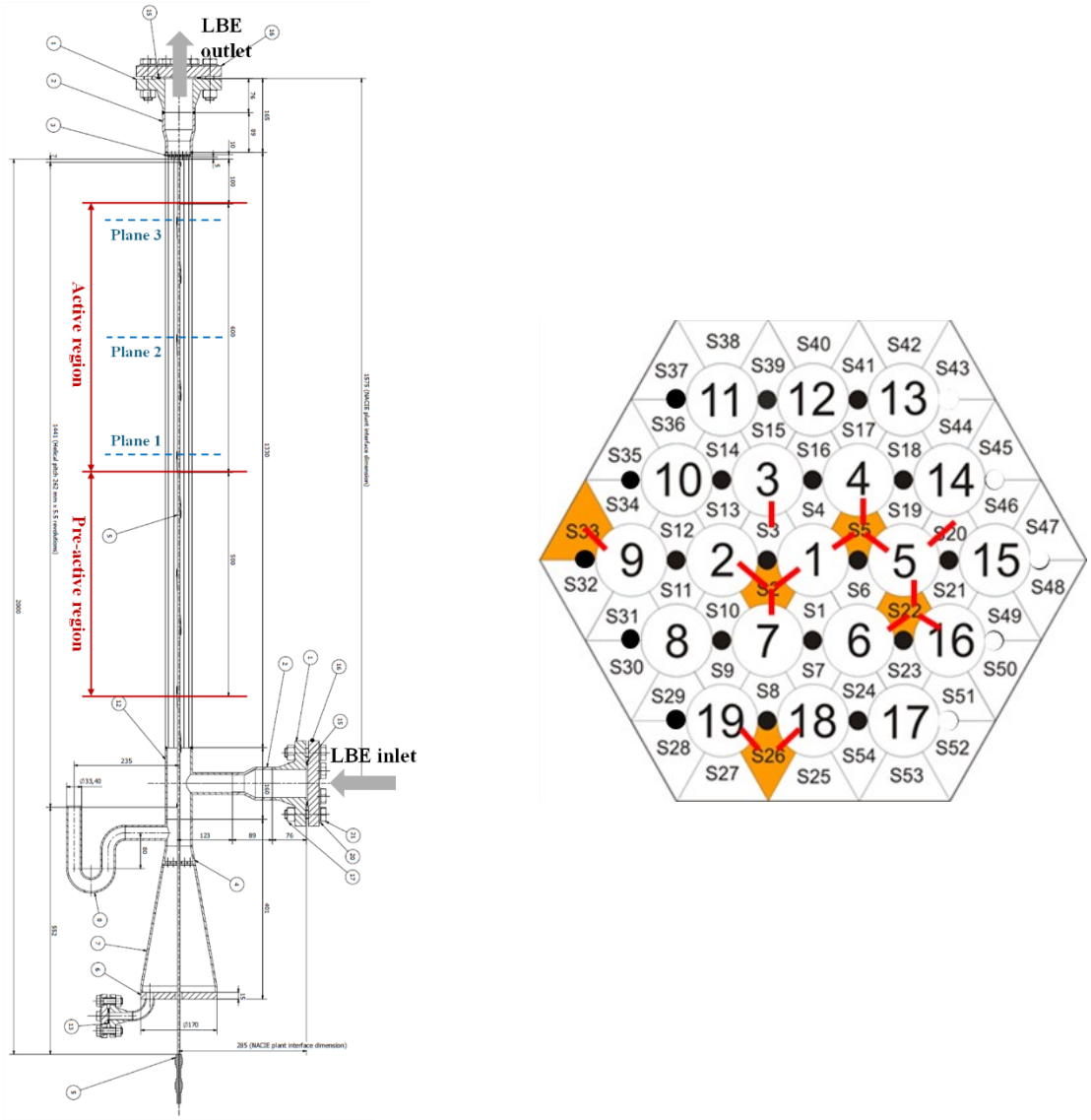


Figure 4.14 – NACIE-UP FPBS layout (left) and cross section of the measuring plane view (right) [59].

The new HX is a shell-and-tube heat exchanger with seven double-wall tubes: a gap filled with AISI 316L powder and pressurized air separates the LBE and the secondary water coolant. LBE flows through the tubes from top to bottom. The shell side has two sections: a low-power section (0-30 kW) with cross-flow and a high-power section (30-250 kW) with countercurrent flow. The secondary side is a closed water loop operating at 16 bars, including a pump, pressurizer, and air cooler. During the investigated experiments, only the high-power section was used.

The upgraded version of NACIE is heavily instrumented (Figure 4.15 and Figure 4.16), with TCs monitoring the temperatures of the loop and within the FPBS and the introduction of a prototypical Thermal mass Flow Meter (TFM) [60] for mass flow rate measuring. The latter has been developed by ENEA in collaboration with Thermocoax and it is based on the energy balance between the power delivered by the instrument to the fluid and the fluid temperature variation across the component.

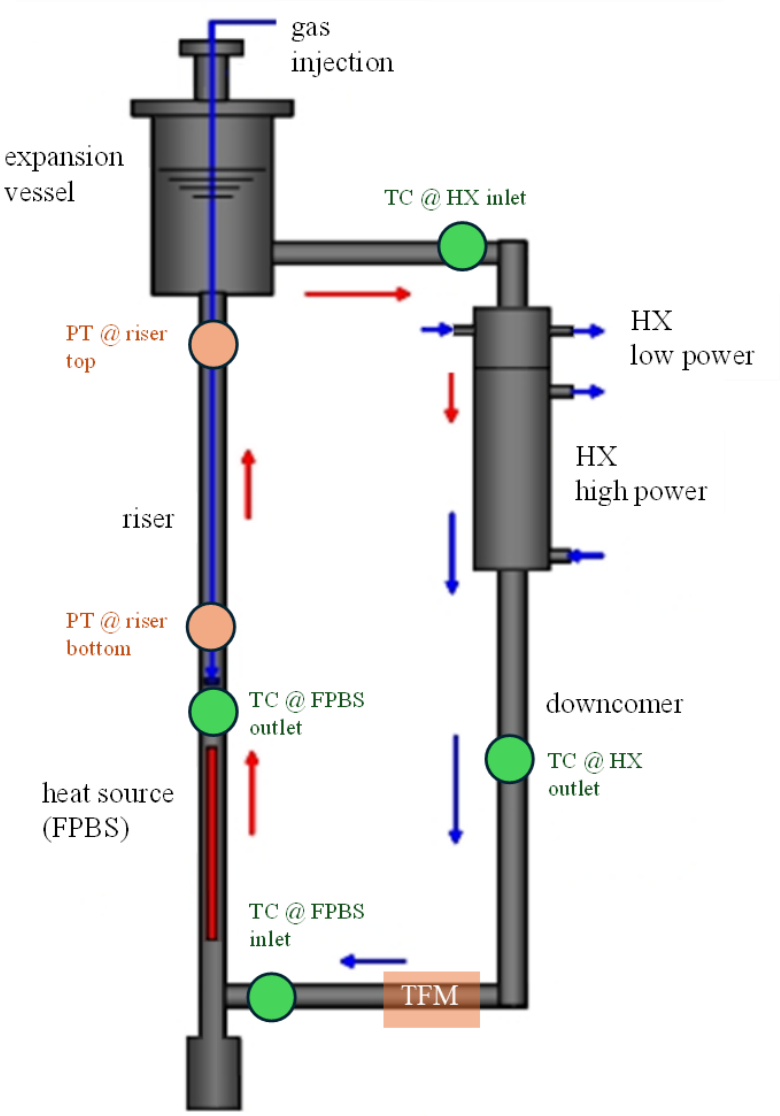


Figure 4.15 – Schematic drawing of the NACIE-UP primary loop [61].



Figure 4.16 – NACIE-UP primary loop.

Experimental setup

The numerical application presented consists of the post-test analysis of the experimental data released in the framework of the IAEA international Coordinated Research Project I31038, named “Benchmark on Transition from Forced to Natural Circulation Experiment with Heavy Liquid Metal Loop”.

The experimental tests, ADP06 and ADP10 [63], examined the transition from forced to natural circulation in a liquid metal loop. Initially, gas injection in the riser line enhanced fluid flow. When gas injection stopped, the LBE mass flow rate decreased due to the reduced driving force. While FPBS power remained constant, LBE temperature downstream of the FPBS and riser temperature gradually increased. Conversely, the cold leg temperature decreased due to the reduced mass flow.

For all the tests, in the initial steady state, the gas is injected at a constant flow rate of 10 Nl/min. Water in the secondary side is kept at 16 bar, with a constant temperature at the HX inlet of 170°C, and the volumetric flow rate is 10 m3/h. At t=0, the gas flow rate drops to zero in 1 s, while all the other parameters remain constant. After the transition, a new steady state condition is achieved, and it is kept for more than 30 minutes. A summary of the experimental conditions is reported in Table 4.3, where BOT and EOT refer to the steady state conditions at the Beginning Of the Transient and the End Of the Transient, respectively.

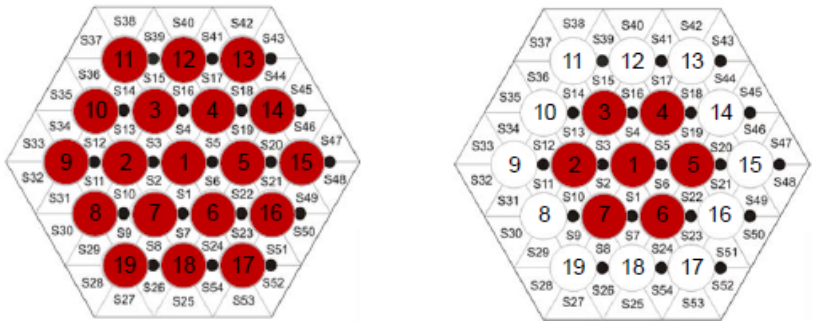
The experimental tests differ from each other in the number and location of the active pins (shown in Figure 4.17):

- in the ADP10 test all the 19 pins are switched on (the fuel assembly is uniformly heated). The total power is 30 kW and the average heat flux on the pins' surface is 127.9 kW/m^2;
- in the ADP06 test only the 7 central pins are switched on, but the total power is the same as the previous test. The average heat flux on the pins' surface is 347.1 kW/m2.

Temperature values are measured in several points of the loop by thermocouples that have an accuracy of ±1.5°C. The LBE mass flow rate is measured by the thermal flow meter whose uncertainty depends on the power provided by the heating element, the temperature at the instrument inlet, and the mass flow rate. The uncertainty can be evaluated by a formula presented in [60], that results in a maximum value of about 5% for the considered experiments.

Table 4.3: Experimental boundary conditions for ADP10 and ADP06 tests [59].

Parameter	**ADP10**		**ADP06**	
	BOT	**EOT**	**BOT**	**EOT**
$\dot{m}_{gas}$ [Nl/min]	10	0	10	0
$\dot{Q}_{tot}$ [kW]	30	30	30	30
q'' [kW/m^2]	127.9	127.9	347.1	347.1
$\dot{m}_{H_2O}$ [m^3/h]	10	10	10	10
T_{inlet,H_2O} [°C]	170	170	170	170
p_{H_2O} [bar]	16	16	16	16



(a) (b)

Figure 4.17 – Active pins (in red) during ADP10 (a) and ADP06 (b) tests [59].

Fuel Pin Bundle Simulator model

The CFD domain adopted both for the CFD standalone analysis of the steady state and the coupled simulation is limited to the 600 mm of the active region of the FPBS to limit as much as possible the CFD domain dimension and in turn the computational cost. The simulated domain comprises the LBE [55] fluid region, the external solid wrapper (AISI316L) that encloses the pin bundle, the wires (AISI316L) and the pins, considering the three constituting different materials: AISI316L, Inconel 600 and copper (Table 4.4). The effect of the Inconel600 inside the pin is neglected and the region included a single Boron Nitride (BN) domain (Figure 4.18).

Table 4.4: Diameters of the different parts of the pin in the active region [59].

Part	Internal diameter [mm]	External diameter [mm]
Clad (AISI316L)	5.08	6.55
Heating tube (Inconel600)	3.35	3.53
Central conductor (Copper)	-	2.31
1st insulant layer (BN)	2.31	3.35
2nd insulant layer (BN)	3.53	5.08

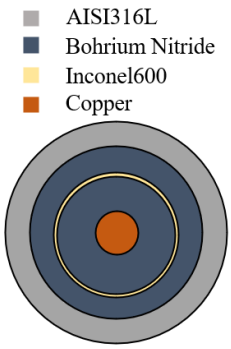


Figure 4.18 – Schematic of the pin materials [62].

To reduce the number of nodes, the mesh is divided into different bodies (Figure 4.19) in both axial and radial directions, creating structured meshes for each region. To allow structured mesh the different bodies are meshed with ANSYS Meshing as different parts. In this way, the obtained mesh is not conformal and has the characteristic of unmatched nodes between adjacent bodies, but the result is a light mesh to be applied for coupled calculation. A second mesh obtained by an in-house developed Python script by the ENEA Bologna team has been tested. This mesh is conformal, is constituted by a similar number of nodes and overall gives very similar results, thus is not included in this thesis.

At the FPBS inlet, a fully developed velocity and temperature distribution is imposed obtained by a previously conducted simulations to retrieve the condition at the FPS inlet. The selected turbulence model is the $SSTk-\omega$ [56] with a constant Pr_t of 1.5. Previous sensitivity analyses showed negligible differences in the range 1.5 – 3.5 [64]. On the external wall of the solid structure, an adiabatic condition is imposed. The fluid boundary layer at the wall is resolved with a $y^+ \sim 1$ on all the fluid-solid boundaries.

The CFX solver's default settings were used, including the Rhie-Chow algorithm and Upwind advection scheme.

A mesh size sensitivity study (Table 4.5) is conducted using ADP10 initial steady-state conditions to determine the optimal number of nodes for balancing accuracy and computational time. From the initial *Reference* mesh, different meshes were evaluated by increasing the resolution separately varying near-wall treatment and element size in radial (*Radial Ref*) and axial directions (*Axial Ref*). The *Coarse Improved mesh* (Figure 4.20 and Figure 4.21) of 4.5M nodes, is the result of the optimization process and it is selected as it achieved a discrepancy of less than 10% compared to the most refined meshes while minimizing mesh size.

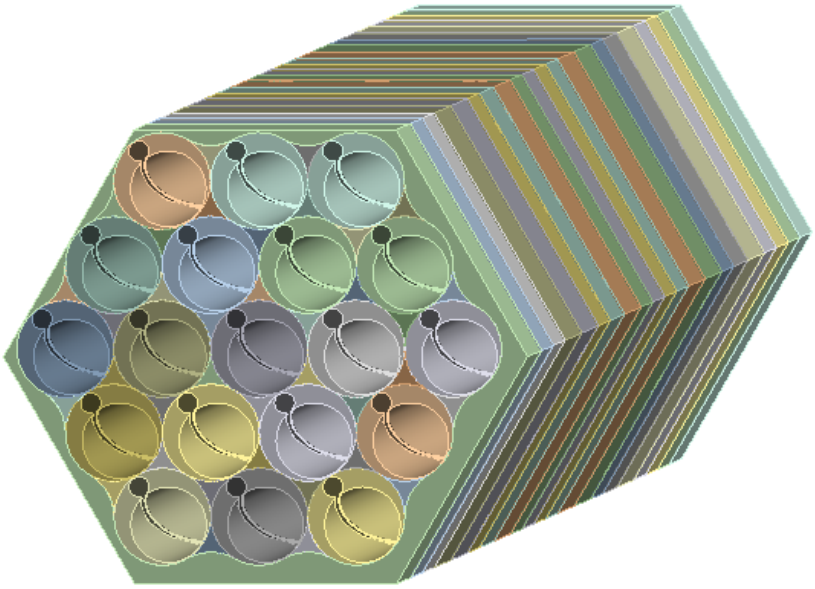


Figure 4.19 – Partition of the fluid region in bodies.

Table 4.5: Mesh size sensitivity study of the Fuel Pin Bundle Simulator CFD model [62].

	Coarse	**Coarse improved**	**Reference**	**Radial ref**	**Axial ref**
n° of nodes [M]	4.2	4.5	6.4	33.5	29.3
Δp [mbar]	28.4	31.1	31.4	33.6	33.8
ΔT in-out [°C]	80.1	80.3	80.3	80.3	80.4
T point [°C]	319.0	321.2	322.5	323.1	323.7

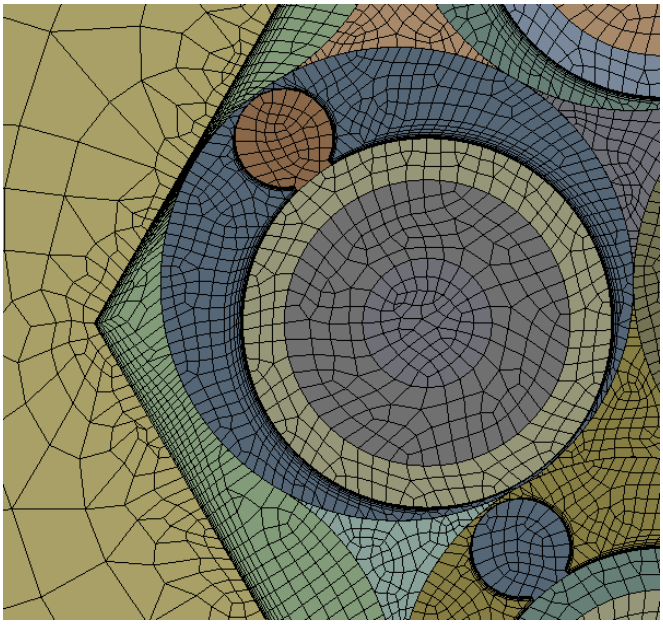


Figure 4.20 – Detail coarse improved mesh.

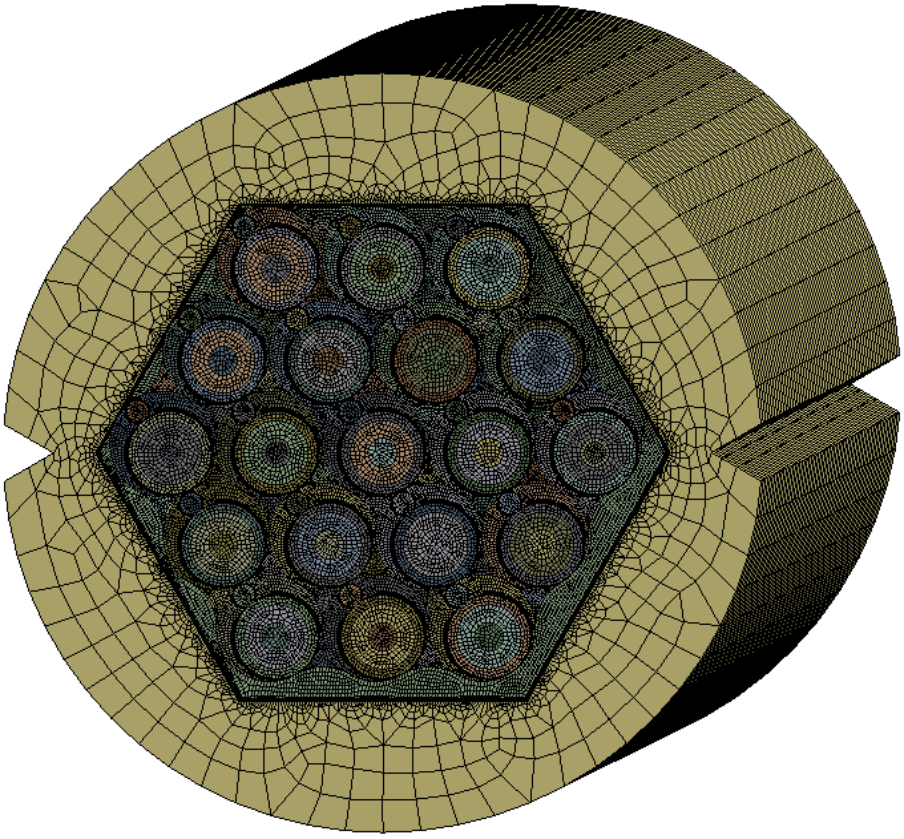


Figure 4.21 – Coarse improved mesh [62].

The CFD stand-alone model is adopted only for the analysis of the steady states, both BOT and EOT. CFD and experimental data are compared focusing on the local temperatures in 67 TCs positions. The TCs locations are reported in [59].

The BOT steady-state simulation results for ADP06 and ADP10 are presented in Figure 4.22 and Figure 4.23, the EOT result in Figure 4.24 and Figure 4.25. The plots report the experimental and numerical data as a function of the thermocouple number. The overall x-axis is divided in three sections referred to bulk, wall and Pin 3 TCs. Data referred to bulk and wall TCs are at their time subdivided considering the three axial instrumented planes, in which the position of the TCs on the section is the same.

Overall, the Ansys CFX model accurately represents the experimental data. An arithmetic average of the absolute value of the difference between CFD and experiment is computed: a mean error of less than 6°C (Table 4.6), that decrease below 3°C if only the ADP10 test is obtained. ADP10 exhibited more uniform characteristics with lower gradients, while ADP06 had a non-heated region in the last rank, leading to non-uniformity that is reproduced with less accuracy by CFX. The CFD model, in general, overestimated internal temperatures and underestimated external temperatures in ADP06, potentially due to underestimation of radial velocities caused by turbulence from the wires. The maximum error per single thermocouple achieved the value of around 17°C in the ADP06 at the BOT. From Figure 4.26 to Figure 4.29, the temperature differences between the CFX results and the experimental values at Plane 3 TCs are reported, indicating the position in the section.

Errors in the first measurement plane might be attributed to the simplified approach of considering only the active length. However, the error magnitude is comparable to that of the second plane, indicating the effectiveness of the imposed velocity map. The third plane generally shows higher differences with experimental results: it is the plane affected by the inaccuracies in the upstream region and where the temperature gradients are more visible.

Pin 3 thermocouples in all the tests demonstrate good qualitative agreement along the heated length. The worst results are obtained in the BOT steady state of the ADP06.

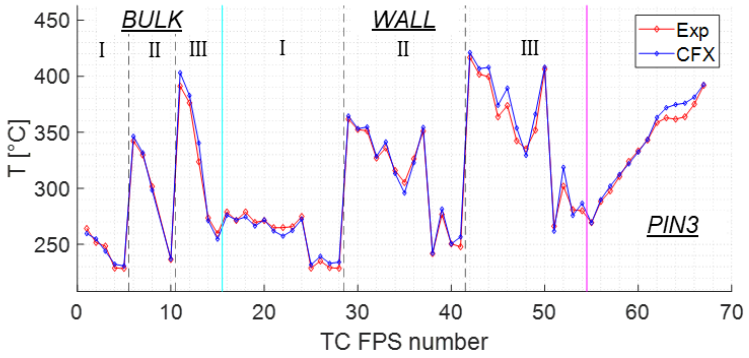


Figure 4.22 – Thermocouples temperature comparison for the BOT steady state, ADP06 [62].

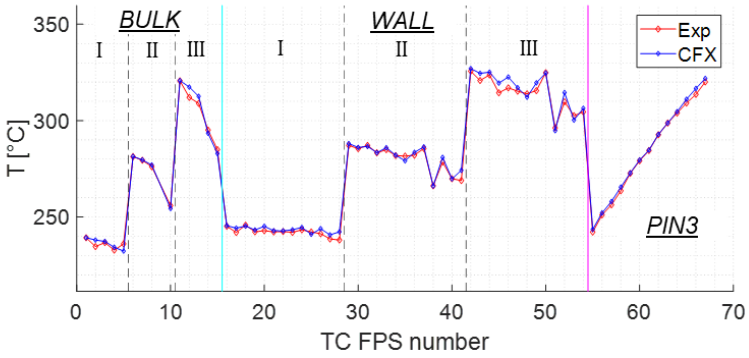


Figure 4.23 – Thermocouples temperature comparison for the BOT steady state, ADP10 [62].

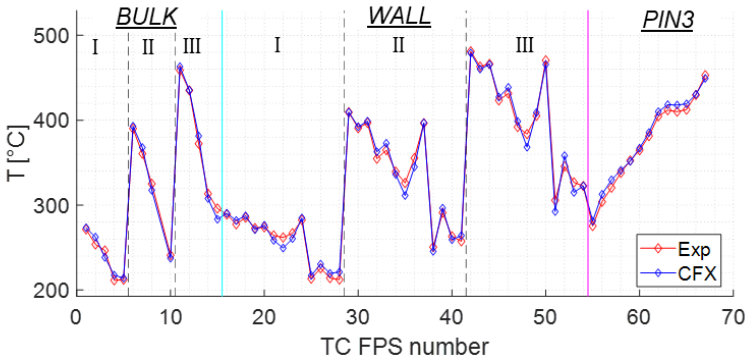


Figure 4.24 – Thermocouples temperature comparison for the EOT steady state, ADP06.

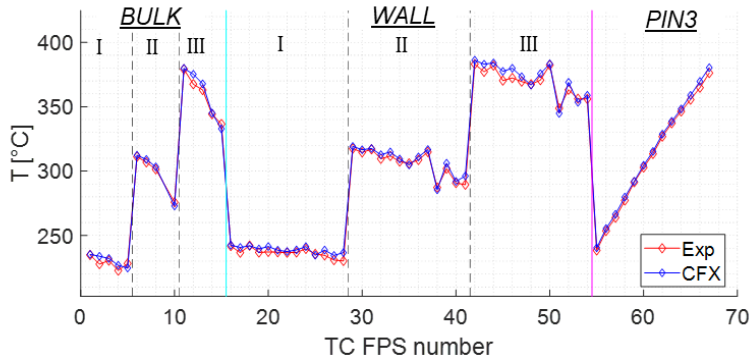


Figure 4.25 – Thermocouples temperature comparison for the EOT steady state, ADP10.

Table 4.6: Mean and maximum temperature difference between CFD and experiment.

$\Delta T_{Exp\ vs\ CFX}$ [°C]	ADP06				ADP10			
	BOT		EOT		BOT		EOT	
	mean	*max*	*mean*	*max*	*mean*	*max*	*mean*	*max*
Plane 1	3.5	7.6	4.8	12.4	1.7	4.3	2.8	6.5
Plane 2	4.1	11.9	5.5	14.8	1.0	5.3	2.3	6.8
Plane 3	7.7	16.8	6.6	15.5	2.7	5.6	3.8	7.7
Tot	5.0	16.8	5.4	15.5	1.7	5.6	2.9	7.7

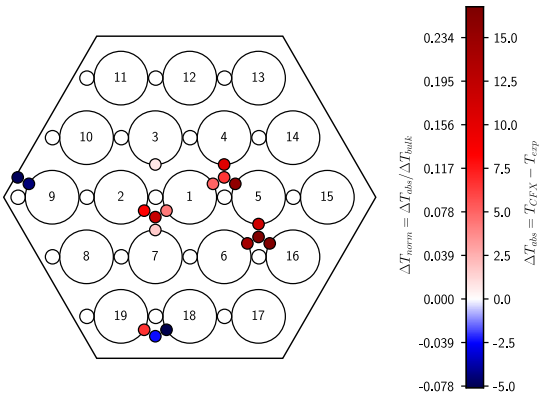


Figure 4.26 – Ansys CFX BOT steady state, temperature comparison on Plane 3 (ADP06) [62].

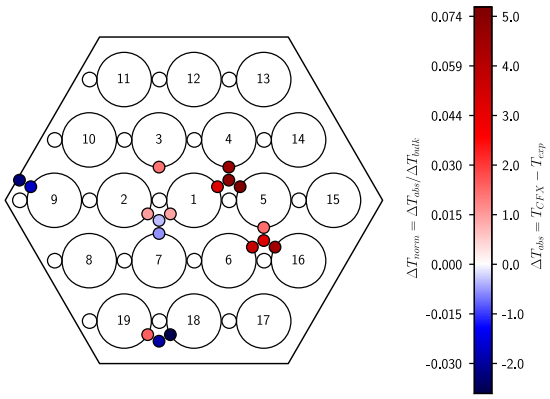


Figure 4.27 – Ansys CFX BOT steady state, temperature comparison on Plane 3 (ADP10) [62].

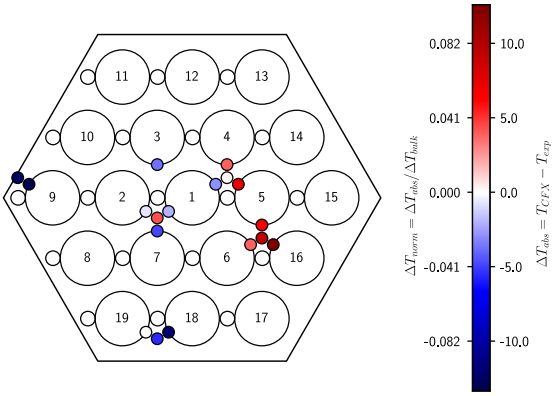


Figure 4.28 – Ansys CFX EOT steady state, temperature comparison on Plane 3 (ADP06).

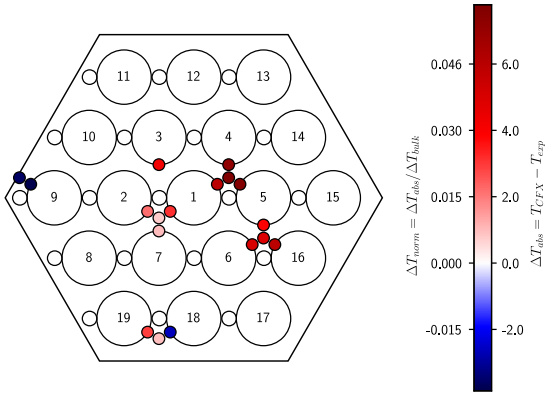


Figure 4.29 – Ansys CFX EOT steady state, temperature comparison on Plane 3 (ADP10).

System scale modelling

Initially, the R5 standalone model is developed. Nodalization of 5 cm is used in active regions (FPBS and HX) to accurately capture heat exchange and thermal gradients. In non-active regions, the nodes size increased to 12 cm, with a smooth transition between the two. The sliced modelling approach [65] is adopted to simulate natural circulation conditions. This methodology involves using the same volume height (or a submultiple) for the vertical control volumes across different nodalization regions at the same axial level. Implementing the sliced approach enhances the code's ability to accurately simulate natural circulation. With this

approach, fluid properties are consistently evaluated at the same axial elevations for all nodalization regions, ensuring that the density difference is accurately captured, thus reducing potential errors in the simulation results [66].

Only the active secondary side of the HX is modelled, with inlet/outlet conditions defined by time-dependent volumes and junctions. The thermal conductivity of the gap between the coaxial tubes in the HX is calculated using the formula [23]:

$$k_{powder} = 0.3 + 0.005 \cdot (T - 200) \quad (9)$$

where T is in °C and k is in W/(m·°C). A graphical representation of the nodalization is given in Figure 4.30.

The primary loop is also thermally insulated using a mineral rock-wool layer with binding thermosetting resin. The thermal conductivity of this resin varies with the temperature, as reported in Table 4.7 (data provided by the manufacturer). The thickness of the thermal insulator is 100 mm in the whole loop.

Table 4.7: Thermal conductivity (k) of the thermal insulator [59].

T [°C]	*k* [W/(m*K)]
0	0.035
50	0.037
100	0.043
150	0.052
200	0.062
250	0.074
300	0.089

The boundary condition for heat loss calculations is set to 8 W/(m²K) for the wall heat transfer coefficient and 10°C for the room temperature. These values were consistent across all simulations.

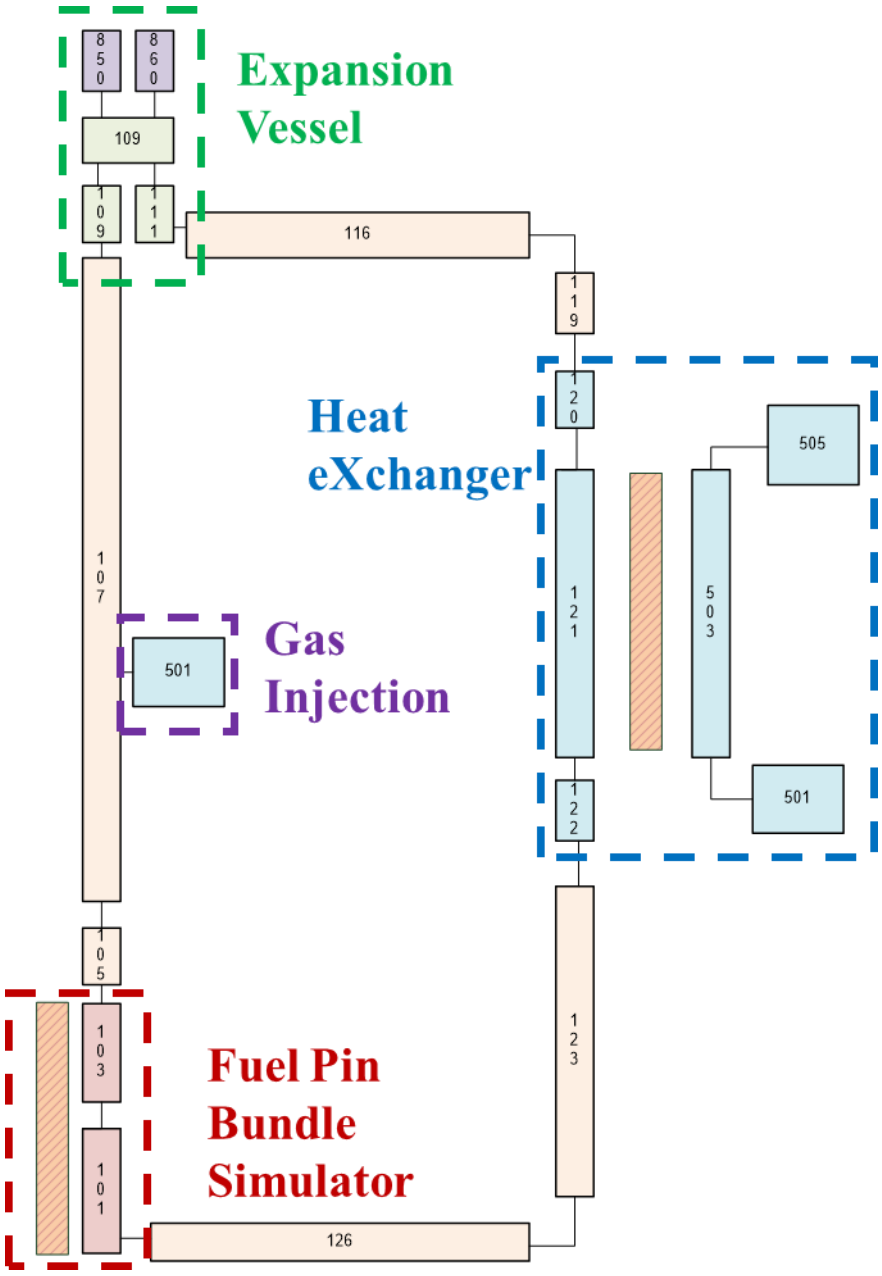


Figure 4.30 – Nodalization of the RELAP5 model of the NACIE-UP loop [62].

R5 allows for customized Reynolds-dependent friction factors and form loss coefficients. Different correlations were used in various facility sections. Localized pressure drops were calculated using formulas from [67], while the Cheng and Todreas correlation for wire-wrapped tube bundles is applied to the FPBS [68][69].

R5 offers options for laminar (Re^{-1}) and turbulent (Re^{-C}) friction factors (equation 10). In the transition region (Re 2200-3000), friction factors are linearly interpolated between the two.

$$\begin{cases} f_L = \dfrac{64}{\Phi_S \cdot Re} & if\ Re < 2200 \\ f_{L,T} = \left(3.75 - \dfrac{8250}{Re}\right)\left(f_{T,3000} - f_{L,2200}\right) + f_{L,2200} & if\ 2200 < Re < 3000 \\ f_T = A + B \cdot Re^{-C} & if\ Re > 3000 \end{cases} \quad (10)$$

The actual correlation is approximated by equations with calibration coefficients listed in Table 4.8. Figure 4.31 graphically compares the approximated and actual correlations.

Table 4.8: Coefficients for the calibration of the Fuel Pin Bundle Simulator pressure drops in the RELAP5 model.

Constant	Φ_S	A	B	C
Value	0.45	0.021	31.66	0.856

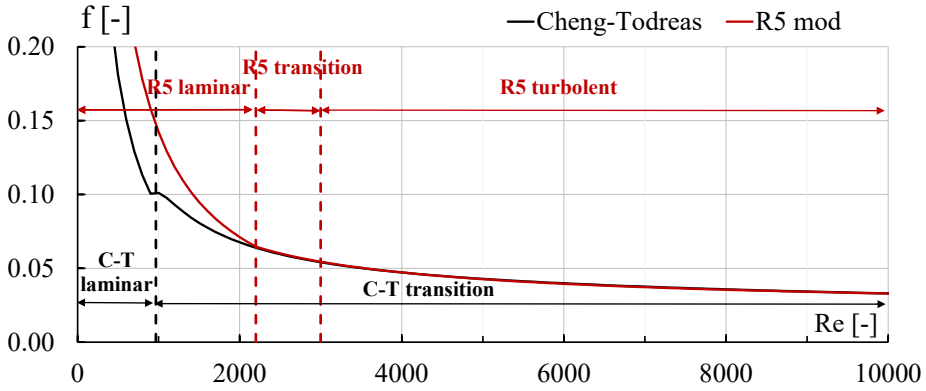


Figure 4.31 – Cheng and Todreas vs RELAP5 correlations for wire wrapped tube bundles [62].

Further analysis of the experimental data identified modelling challenges related to the steady-state natural circulation regime (EOT). The temperatures of the hot and cold legs, based on TC readings at the FPBS and HX outlet, were determined to be 362.5°C and 199.5°C, respectively. The resulting pressure head for the natural circulation can be computed as follows:

$$\Delta p_{head} = \Delta\rho \cdot g \cdot H = (\rho_{@199.5°C} - \rho_{@362.5°C}) \cdot g \cdot H = 9.7\ kPa \quad (11)$$

where Δρ is the density difference between the cold and hot leg, g is the gravitational constant, and H is the relative height between the HX and FPBS thermal barycentres.

The experimental mass flow in the final steady state is similar for both the ADP06 and ADP10 tests since the power in natural circulation is the same and corresponds to Re~3600, from which a friction factor in the FPBS equal to 0.05 can be retrieved from equation 10. The pressure drops in the FPBS can be calculated as follows:

$$\Delta p_{FPBS} = \left(f \cdot \frac{L}{D_H}\right) \cdot \left(\frac{1}{2} \cdot \rho \cdot u^2\right) = 3.5\ kPa \quad (12)$$

Pressure drops in the rest of the facility were calculated both analytically and numerically using the R5 model. Both methods yielded very low values, confirming the low velocities in the LBE primary loop, including the HX, where the flow area is significantly larger than in other sections, excluded the FPBS. Detailed pressure drop distributions are provided in Table 4.9.

Table 4.9: Numerical pressure drops along the loop in the end of the transient steady state [62].

Location	Pressure drop [kPa]
FPBS inlet elbow	0.11
FPBS pins	3.47
FPBS outlet grid	0.91
Riser	0.04
Expansion vessel (from inlet to outlet)	0.03
Upper horizontal leg	0.04
Upper bend	<0.01
HX	0.02
Downcomer	0.02
Lower bend	<0.01
Lower horizontal leg (including TFM)	0.10

In conclusion, the most significant contribution to the total loop pressure drops is the one in the FPBS. The discrepancy between the values obtained with equation 11 and the sum of all the pressure losses, i.e., between natural circulation driving force and circuit hydraulic resistance, could be attributed to an eventual additional pressure drop not considered in the models. One possible explanation for the pressure drop is the presence of oxide deposits in the coldest part of the loop (the downcomer bottom), where oxygen solubility is lowest. Such deposits could have reduced the flow area, leading to increased pressure drops. Since the experimental campaigns lacked an online oxygen control system, a concentrated pressure drop is added to the downcomer in the form of a constant K-coefficient to calibrate the numerical model.

The calibrated model underestimated mass flow rates in the forced circulation regime. This is primarily due to an underestimation of the void fraction profile within the riser. The gas lift is simulated with a fixed argon mass flow rate using a time-dependent junction and volume. The code modifications allowed for gas-LBE coexistence in the riser. However, the calculated average void fraction is only around half the experimental value. RELAP5 Mod3.3 uses water-based models for non-condensable gas bubble rise velocity, which are not suitable for HLMs. To compensate, the riser is injected with double the gas mass flow rate.

Based on the R5 model, the coupled model is defined opening the loop at the FPBS location (Figure 4.32): the volumes corresponding to the active region are removed and the extremities connected to a time time-dependent junction and volume at the inlet and a single junction and time-dependent volume at the outlet. In the coupled simulations, the FPBS is modelled with CFX, adopting a decomposition domain approach. The remaining part of the system is modelled in R5 as previously described.

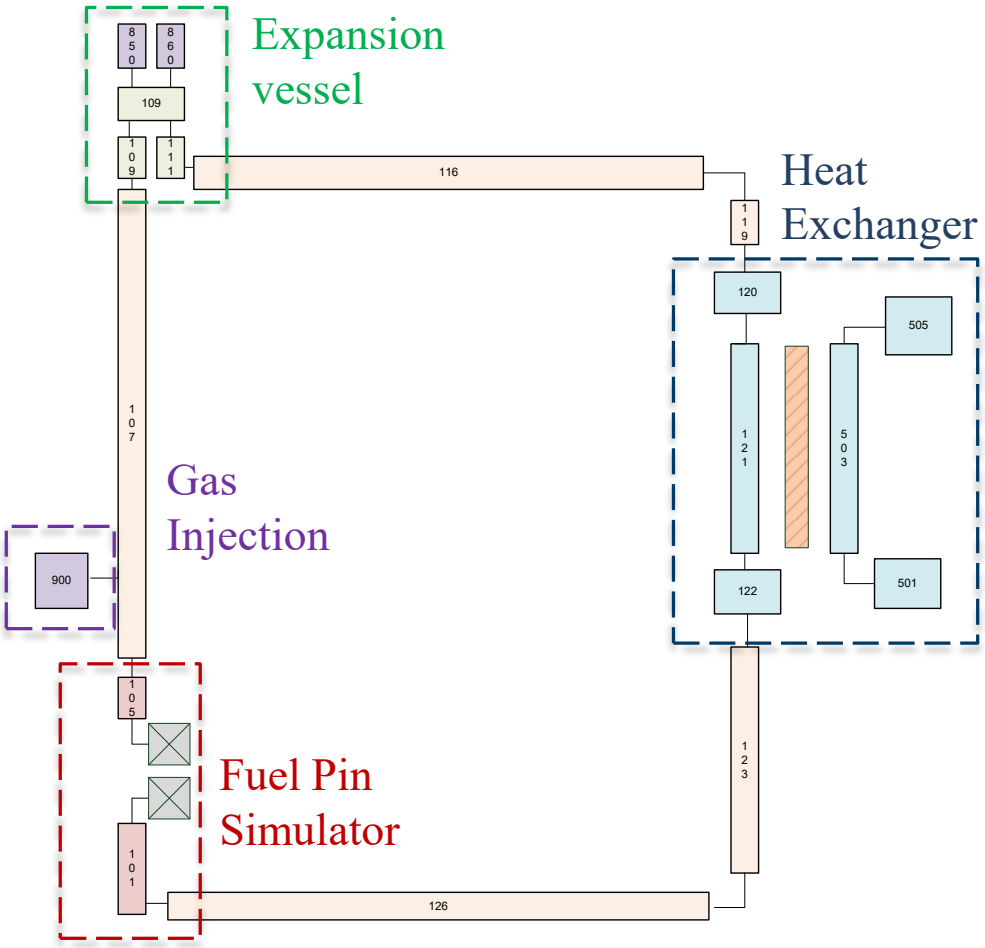


Figure 4.32 – Nodalization of the NACIE-UP open loop adopted for the coupled simulations.

The comparison of the experimental results with R5 standalone and coupled simulations is reported in the next section.

Coupled tool simulation results

For the coupled simulation, a preliminary R5 steady state calculation with the "open loop" model (see Figure 4.32) has been performed to prepare a restart file to be used for the coupled simulation. The boundary conditions adopted for the "open loop" are the steady state values obtained with the entire loop.

During the decomposition approach coupled run the two-way exchange of information regards (see Figure 4.33 or a graphical representation):

- the outlet mass flow rate (from CFX to R5);

- the outlet temperature (from CFX to R5);
- the total pressure drops along the active length of the FPBS (from CFX to R5);
- the inlet mass flow rate (from R5 to CFX);
- the inlet temperature in the FPBS (from R5 to CFX).

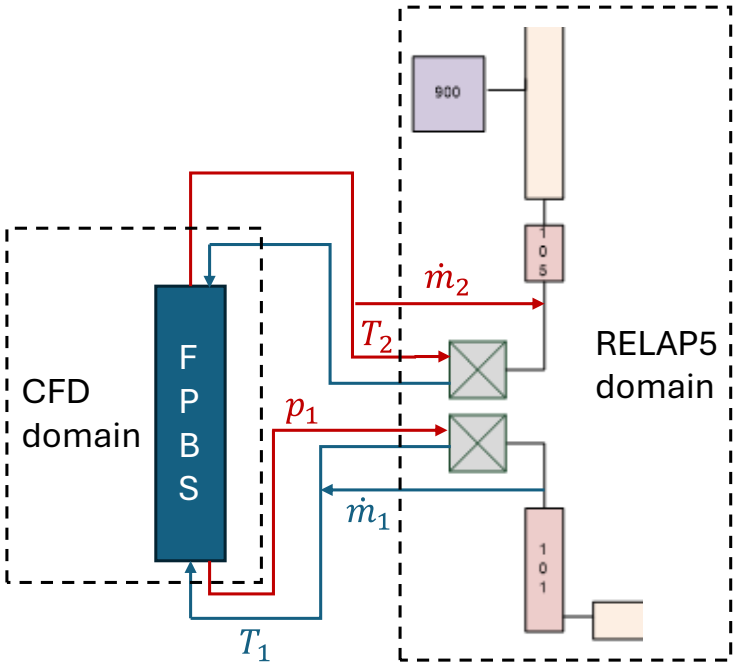


Figure 4.33 – Exchanged parameters in the coupled NACIE-UP simulation [62].

The pressure drop considered in the calculation is computed following the procedure described in section 3.3.1. The CFD inlet mass flow rate is set equal to the RELAP5-calculated value at the outlet of the 'open loop.' A non-dimensional velocity map, created by averaging the fully developed flow maps from the initial and final steady-state CFD simulations, is applied at the CFD inlet. A similar approach is used to impose an inlet temperature distribution. These choices were considered the best way to reduce computational time without sacrificing the overall simulation accuracy.

In the coupled simulations, the R5 time step is set to 1/10 of the CFX time step to ensure stability. A sensitivity analysis showed that varying the time step within the 10^{-3} s to $2 \cdot 10^{-2}$ s range had minimal impact on the results. An adaptive timestep is applied in the simulation with a minimum of $5 \cdot 10^{-3}$ s to $2 \cdot 10^{-2}$ s.

To establish a new steady state before the transient began, a 20-second null simulation is performed after the codes starts exchanging variables. At that moment, gas injection was then stopped to trigger the transient.

For the presented results, a semi-implicit advancing scheme is adopted. In Figure 4.34, the mass flow rate obtained using a preliminary decomposition-coupled model of the NACIE-UP loop with an explicit time-advancing scheme is compared to the one discussed in the following paragraph (semi-implicit) and the experimental result. Initially, the explicit scheme was used due to its faster execution; however, some numerical instabilities were observed. For this reason, the semi-implicit scheme was selected to continue the analysis.

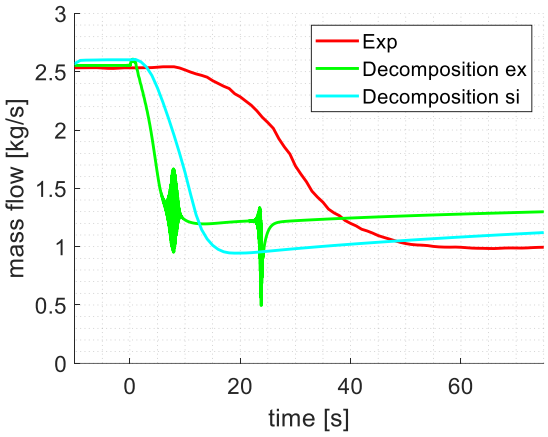


Figure 4.34 –Preliminary comparison between the explicit and semi-implicit decomposition coupling approach [70].

The results of the two steady states are compared for each experiment. The results for the BOT and EOT for the R5 standalone and for the BOT for the coupled simulation are summarized in Table 4.10 and Table 4.11. Th EOT state is not fully reached in the coupled simulation and so the result not reported in the table.

The ADP10 and ADP06 tests had similar loop parameters, differing only in power distribution. Comparing simulation and experimental results, the largest discrepancy in the mass flow rate is found in the ADP06 test at BOT. This discrepancy is comparable to the measurement uncertainty. The maximum temperature difference is found at the FPBS outlet in the EOT of the ADP06 (about 12°C).

As expected, the coupled simulation results closely matched the R5 stand-alone results. The two coupled calculations produced almost identical results, except for the FPBS outlet temperature, which is calculated by the CFX domain.

Table 4.10: Experimental vs RELAP vs coupled results (ADP10 test).

	Parameter	Unit	Exp	RELAP5	Error	Coupled	Error
BOT	LBE ṁ	kg/s	2.56	2.52	-1.6%	2.60	1.6%
	T_{in} FPBS	°C	225.6	223.2	-2.4°C	223.3	-2.3°C
	T_{out} FPBS	°C	305.2	299.0	-6.2°C	299.7	-5.5°C
	T_{in} HX	°C	301.6	296.9	-4.7°C	295.1	-6.5°C
	T_{out} HX	°C	220.5	218.6	-1.9°C	218.8	-1.7°C
EOT*	LBE ṁ	kg/s	1.31	1.34	2.3%	-	-
	T_{in} FPBS	°C	207.5	207.2	-0.2°C	-	-
	T_{out} FPBS	°C	362.4	350.5	12.0°C	-	-
	T_{in} HX	°C	353.3	345.9	-7.3°C	-	-
	T_{out} HX	°C	199.4	200.0	0.7°C	-	-

* Results of the coupled calculation at EOT are not available since it ends at 1500 s

Table 4.11: Experimental vs RELAP vs coupled results (ADP06 test).

	Parameter	Unit	Exp	RELAP5	Error	Coupled	Error
BOT	LBE ṁ	kg/s	2.66	2.52	-5.3%	2.60	-2.3%
	T_{in} FPBS	°C	227.7	223.4	-4.3°C	223.3	-4.4°C
	T_{out} FPBS	°C	304.4	299.3	-5.1°C	300.3	-4.0°C
	T_{in} HX	°C	301.4	297.2	-4.2°C	295.1	-6.3°C
	T_{out} HX	°C	222.7	218.8	-3.9°C	218.8	-4.0°C
EOT*	LBE ṁ	kg/s	1.33	1.34	-0.8%	-	-
	T_{in} FPBS	°C	207.7	207.3	-0.3°C	-	-
	T_{out} FPBS	°C	359.9	350.6	-9.4°C	-	-
	T_{in} HX	°C	351.2	346.2	-5.0°C	-	-
	T_{out} HX	°C	199.6	200.1	0.5°C	-	-

*** Results of the coupled calculation at EOT are not available since it ends at 1500 s**

The start of the transient is defined as the moment when gas injection stops. This is assumed to occur at t=0 s for both R5 and coupled simulations. The thermal power from the FPBS remains constant, as do the water temperature and mass flow rate at the HX secondary side.

As shown in Figure 4.35 and Figure 4.36, the LBE mass flow rate rapidly decreases to ~1 kg/s after gas injection stops. The EOT steady state is approached around 1500 s, when the system transitions to natural circulation. The delay in the experimental mass flow rate drop is likely influenced by the measurement system's

response time. This is supported by the consistent timing of temperature excursions in Figure 4.37 and Figure 4.38.

Figure 4.39 and Figure 4.40 illustrate the focus on the variation of mass flow rate and temperatures at the start of the transient, to better show that the discrepancies visible in the first few tens of seconds are not noticeable in the temperature variation. However, some small discrepancies between the experimental mass flow rate and the numerical results remain visible.

Figure 4.37 and Figure 4.38 show good agreement between experimental and numerical values of FPBS inlet and outlet temperatures, confirming the accurate representation of mass flow rate transition. However, a delay is observed in HX inlet and outlet temperatures (Figure 4.41 and Figure 4.42). This might be due to an incomplete representation of the system's heat capacity, as parts of the metallic shell were not simulated.

The numerical trends predicted by R5 and the coupled tool are very similar, suggesting that a 1D representation of the entire system is adequate for describing loop TH phenomena in these conditions. Discrepancies can be attributed to more detailed FPBS modelling and pressure drop evaluations.

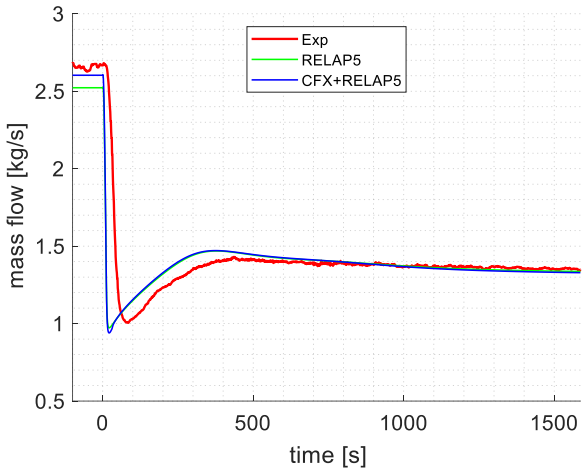


Figure 4.35 – Experimental vs RELAP5 vs coupling mass flow rate comparison (ADP06) [62].

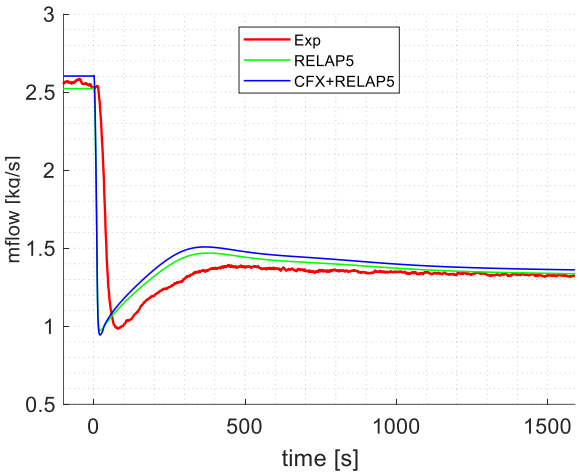


Figure 4.36 – Experimental vs RELAP5 vs coupling mass flow rate comparison (ADP10)[62].

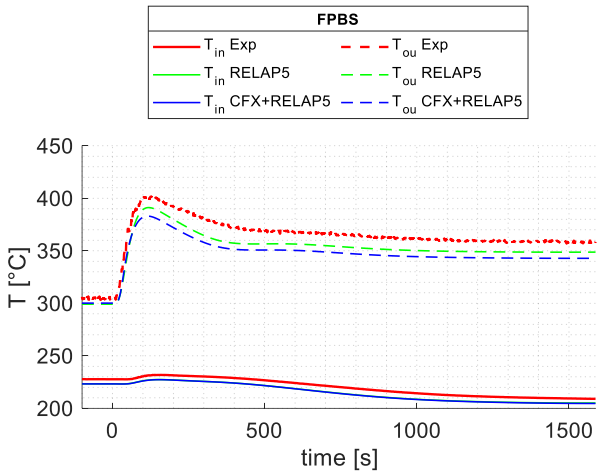


Figure 4.37 – Experimental vs RELAP5 vs coupling FPBS temperature comparison (ADP06)[62].

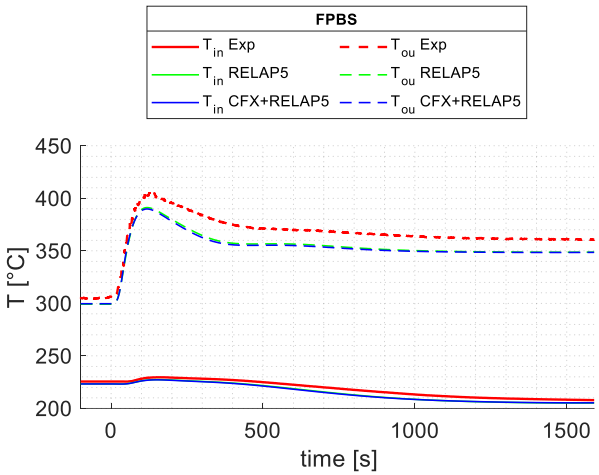


Figure 4.38 – Experimental vs RELAP5 vs coupling FPBS temperature comparison (ADP10)[62].

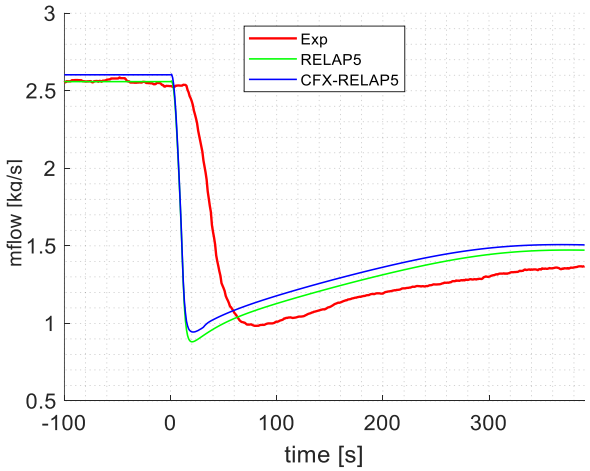


Figure 4.39 – Experimental vs RELAP5 vs coupling mass flow rate comparison, beginning of the transient (ADP10).

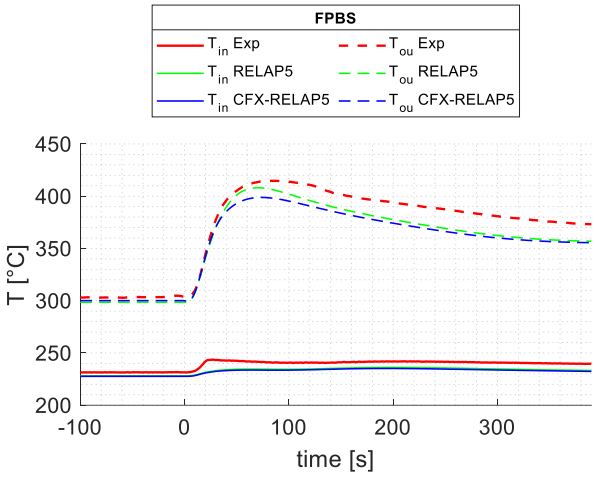


Figure 4.40 – Experimental vs RELAP5 vs coupling FPBS temperature comparison, beginning of the transient (ADP10).

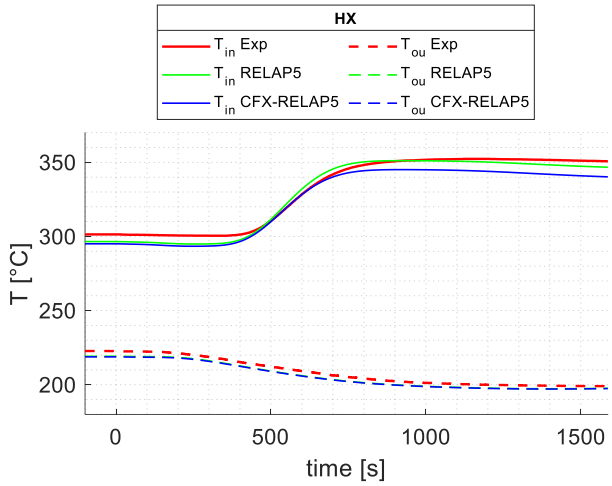


Figure 4.41 – Experimental vs RELAP5 vs coupling HX temperature comparison (ADP06) [62].

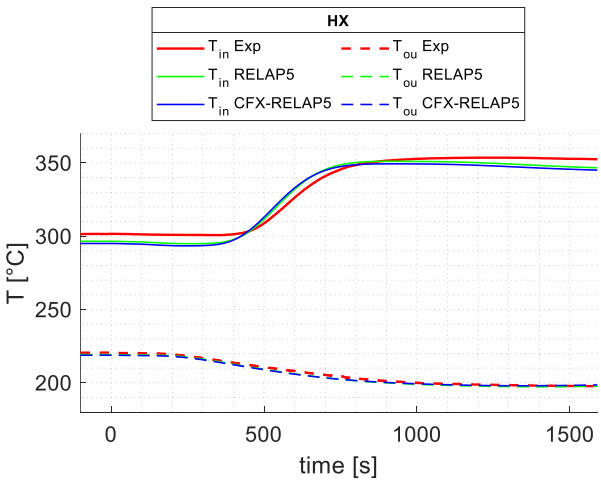


Figure 4.42 – Experimental vs RELAP5 vs coupling HX temperature comparison (ADP10) [62].

An advantage of the coupled tool is the ability to perform CFD-level analysis on the FPBS while obtaining appropriate boundary conditions (mass flow rate and inlet temperature) from a system-level calculation (R5). Figure 4.43 and Figure 4.44 show the comparison between the experimental results and the numerical trends, obtained by the coupled tool, of local temperatures inside the FPBS, in particular TC 12 (bulk) and TC 49 (wall), reported as example. The CFD calculation demonstrates to reproduce with similar behaviour the experimental results. The

error is lower at the BOT and going toward the EOT, thus approaching steady state conditions. The differences in the transient region could be explained by considering the discrepancy between experimental and numerical LBE mass flow rate, already discussed in the previous section, but overall, also the local temperature representation could be considered satisfactory.

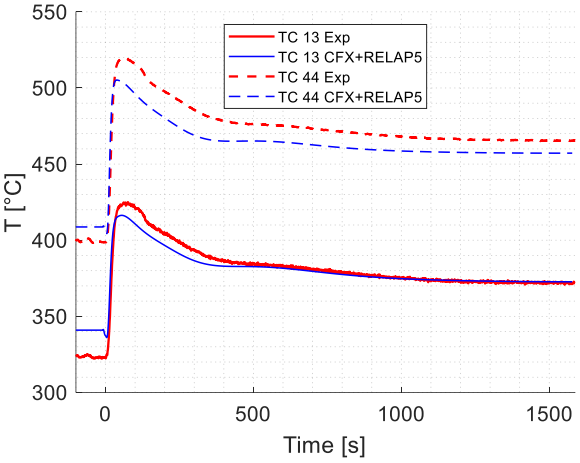


Figure 4.43 – Experiment vs coupling TC13 and TC44 temperature comparison (ADP06) [62].

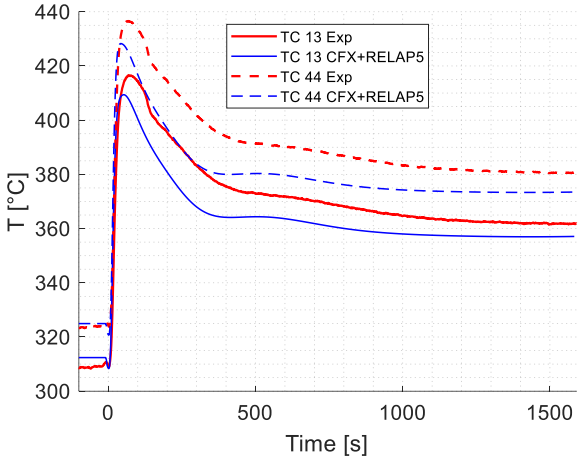


Figure 4.44 – Experiment vs coupling TC13 and TC44 temperature comparison (ADP10) [62].

In conclusion, the obtained mass flow rate and temperatures are close to the R5 stand-alone results, with small discrepancies in the investigated time window (1500 s transient). Even though the coupling approach has given similar results compared to the R5 stand-alone simulation, the main advantage of the application of the coupled tool is a detailed local description of the FPBS active region (CFD domain), being the main TH phenomena governing the considered transients analysable with 1D codes. Errors in the local FPBS temperatures during the coupled transient simulation are mainly linked to the inaccuracies in reproducing system level quantities such as the mass flow rate.

4.2.3 TALL-3D

The TALL-3D facility was conceived to assess the benefits of coupled CFD-STH tools and compare their predictions with experimental data. Because of the link between natural circulation in the loop and complex 3D mixing and stratification patterns in the axisymmetric pool-type test section, this facility presents an ideal scenario for validating coupled tools.

It is important to reference the studies of the facility behaviour within the already mentioned European project THINS [30] and SESAME [31]. From the latter, a forced to natural circulation transition experiment is selected for the analysis here reported. During the two projects, various coupling tools were tested and compared.

TALL-3D does not add to the modelling complexity when validating the Ansys CFX – RELAP5 Mod3.3 tool: the NACIE-UP application allows the study of the complex geometry of the FPBS and the effect of multiphase flow in the riser during the gas enhanced circulation. Nevertheless, in the studied TALL-3D transient, novel reactor relevant phenomena are present: even if the R5 and especially the CFX models are simpler to be developed, the coupled approach is tested for mass flow inversion, thermal mixing and stratification and more relevant mutual feedback between the codes.

Facility description

The facility (Figure 4.45) is composed of the primary loop in which LBE circulates, and the secondary loop, with the synthetic organic heat transfer fluid Dowtherm RP. The total facility height is 6.5 meters.

The primary loop [71] comprises the sump tank (on the left) for storing, melting, and supplying LBE to the main loop, three vertical legs, and two horizontal sections connecting each pair of elbows and a T-junction. The Main Heater (MH) leg (left leg) contains a 27 kW rod-type electric heater (pin outer diameter 8.2 mm, heated length 870 mm) at the bottom (Figure 4.47a) and an expansion tank at the top. The Heat Exchanger (HX) leg (right leg) consists in a counter-current heat exchanger (Figure 4.47b) at the top and an Electric Permanent Magnet (EPM) pump at the bottom (Figure 4.47c). The middle 3D leg connects a pool-type 3D test section to the loop.

The 3D Test section (3D-TS) is an axisymmetric cylindrical stainless steel vessel with a bottom and a top connection to the loop (see Figure 4.48a). The geometrical description and the instrumentation position can found in [71]. The upper two-thirds of the test section are equipped with a 15 kW band heater to induce thermal stratification within the LBE pool. Inside, a circular plate is positioned perpendicular to the flow to enhance mixing by redirecting the incoming flow toward the pool's periphery. This plate is suspended from the ceiling using four fin-shaped separators to minimize flow disruption. The inlet tube of the 3D-TS is narrower than the outlet tube (inner/outer diameter correspond to 17/23 mm vs.

27.8/33.4 mm), matching the dimensions of the pipes in the primary loop's main components.

Two types of thermal insulators are used: ISOVER Tape Lock 7300 and Nano T Ultra. Nano T Ultra is used only for some regions around the test section, ISOVER Tape Lock 7300 is used in the rest of the loop.

Figure 4.48b shows the thermocouples (TCs) inside the 3D-TS for a generic plane, indicated by the “x” letter, among the four measuring planes present. For the validation of the pool modelling an ordinated vector is built, only considering the instruments in the fluid, with the following order: CIP, BP, IPT, ILW (for the nomenclature see Figure 4.48b). This vector will be used to compare in a single plot the TCs simulation results with the experimental data.

Under forced circulation, LBE flows downward in the HX leg and upward in the MH and 3D legs. However, during transient events, the flow direction in any of these legs can reverse, influenced by factors such as heater power and initial conditions.

The secondary loop is a closed system using synthetic organic Dowtherm RP heat transfer fluid to cool the main loop. The fluid flow is clockwise (refer to Figure 4.45). The oil circulates through the system, starting from the oil tank, passing through the rotary pump, then flowing to the main loop heat exchanger. From there, it proceeds to the secondary heat exchanger, which is capable of removing up to 40 kW, before returning to the oil tank.

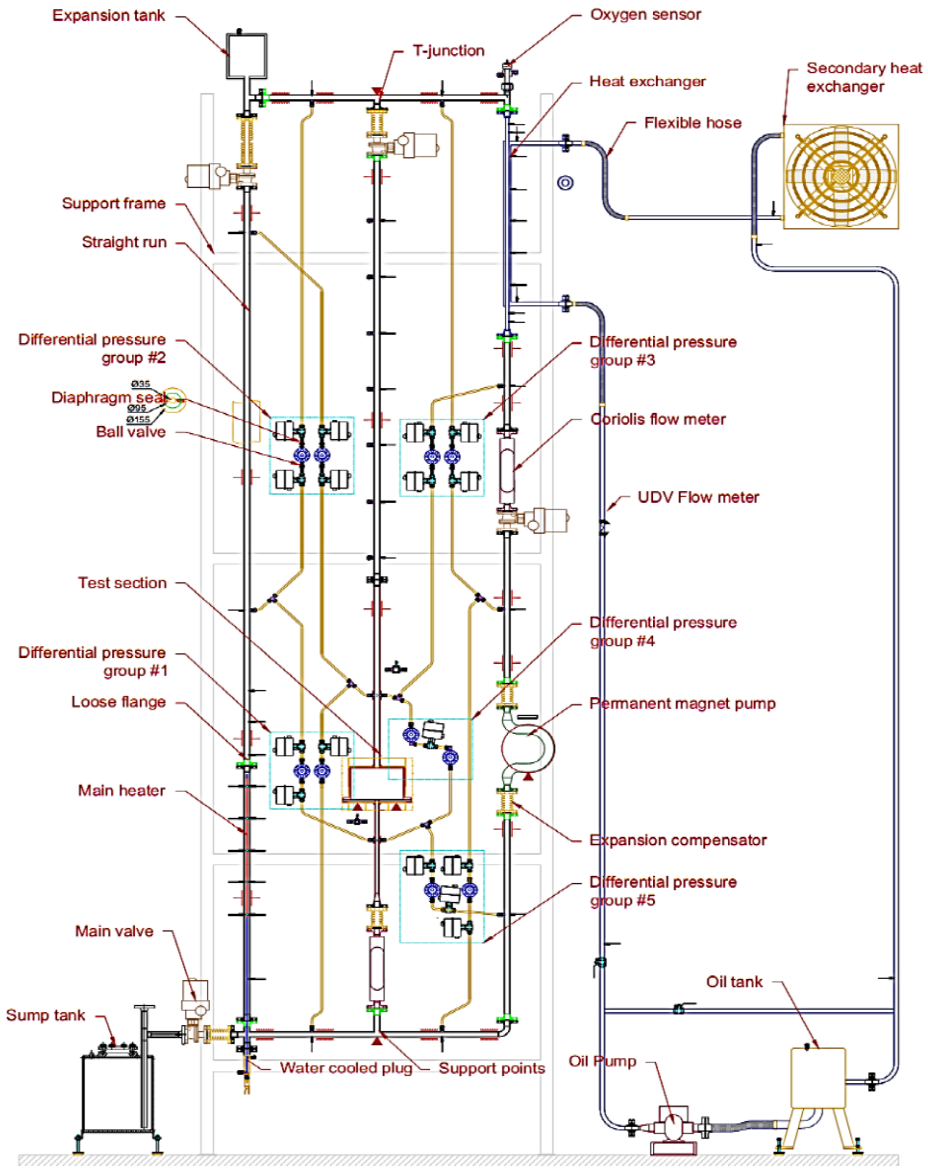


Figure 4.45 – TALL-3D facility main components [71].



Figure 4.46 – Picture of the TALL-3D facility [71].

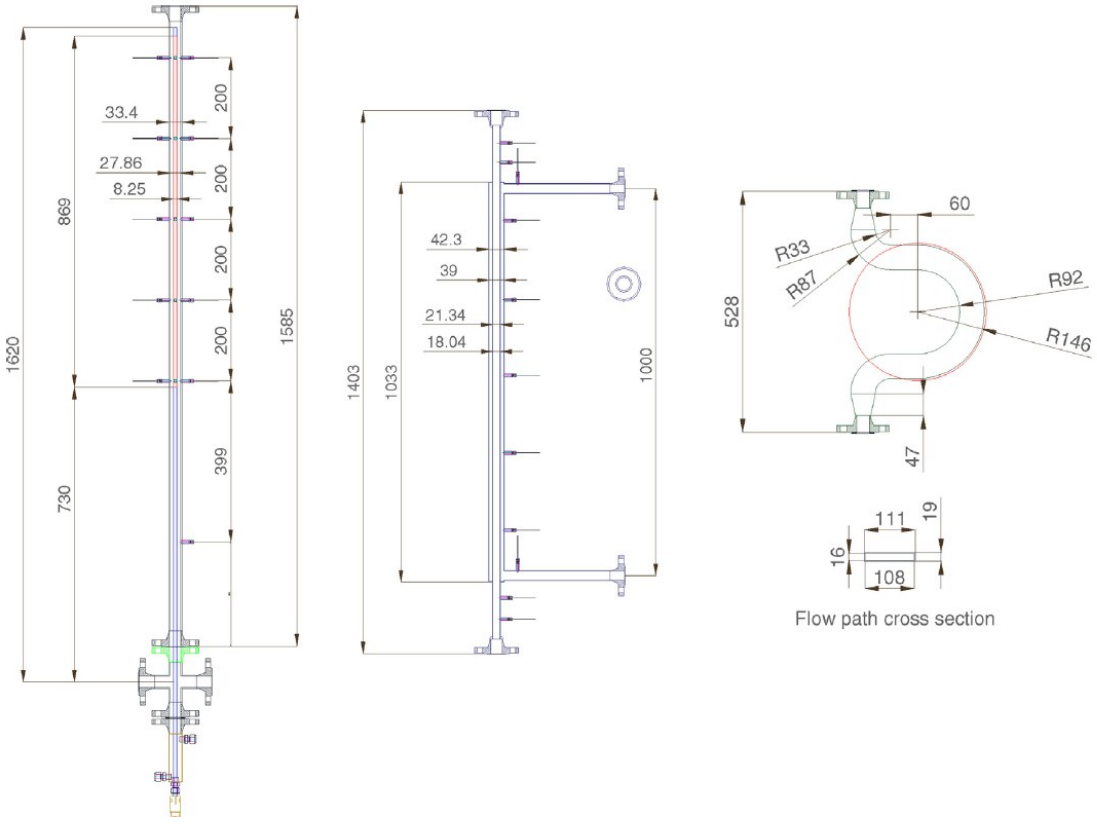
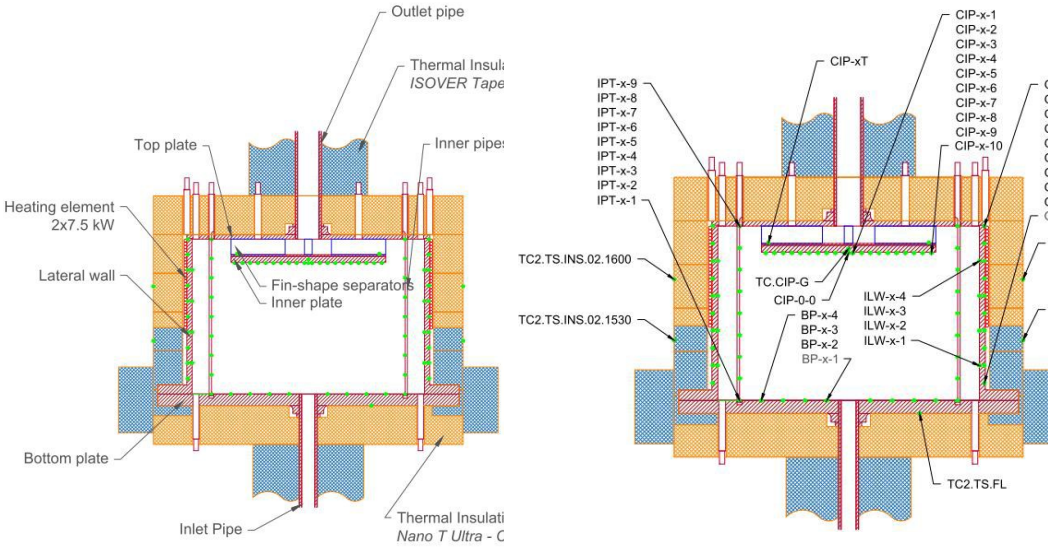


Figure 4.47 – Design drawings of main loop components (main heater (left); heat exchanger (centre); LBE pump (right)) [71].



(a) (b)

Figure 4.48 – TALL-3D test section: components (a) and thermocouples position and nomenclature (b) [71].

Experimental setup

For validation of the coupled tools, the transition from forced to natural circulation is considered to emphasize the importance of feedback mechanisms and the efficacy of the coupling methodology. The transient initiates from a forced steady-state circulation with a mass flow rate of 3.34 kg/s in the HX leg, divided between the MH leg (2.03kg/s) and the 3D-TS leg (1.31 kg/s). Throughout the transient, both the MH and the 3D-TS heater operate continuously with 3.2 kW and 4.0 kW, respectively.

The theoretical principle behind the 3D-TS's ability to exploit three-dimensional effects is based on the opposing influences of the entering nozzle jet and the buoyant boundary layer on the heater wall. The jet enhances fluid mixing within the test section, while the boundary layer contributes to the formation of thermal stratification.

In forced steady-state circulation (FC) the jet at the 3D-TS bottom is powerful enough to mix the fluid inside the volume; once the EPM pump is turned off, the mass flow rate in all legs declines leading to the onset of natural circulation (NC), driven by temperature gradients between the hot and cold legs, determining the reduction of the mixing effect of the jet and the formation of thermal stratification within the pool [72].

The transient initial and final steady state conditions are reported in Table 4.12. Reference to the studied test could be found within the SESAME project [73] under the name TG03.S301.04.

Table 4.12: Experimental test initial and final steady state conditions [74].

Parameter	Units	Initial steady state (FC)	Final steady state (NC)
Main heater electric power	W	3234	3235
3D-TS electric power	W	4048	4027
Heat exchanger LBE mass flow rate	kg/s	2.03	0.25
3D-TS LBE mass flow rate	kg/s	1.31	0.27
MH down section LBE temperature	°C	234.5	202.0
MH top section LBE temperature	°C	246.5	283.92
HX top section LBE temperature	°C	250.2	280.0
HX down section LBE temperature	°C	236.0	211.9
3D-TS down section LBE temperature	°C	235.4	201.8
3D-TS top section LBE temperature	°C	254.1	294.7

3D-Test section model

The axisymmetric pool in a STH code can be modelled using a one-dimensional component with axial discretization along the flow direction. To simulate the transition from the loop pipeline to the 3D-TS, control volumes with varying flow areas can be employed. At the junctions between volumes with different areas, appropriately defined localized pressure drop coefficients should be established.

The modelling using a CFD code could benefit from the quasi-axisymmetric conditions within the test section. The parts that do not meet the axisymmetric condition are the fin-shaped separators. However, the impact of the separators can be neglected. The thermocouples are positioned on four equally spaced planes therefore, to obtain axisymmetric experimental data comparable with simulation results, the average values from the four planes were considered.

An experimental error is computed as the sum of three contributions [74]:

$$\sigma_{tot} = \sqrt{\sigma_{man}^2 + \sigma_{sym}^2 + \sigma_{std}^2} \tag{13}$$

where:

- σ_{man} correspond to the accuracy indicated by the manufacturer, equal to 1.5°C;
- σ_{sym} indicates the agreement between the four measuring planes and it is computed as the standard deviation among the four steady state values;
- σ_{std} represent the dispersion, thus the noise of the measures in time and it is computed as the square root of the sum of the square of the four standard deviations in the steady state time interval.

The Ansys CFX simulation setup has the following characteristics:

- the CFD domain includes the fluid, the steel 316L, the heaters (considered made entirely of steel 316L) and the insulation. Materials properties are taken respectively from the handbook of liquid metals for the LBE [55], from Ref. [75] for the steel, and from Ref. [71] for the insulator;
- at the top (Up) and bottom (Down) section of the domain, two opening boundary condition are imposed, setting the mass flow rate at the bottom section with uniform velocity distribution on the area and relative pressure equal to zero at the top;
- buoyancy is activated;
- in the heaters' domain, a uniform volumetric heat source is imposed to provide the power to the test section;
- the SST k-ω turbulence model [56] is implemented with a constant turbulent Prandtl number equal to 2 [64]. Variation of the constant turbulent Prandtl number in the range 1.5 - 3 have been tested showing negligible differences;
- the selected advection scheme in the solver is the CFX implement upwind scheme.

In CFX, the axisymmetric condition can be leveraged using either a 2D or 3D approach. The 2D approach involves a single cell in the azimuthal direction. Both periodic and symmetry boundary conditions can be applied to the azimuthal boundaries.

On the 2D model, a grid independence study is carried out with the condition corresponding to the first steady state of the transient previously described and reported in Table 4.13.

Table 4.13: Grid independence study of the 2D model of the 3D Test Section [74].

Quantities	Mesh 1	Mesh 2	Mesh 3
N° of cells [-]	187.5 K	109.2 K	38.9 K
Temperature Up section [°C]	256.1	256.1	256.1
ΔP [Pa]	1001	1011	999
Average Temperature error at the TCs with respect Mesh 1 [°C]	-	0.15	0.62
Maximum TCs error respect Mesh 1 [°C]	-	1.11	6.88

While the overall variation in global quantities remains relatively unchanged among the three meshes, the temperature at the TC locations is influenced by spatial discretization. Mesh 2 is selected because it reaches sufficient level of independence of the result: in fact, the maximum temperature difference with Mesh 1 is lower than the TCs accuracy indicated by the manufacturer (1.5°C).

The Mesh 2 (Figure 4.49) setting parameters are adopted also for all the 3D models on the azimuthal faces, and then swept around the axis.

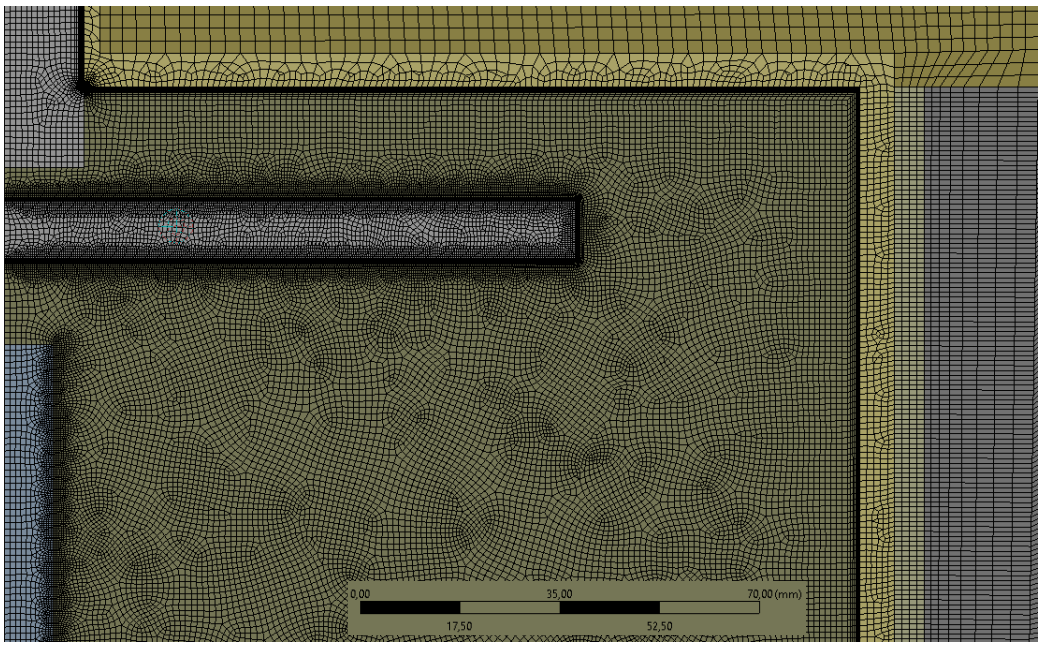


Figure 4.49 – Detail of the discretization in Mesh 2 [74].

To follow, the effect of 2D or 3D modelling, and the dimension of the circumferential angle considered in the 3D cases is evaluated by comparing the results with the experimental ones (see Figure 4.50 and Figure 4.51). Models with 3° and 90° angles were constructed using 5 and 150 radial points. To evaluate the

impact of boundary conditions, both symmetric and periodic conditions were tested on the 3° model.

In the initial steady state, the qualitative fluid temperature trend inside the box is well captured by all the models except for concern the ILW TCs (i.e., the ones on the internal faces of the box), where, in any case, the error is limited (lower than 7°C). Among the presented cases, negligible differences can be noticed, also on the pressure drops across the test section. In particular the differences between the 3° and 90° models could not be noticed in the plots. The 2D model is adopted for the coupled approach, in order to reduce as much as possible the computational cost.

The error in fluid temperature measurements at the TC positions within the test section remained below 10°C during both steady states. However, the CFD model consistently underestimated thermal losses through the insulation, leading to discrepancies in the energy balance. This discrepancy is likely due to thermal bridges formed where instrumentation support penetrates the insulation, particularly at the top and bottom surfaces of the 3D-TS. To address this issue and improve the model's accuracy in reproducing the thermal balance, a new region within the insulation is defined with an increased thermal conductivity, calculated as the average of the insulation and steel values. This modification enabled the CFD model to accurately represent the experimentally measured thermal losses and resulted in improved temperature predictions at the outlet of the test section. The impact on the TCs inside the 3D-TS, as reported in Figure 4.50 and Figure 4.51, shows slightly worse results in the first steady state, where the average error increases from 2.0°C (*2D* blue trend) to 2.6°C (*2D improved* red trends). However, improvements are observed in the second steady state, where the error decreases from 3.6°C to 2.0°C.

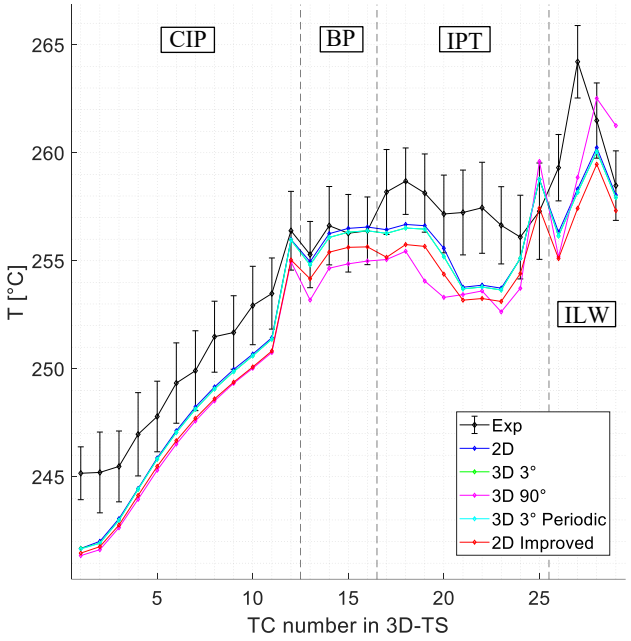


Figure 4.50 – Comparison with experimental data of the different modelling approaches of the 3D-Test Section during the initial steady state [74].

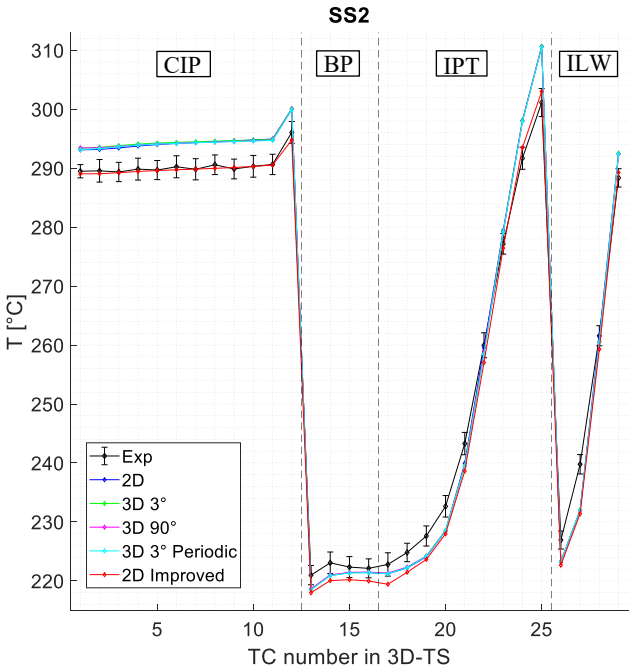


Figure 4.51 – Comparison with experimental data of the different modelling approaches of the 3D-Test Section during the final steady state [74].

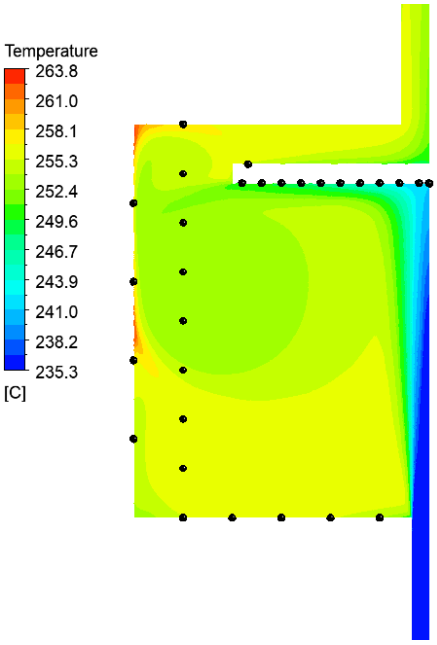


Figure 4.52 – Temperature distribution inside the 3D-Test Section during the initial steady state with the 2D improved model [74].

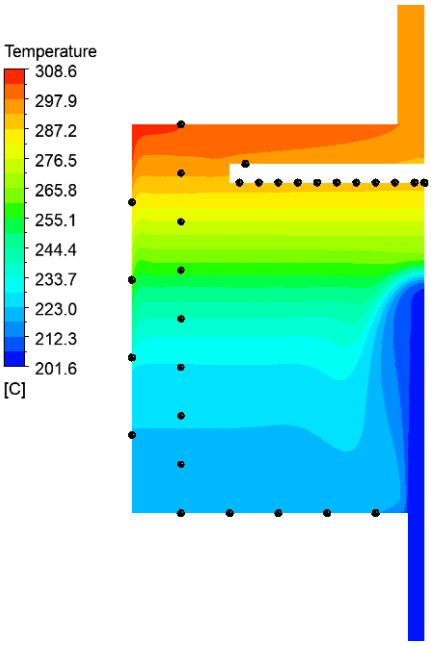


Figure 4.53 – Temperature distribution inside the 3D-Test Section during the final steady state with the 2D improved model [74].

Figure 4.52 and Figure 4.53 report the temperature distributions inside the 3D-TS for the initial and final steady states. Since the provided power from the heaters is the same, the thermal gradients are much higher in the final steady state. The contours clearly show how the inlet jet is able to achieve a good pool mixing in the initial steady state, with temperatures at the lower face of the pool close to the exit one. Once the final steady state is reached, thermal stratification becomes evident throughout the pool, except for a small region above the inlet section, where a small effect of the inlet jet could be noticed.

After the assessment of the overall behaviour of the CFD model in steady state conditions, a transient simulation is performed to give confidence in the application of the CFD model within the coupled tool. Imposing the experimental mass flow rate and inlet/outlet temperatures, the model is tested evaluating the capability to reproduce the phenomena inside the pool.

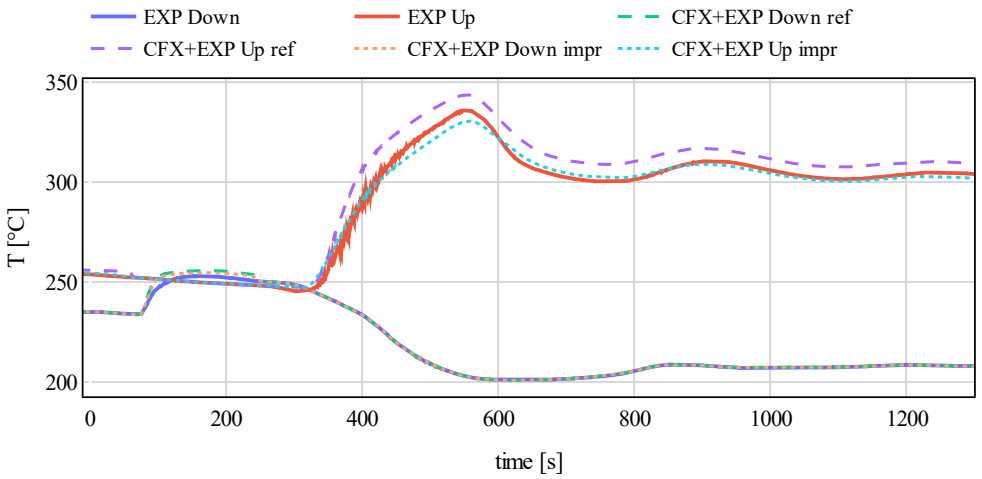


Figure 4.54 – Transient simulation with the Ansys CFX model and boundary conditions from experimental results [74].

In Figure 4.54, the temperatures monitored at the lower (Down) and upper (Up) 3D-TS boundaries are reported for the *reference* case without correction on the thermal conductivity of the insultation and the *improved* model defined to match the heat losses (which has already proven to better estimate the temperature field in steady state condition).

In the transient plots, the time axis zero point coincides with the moment the magnetic pump is shut down. The simulation is configured such that the experimental temperature is imposed at the upper section during the time interval

when the mass flow rate reversed (75-260 seconds) and at the lower section otherwise. Analysing the temperature trends, differences are observed in the predicted system thermal dynamics, particularly regarding the peak temperature reached at the upper boundary during the transient. The *reference* case overestimates the maximum value, while the *improved* model slightly underestimates it but exhibits excellent agreement with experimental data during the remaining part of the transient. Given these results, the performance of the 2D *improved* CFD model is deemed satisfactory for the coupled application.

System scale modelling

The R5 standalone model of the facility is composed by pipes, junctions and pump components (Figure 4.55). A total of 380 fluid volumes discretizes the entire domain. The average volume length corresponds to 5 cm, maintaining a node length-to-diameter ratio greater than 1, and adopting the sliced modelling approach [65] already introduced in section 4.2.2. The primary fluid is LBE, and the free level is set in PIPE 134 corresponding to the expansion vessel. Here the pressure boundary condition is imposed with a time dependent volume. The electromagnetic pump (in the green box in 4.51) is simulated with the PUMP component, that is intended to be a mechanical pump in R5. Therefore, proper modifications have been done to adjust the power provided to the LBE by the pump. Evaluation of T-junctions pressure loss coefficients is performed according to Ref. [67], while flow meters and ball valves pressure losses have been calibrated according to Ref. [71].

The secondary fluid in the heat exchanger is Dowtherm RP, a diathermic oil. However, due to RELAP5's limitations, water with modified operating conditions is used instead. Water with respect to the oil has similar density, higher heat capacity and thermal conductivity. A calibration of the secondary side conditions is carried out to match the initial and final steady state. The temperature, pressure, and mass flow rate of the secondary fluid are controlled by time-dependent volumes and a time-dependent junction.

Heat transfer with the solid structures is simulated by heat structures components. The MH rod and the 3D-TS heating are simulated by structures with volumetric heat generation, while the heat transfer from LBE to the secondary fluid is modelled through a heat structure that take into account the thickness of the tube. The additional thermal inertia of the metal of solid structure such as valves and flow meters are considered. Heat loss to the surrounding environment was accounted for

by including an insulating layer. The environment was modelled as having a constant heat transfer coefficient of 8 W/m^2 K and a constant temperature of 10°C.

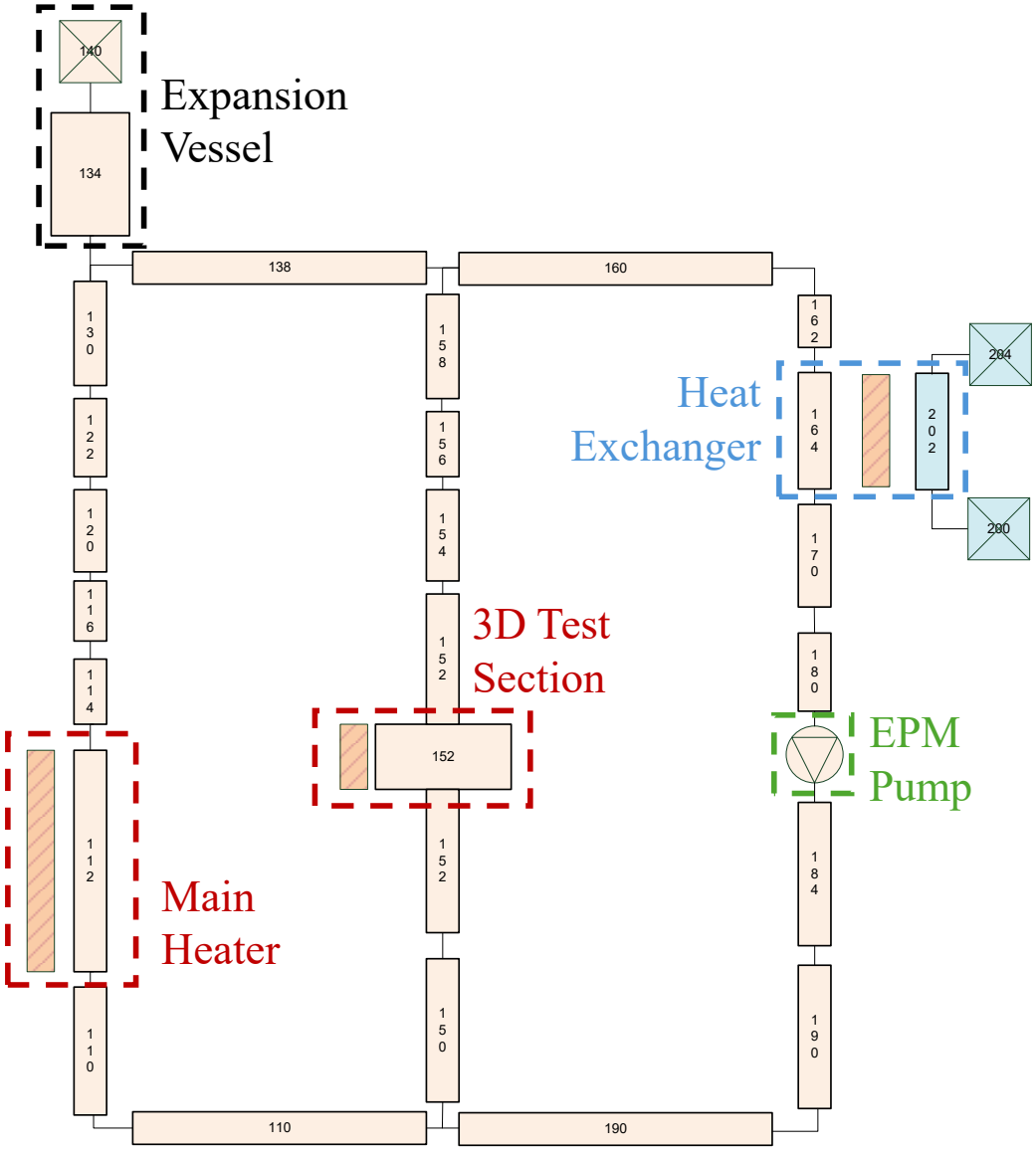


Figure 4.55 – RELAP5 nodalization of TALL-3D facility [74].

The coupled simulations adopt two different RELAP5 models according to the spatial discretization approach:

- decomposition approach: the 3D-TS leg is opened, and short horizontal volume, time dependent volumes and junction are included to allow information exchange at the boundaries of the domain;

- overlapping approach: the overlapped domain is substituted by two small horizontal volumes and a single volume with dimension equivalent to the CFD domain.

A full description of the strategy is reported in chapter 3. The 3D-TS is modelled in both approaches with the Anys CFX domain previously described.

Coupled tool simulation results

For the TALL-3D the decomposition, overlapping CU and overlapping CA approaches are tested. The information exchanged for each approach are summarized in Table 4.14.

Table 4.14: Information exchanged during the TALL-3D coupled simulation for the different approaches.

	Decomposition	**Overlapping CU**	**Overlapping CA**
From R5 to CFX	- Mass flow rate - Temperature at the boundaries	- Mass flow rate - Temperature at the boundaries	- Mass flow rate - Temperature at the boundaries
From CFX to R5	- Mass flow rate - Temperature at the boundaries - Pressure at the boundaries	- Temperature at the boundaries - Volume averaged temperature - Junction pressure loss coefficient	- Temperature at the boundaries - Volume averaged temperature - Friction factor

The first test of the tool consists in the application of the decomposition approach with both the explicit and semi-implicit time advancing schemes at different coupling timesteps. The results of the mass flow rate in the 3D-TS leg are reported in Figure 4.56. The legend of the figures indicates the method ('ex', explicit or 'si', semi-implicit) and the timestep between two exchanges of information that coincides with the CFX timestep. The R5 timestep is kept constant and equal to $2 \cdot 10^{-2}$ s to highlight the effect of the coupled timestep.

Other tests with smaller timestep give strange results like oscillatory behaviour or numerical instability. Preliminary analysis shows that the two models (R5 and CFX) could be the cause of this behaviour when small timesteps are adopted. For what concern CFX this was visible also in standalone transient simulation, while regarding R5 it was visible with successive restart of the code with small timestep. These problematics are not visible with the timestep presented in this thesis. Further

investigations are required on the topic, extending the analysis to the overlapping approach, for which the analysis was conducted only for the showed timestep.

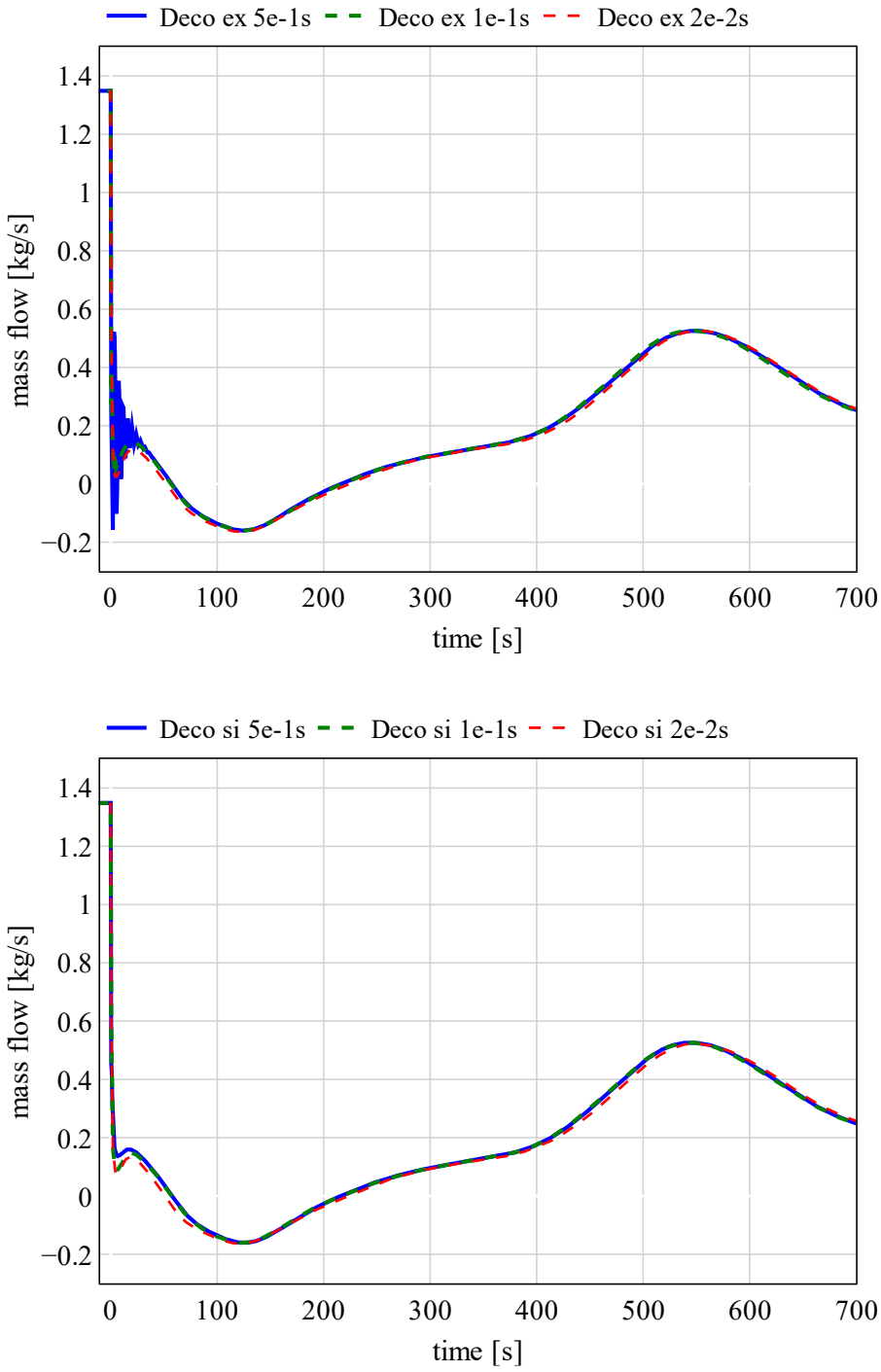


Figure 4.56 – Coupled simulation with the decomposition domain approach at different coupling timestep with the explicit (top) and semi-implicit (bottom) time advancing schemes [74].

Table 4.15: Computational time with the decomposition domain approach at different timestep for the explicit and semi-implicit time advancing schemes [74].

Coupling timestep	Explicit	Semi-implicit	Semi-implicit/explicit ratio
2e-2 [s]	5.399e5 [s]	7.618e5 [s]	1.41
1e-1 [s]	1.336e5 [s]	2.186e5 [s]	1.64
5e-1 [s]	4.092e4 [s]	6.461e4 [s]	1.58

The explicit scheme exhibited numerical oscillations when using a large time step (5e-1s) at the onset of the transient. However, a suitable time step could be determined to eliminate these oscillations. In contrast, the semi-implicit scheme did not produce any oscillations. Any numerical oscillations that did occur were damped out within a short time, and the final results were essentially identical to those obtained without oscillations.

Employing both time advancing schemes, the major discrepancies could be noticed during the fast reduction of mass flow rate due to the magnetic pump stop. However, the results almost coincide after around 100 s and there are no notable differences between explicit and semi-implicit schemes. The difference between 1e-1s and 2e-2s timestep simulations are barely visible.

In Table 4.15, a comparison of the computational time required by the different simulations at various timesteps and with both the time advancing schemes are reported. The comparison is carried out with the same solver setup and the same computational power (24 CPU). The ratio between the computational time of the semi-implicit scheme over the explicit one is around 1.5.

The same calculations are repeated with the overlapping CA approach for both the explicit and semi-implicit time advancing schemes (Figure 4.57), along with a comparison with the results obtained adopting the overlapping CU simulated with only the 1e-1 timestep. The dependence on the time step was minimal for all schemes except the explicit scheme at the highest time step. In this case, numerical distortions in the mass flow rate were observed when the velocity approached zero or changed direction. These distortions were caused by numerical discontinuities in the friction factor calculation, resulting in localized spikes. A deeper study to reduce the numerical distortion when velocity approaches zero should be carried out in the prosecution of this thesis. No oscillations were present in the overlapping simulations. The differences between the CU and CA overlapping approaches were minimal, confirming the validity of both formulations.

The analysis on the computational time needed for the simulations with the overlapping approach has negligible differences with respect to the decomposition one (Table 4.15), not adding any new information and thus not showed.

Eventually, Figure 4.58 shows the overlay of the results obtained with a timestep of 1e-1s for both explicit and semi-implicit time advancing schemes, implementing the decomposition and both overlapping domain approaches. The plot shows that the variance of the solution is limited, demonstrating the independence of the results with respect to the selected coupling approach.

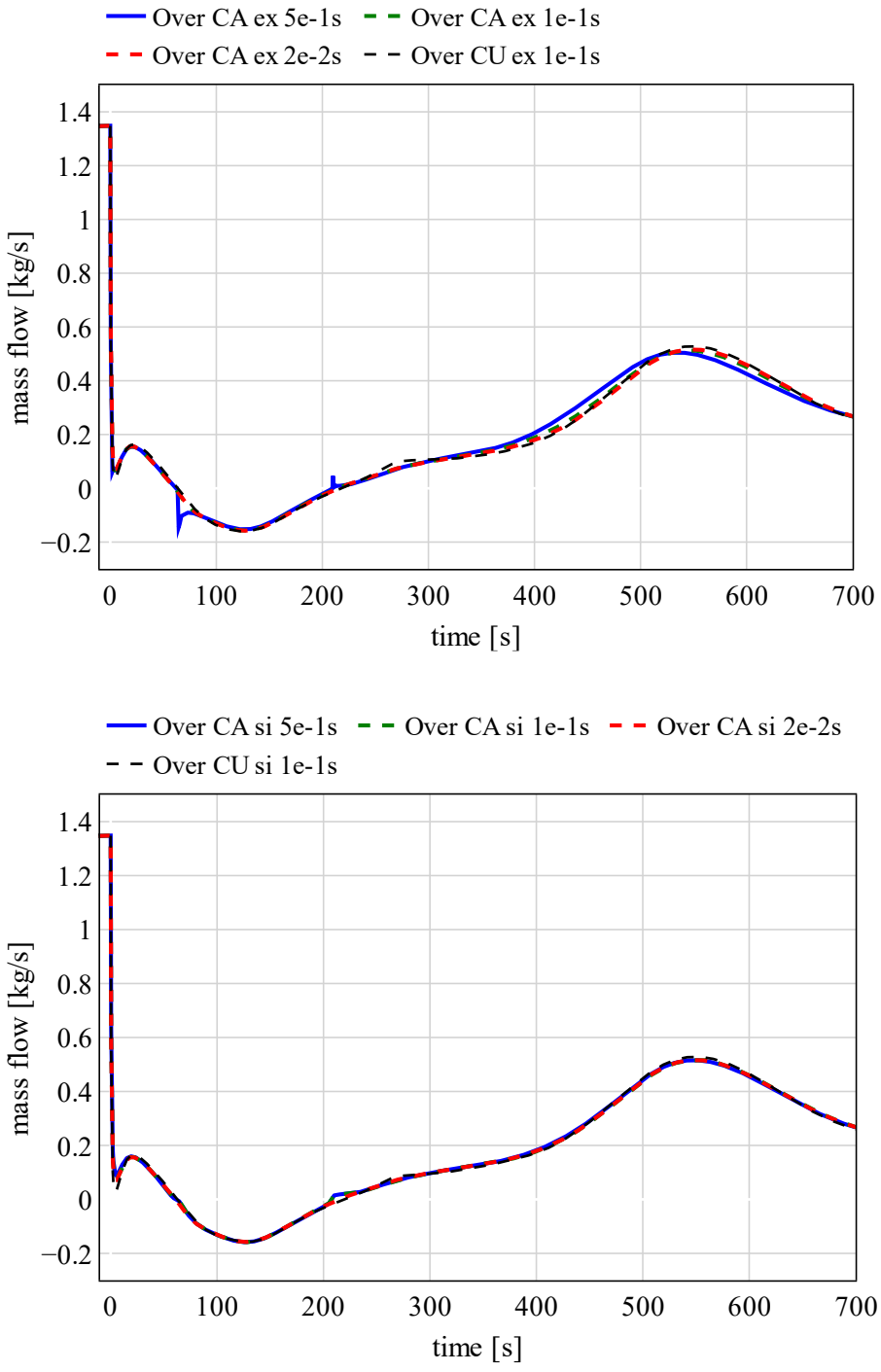


Figure 4.57 – Coupled simulation with the overlapping domain approach at different coupling timestep with the explicit (top) and semi-implicit (bottom) time advancing scheme [74].

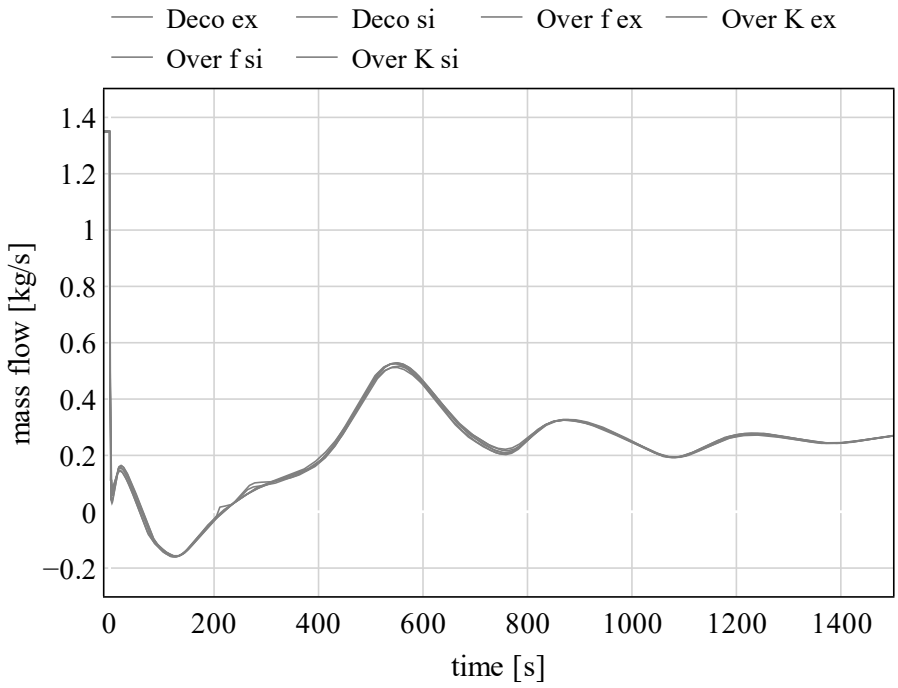


Figure 4.58 – Overlay of the mass flow rate in the 3D test section leg for all presented coupling approaches with a timestep of 1e-1s [74].

The comparison of the coupled tool with experimental data and the standalone RELAP5 Mod3.3 simulation demonstrates the improvement given by the CFD model in accurately representing the phenomena occurring within the 3D-TS and their impact on the overall facility behaviour. The coupled simulations using the decomposition approach, semi-implicit time advancement scheme, and a time step of 1e-1s is selected as the reference for the plots. In Figure 4.59, the coupled simulation with the decomposition approach shows improvements in reproducing the frequency of the experimental oscillations of the mass flow rate in the 3D-TS, even though their amplitude is slightly higher than the numerical ones. Similar conclusions could be drawn analysing the mass flow rate on the MH leg (Figure 4.60), with a notable improvement in the phenomena representation by the coupled approach.

The reason behind this behaviour could be found especially in the temperature at the 3D-TS model boundaries (Figure 4.61):

- the CFX-RELAP5 tool accurately predicted the initial temperature rise in the lower section caused by the mass flow rate reversal, demonstrating its ability to represent the initial steady-state conditions and flow reversal

within the test section. However, both the coupled and standalone simulations underpredicted the temperature trend for the remainder of the transient. This discrepancy is likely due to the use of a different secondary fluid in the heat exchanger instead of the synthetic organic Dowtherm RP fluid, resulting in different component performance;

- the temperature at the upper section is slightly underpredicted at the peak occurring around 580 s after the transient begins. Some possible explanations are to the higher thermal capacity of the CFD model, already demonstrated in Figure 4.54 and the lower temperature at the Down section, but an improvement in the representation of the oscillation frequency is, in any case, visible;
- at the final steady state, the temperature variation across the 3D-TS is slightly lower in the experiments caused by the slightly higher mass flow rate.

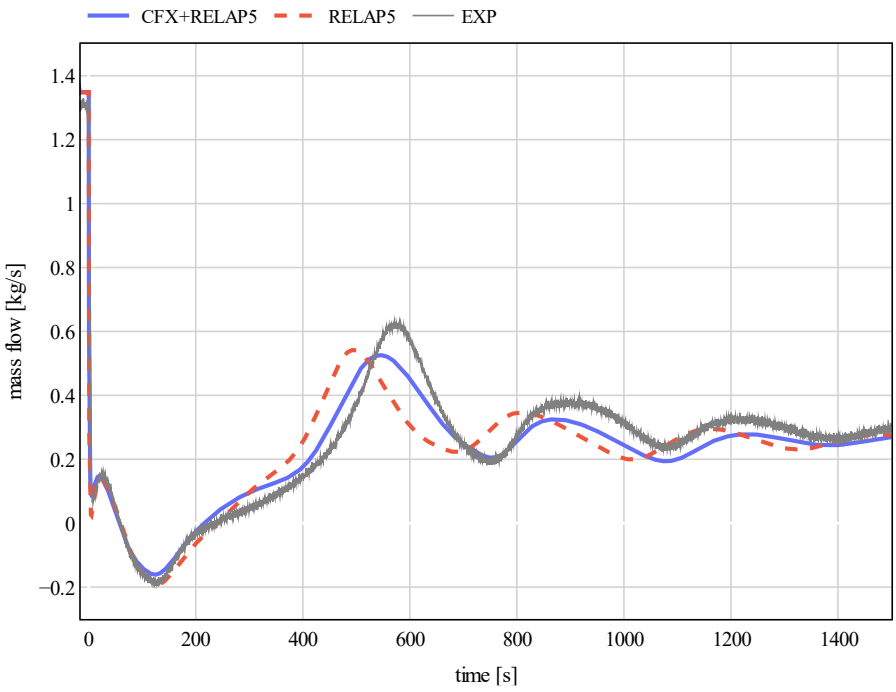


Figure 4.59 – Comparison between experiment, RELAP5 standalone and coupled simulation of the mass flow rate in the 3D test section leg [74].

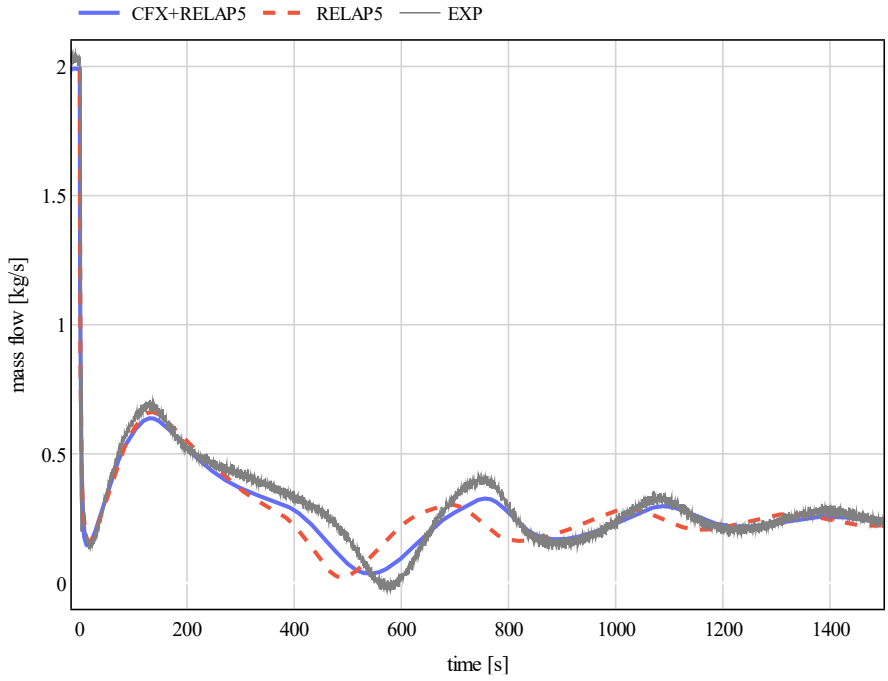


Figure 4.60 – Comparison between experiment, RELAP5 standalone and coupled simulation of the mass flow rate in the Main Heater leg [74].

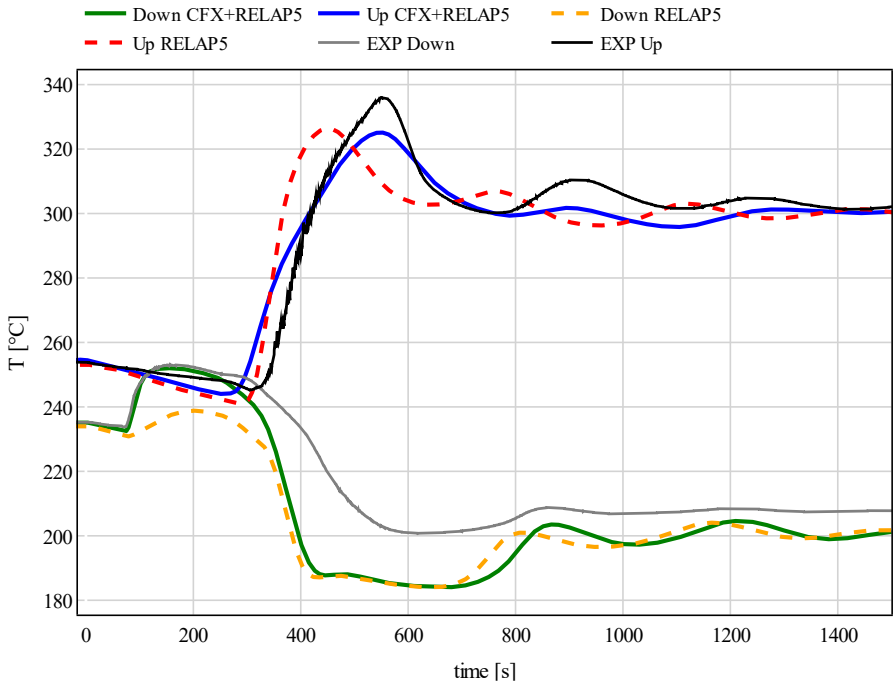


Figure 4.61 – Comparison between experiment, RELAP5 standalone and coupled simulation of the upper and lower surface temperature of the 3D test section [74].

The Ansys CFX - RELAP5/Mod3.3 tool gives the possibility to compare the results of the TCs inside the pool also during the transient. The IPT and CIP TCs are selected for this purpose. The IPT TCs are mounted on the vertical support, covering the entire length of the pool, while the CIP TCs are positioned on the horizontal plate. (Figure 4.48a). The results of the decomposition approach simulation (CFX+RELAP5) in Figure 4.62 clearly show the transition from a thermal mixing to thermal stratification condition inside the pool. A good agreement with experimental data is achieved in the upper region of the pool (IPT 1-3) located closer to the heaters. Going down in the pool the IPT temperatures are under-predicted: the reason could be found in a local bad prediction of the thermal losses, that gain more importance when the mass flow rate is reduced, or a slightly worse performance of the CFD model in the transition toward an almost fully conductive heat transfer condition within the fluid, or behind the underestimation of the temperature entering the pool from the lower section. In Figure 4.62 the dot lines represent the results obtained with the CFX model in which the experimental boundary conditions are applied (CFX+EXP), already discussed in the 3D test section model subchapter (*improved* model). The results are closer to the experimental ones with respect to the coupled simulation, also for what concern the IPT TCs located in the lower part of the pool. This fact supports the idea that the errors are related to the underestimation of the temperature entering the pool from the lower section.

In Figure 4.63, the CIP temperatures could be described as follows:

- in the first 450 s the CFX+EXP and CFX+RELAP5 results under-predict the experimental value;
- from 630s toward the final steady state of the CFX+RELAP5 calculation under-predicts the results, with a similar behaviour seen in the IPTs and lower section temperatures;
- between 450 s and 630 s, the experimental results show a drop of temperature due to the injection of cold fluid in the pool. This is captured for the central TCs in the horizontal plate (e.g. CIP 1) by the CFX+EXP simulations, but not for all the one presents (e.g. CIP 5). In the CFX+RELAP5 simulations the drop of temperature is not predicted for any TCs, mainly due to the differences in the mass flow rate and the temperature at the lower section.

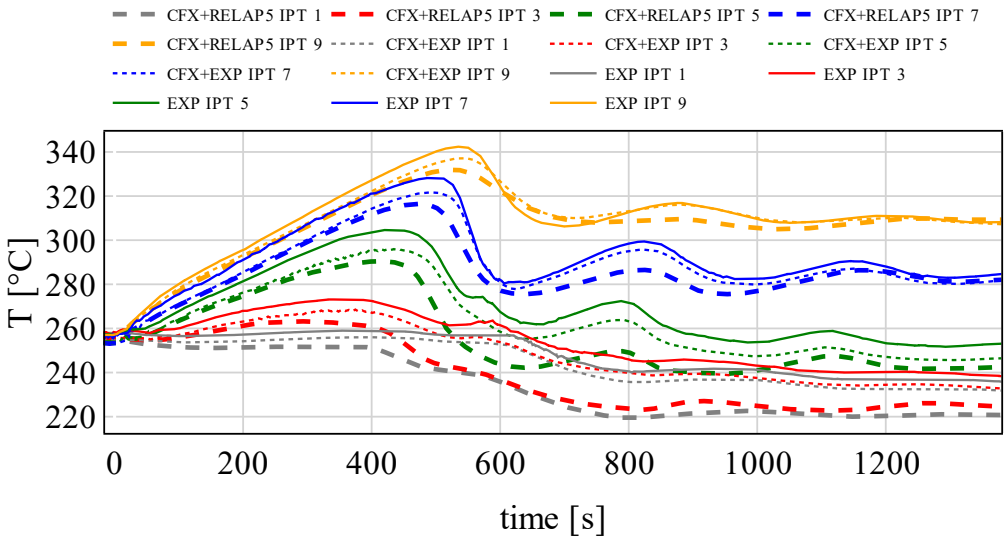


Figure 4.62 – Comparison between experiment, coupled decomposition simulation and CFX transient simulation of IPT thermocouples inside the 3D test section [74].

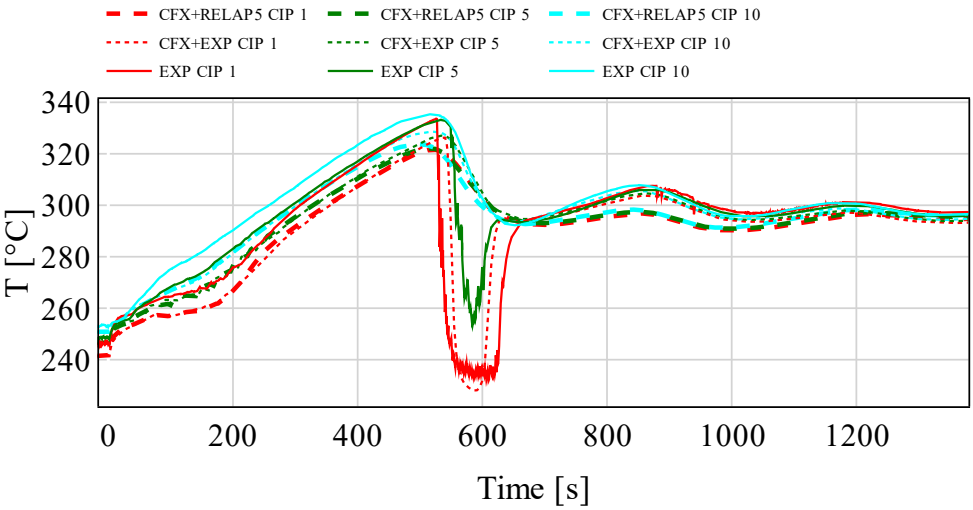


Figure 4.63 – Comparison between experiment, coupled decomposition simulation and CFX transient simulation of CIP thermocouples inside the 3D test section [74].

4.2.4 Lesson learned from loop type facility test cases

The experience gained with the Ansys CFX – RELAP5 Mod3.3 coupling tool applied to loop type facilities is fundamental for demonstrating the tool capabilities and for reaching important conclusions.

For the coupling approach, the three applications (NACIE, NACIE-UP, TALL-3D) are characterized by an increased level of complexity:

- NACIE could be considered a simple loop. All the components could be easily modelled and for all of them a mono-dimensional approximation is likely effective. Well known correlations and modelling strategies can be applied to define a loop model that is able to represent the system condition. This application can be considered among the ones where STH performances are likely to be satisfactory. The results presented in section 4.2.1 confirm the correctness of the coupling approaches under condition coming from experiment, beyond the test case presented in section 4.1. The coupling does not introduce significant errors or distortions in the representation of the phenomena.

- The NACIE-UP experiment represents a further step up in complexity, as each code (CFD and STH) is applied to increasingly challenging conditions and geometries. The activities for the development of the coupled model are strictly correlated to the two standalone models, which have required to be refined for effectively reproducing the experimental results. For what concern the physical phenomena studied by the coupled tool, the level of complexity is similar to the NACIE one.

- The TALL-3D case includes a strong simplification of the CFD model with respect to the NACIE-UP application, but the thermal mixing to stratification transition in the 3D-TS and the strong feedback of the phenomena occurring in the pool to the entire system behaviour determine a more complex system scale analysis. The coupled tool has been tested also to represent a case with inversion of the flow rate, a condition that shall be included within a validation process.

Chapter 4.2 reports the first set of validation cases that enhances the maturity of the coupled tool and poses the basis for more complex applications. To follow

the lesson on the application of the tool and on the choice of the coupling approach among the one discussed in this work are presented.

Application of CFD-STH coupled tool

The following general lessons can be learned from the carried out activities:

- **The coupled tool is really effective for cases in which an improved component representation influences the system behaviour**. The NACIE-UP case is the demonstration of an application where a CFD model allows to have more accurate and complete information on the TH behaviour of a component (FPBS); however, the feedbacks on the system behaviour (pressure drops, thermal balance, inlet and outlet temperature) are well captured by the STH code, thus not requiring resorting to the coupled tool to accurately predict the system behaviour. On the other hand, TALL-3D clearly shows how the CFD model is capable to capture the condition occurring in the test section and the effects on the overall system influencing in particular the temperatures at the 3D-TS boundaries.
- **The coupled tool relies heavily on the reliability of the models developed independently within the CFD and STH codes.** This is a straightforward conclusion, but it is important to highlight how the application of coupled tool follow the demonstration of maturity of CFD and STH codes in relevant application for LFR safety analysis.
- **A coupling approach, no matter how well-developed and efficiently optimized, introduces complexities that should be avoided if not essential**. Standalone CFD steady state simulations can be, for example, adopted for the characterization of the pressure drops or heat transfer behaviour of an innovative system for which reliable correlations are not available. The data coming from this previous numerical activity can be used for refining the STH parameters and correlations. On the other hand, the standalone STH code can be run to generate boundary conditions for a subsequent standalone CFD transient simulation. A proper phenomenological analysis of the system and the transient that is intended to be studied is necessary before deciding to apply a coupled CFD-STH tool.
- **In the validation process of a newly developed coupled code, experiments in loop type facilities are fundamental.** Data coming from campaigns conceived for the validation of this kind of TH tools, like TALL-3D, demonstrate to be capable of introducing important challenges to the

coupled approach that need to be addressed before the application to pool type facilities.

Choice of the coupling approach

If the previous subsection aims to answer to the question “when is it worthy to adopt a CFD-STH coupled tool?”, in this section conclusion regarding the choice of the coupling approach among the ones here presented is discussed:

- decomposition explicit
- decomposition semi-implicit
- overlapping CU explicit
- overlapping CU semi-implicit
- overlapping CA explicit
- overlapping CA semi-implicit

The analyses presented in chapter 4.1 and 4.2 are not intended as complete and definitive analysis of the possible choices, rather, they represent an initial study to guide future development.

The domain decomposition approach is easier to implement. As the complexity of the problem increases, the implementation remains largely the same, with only an increase in the number of variables to be exchanged. In the cases discussed, it is evident that the explicit scheme is less numerically robust than the semi-implicit one, leading to numerical oscillations when rapid variations in hydraulic parameters occur. Generally, the properties of heavy liquid metals tend to smooth thermal fluctuations, while mass flow rate can change rapidly in a nuclear scenario. Here, "rapid variation" refers to fast changes with respect to the adopted timestep. Another important consideration is ensuring the conservation of quantities, particularly when distribution maps need to be applied at the Ansys CFX boundaries.

The overlapping CU approach appears to be superior to the CA method only when mass flow inversion occurs. The development of the CU method is easier but requires tuning of some parameters that are case dependent. The overlapping CA method seems to be the most promising due to the possibility of directly computing values to match the CFD result, while ensuring conservation of quantities in the domain.

The achieved maturity and future developments of the approaches are here presented:

- decomposition approach:
  - an analysis of the relaxation factor implemented in the tool needs to be conducted for the semi-implicit scheme;
- overlapping approach:
  - cases where more than 2 boundaries are present (multiple inlet and/or multiple outlet) shall be addressed;
  - improvement in the representation of mass flow inversion with the CA method are necessary;
  - modification of the RELAP5 code to allow the definition of the friction factor through a control variable can increase the implicitness of the CA method, strongly reducing the differences between the explicit and semi-implicit result;
- both the approaches:
  - tests with thermal boundaries conditions need to be addressed;
  - advancement in the RELAP5 data management during the restart file generation and extraction of data from the restart file should be investigated (e.g. double precision);
  - user-interface can be improved to facilitate the tool application.

Overall, at the current stage, the decomposition approach with a semi-implicit scheme can be considered the most ready-to-use method. The overlapping CU method with the explicit scheme shows promise as the most advanced approach, provided the issues presented are resolved.

4.3 Modelling of the ATHENA pool type facility

Within the ALFRED Research – Infrastructure program [76], ATHENA (Advanced Thermal-Hydraulics Experiment for Nuclear Application) is being constructed in Mioveni (Romania) at the Institutul de Cercetari Nucleare (ICN) research centre. It is an electrically heated 2.21 MW pool type multipurpose facility with a large size vessel of 10 m in height and 3.2 m in diameter. A wide range of LFR system aspects will be examined in the pool, including full-scale tests of single ALFRED components and their interactions, as well as specific separate-effect tests relevant fot safety and/or design. Furthermore, it represents an important

demonstration of coolant chemistry control capabilities in large pool, and it will provide a large experimental database suitable for code validation and model development to support a broad spectrum of LFR projects and associated licensing activities.

ATHENA will be fundamental toward the licensing of ALFRED, but it is not intended to be adopted for the simulation of reactor safety relevant transients. For this purpose, the ELF (Electric Long running Facility) facility will be designed, with the goal to assess system performance and long term reliability of the components (e.g. the pump) [76].

The commissioning of the ATHENA facility will be carried out in early 2025. Among the different activities, ATHENA is part of the facilities involved in the LESTO (LEad fast reactor Safety design and Tools) [77] European project, coordinated by ENEA, started in November 2024, in which a Protected Loss Of Flow Accident (PLOFA) is foreseen.

In this chapter, after the description of the facility, three cases are considered for evaluating the performance of the Ansys CFX – RELAP5 Mod3.3 tool applied to ATHENA:

- in section 4.3.2, the mixing zone above the multi assembly main heater system is simulated during a mass flow reduction transient;
- in section 4.3.3, the main pool is simulated with the CFX and R5 standalone models to evaluate the difference in time required to detect a temperature increase at the heat exchanger outlet to be noticed at the inlet of the conduit that feeds the Core Simulator;
- in section 4.3.4 a PLOFA of the entire facility is reported, adopting the CFD code to simulate the Core Simulator, with focus on the heat transfer in the inter-wrapper region.

For all the three test cases, no experimental data are available, thus a code to code analysis is performed.

4.3.1 ATHENA facility

ATHENA is a large pool-type multipurpose facility, having a power installed of 2210 kW. It uses pure lead as primary coolant and pressurized single phase water as secondary cooling fluid. The main features of the ATHENA design are represented by a large size vessel, with the same height currently foreseen in

ALFRED, which is capable to host and test single and coupled full scale components.

The internals (Figure 4.64) comprise:

- the suction duct from the main pool (Feeding Conduit), equipped with a Venturi flow meter and connected to the heater housing duct;
- the main electrical heater, the Core Simulator (CS), reproducing an ALFRED average FA;
- a riser that contains the main pump and connects the heater outlet to the Separator;
- the Separator, a hot pool that connects the riser to the Main Heat eXchanger (MHX);
- the MHX, the facility main heat sink.

Hosted in the riser. the pump is a vertical one, axial type with axial suction and discharge. The pump impeller, shell and any other part in contact with the heavy liquid metal is made of AISI 316L. The pump impeller and pump shaft are alumina coated by chemical vapour deposition (pack cementation) to better withstand the corrosion induced by high temperature corrosion/erosion environment.

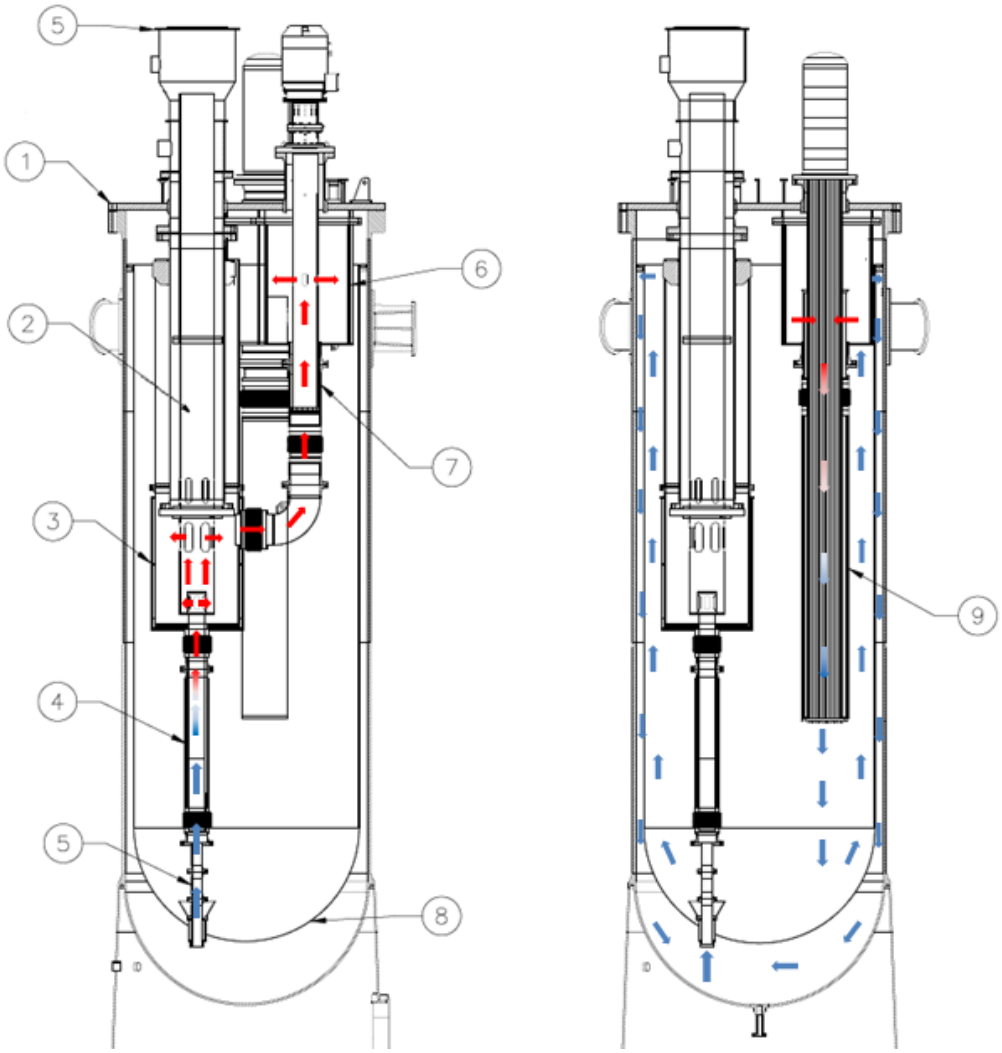
From the pump exit, the hot lead reaches the Separator (or hot pool). After the hot lead has flown downward through the shell side of the MHX, where it is cooled by a dedicated secondary loop, it reaches the bottom of the barrel. In the barrel, the lead rises up to the free surface in the cover gas region and flows in the main pool through a series of holes. Eventually the flow crosses the region between barrel and main vessel to reach the lower part of the main pool, where the inlet of the feeding conduit is located. The barrel covers and tests the function of the internal structure described in section 1.2.1 and reported in Figure 1.2, where the main components of ALFRED are shown.

Since the pins in the CS are electrically heated, an isolated volume, called dead volume, is installed above the CS. Inside the dead volume, there are the pin tails where the heat is generated by residual joule effect. The dispersed heat is removed by air in forced circulation regime avoiding high temperatures on the pin tails.

The main constraint for the design of the internals of the ATHENA facility is the distance between the thermal barycenters of the CS and the MHX, that must be equal to 3350 mm to be representative of the ALFRED layout, allowing to reproduce the main phenomena in natural circulation regime.

The nominal operation conditions are characterized by a thermal cycle of 400 °C to 520 °C, reaching in the hottest spot of the CS value around 550 °C, and a nominal mass flow rate of 126 kg/s.

In the following subsections, the CS and the MHX are described and graphically represented.



Legend					
1	*Main Vessel*	**4**	*Core Simulator*	**7**	*Main Circulation Pump*
2	*Dead Volume*	**5**	*Feeding Conduit*	**8**	*Barrel*
3	*Fitting Volume*	**6**	*Separator*	**9**	*Main Heat Exchanger*

Figure 4.64 – ATHENA main vessel layout and primary coolant flow path [78].



Figure 4.65 – ATHENA main vessel (top left), cover (bottom left) and internals (right).

Core Simulator

One of the first objectives of ATHENA is the thermal-hydraulic characterization of a core mock-up, represented by the Core Simulator (CS), both

in forced and natural circulation, including inter-wrapper flow and thermal coupling among fuel assemblies (FAs).

The CS configuration is characterized by 127 pins and seven FA. A cross section is reported in Figure 4.66, where the wrappers subdivision is highlighted: a hexagonal central one (in blue) with 61 pins (60 active + 1 dummy central element) is surrounded by 6 smaller polygonal wrappers (in blue) with 11 pins each. Around them, a polygonal shroud (in green) is installed to limit lead bypass around the assemblies.

The design configuration aims to be representative of an averaged ALFRED FA, since the effect of the adjacent FAs in the reactor core is simulated by the 6 smaller wrappers surrounding the central one.

The active length of the pin is 810 mm, with a total length in lead of 3070 mm from the bottom grid – which maintains the pins in the correct position – to the flange that isolates the lead from the dead volume through a sealing mechanism. The total length of the pins is composed by the immersed length, the dead volume length, and the final part exiting the vessel flange.

Together with the bottom grid, an upper grid and 3 spacer grids are used to maintain in position the entire pin bundle. In Figure 4.67, the design of the spacer grids for the two kind of bundles is reported.

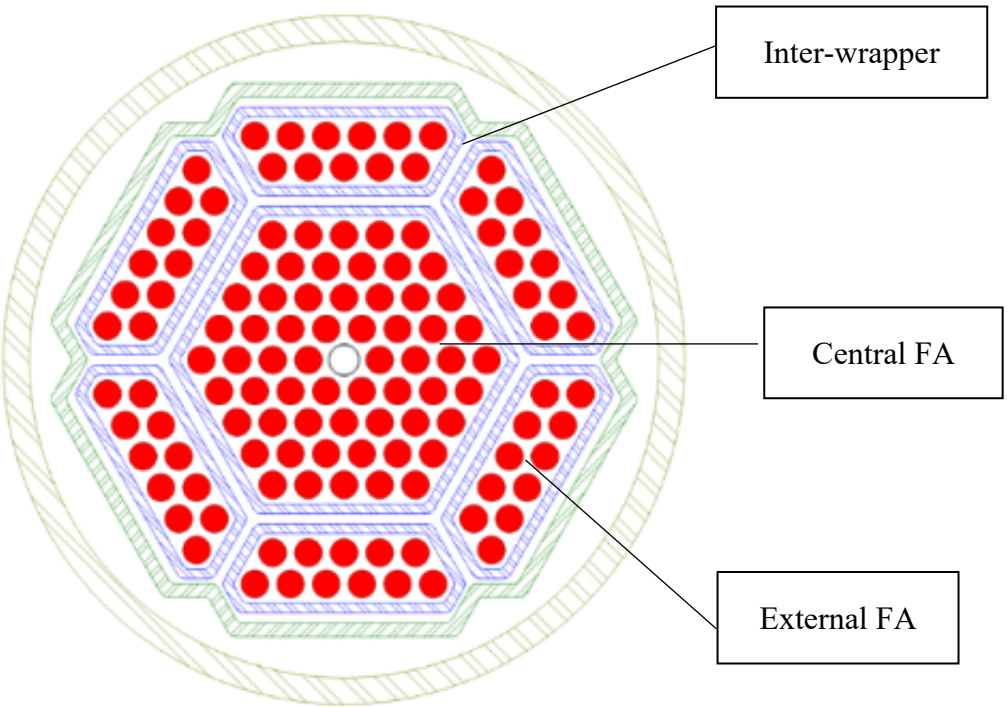


Figure 4.66 – Schematic layout of the ATHENA fuel assemblies [78].

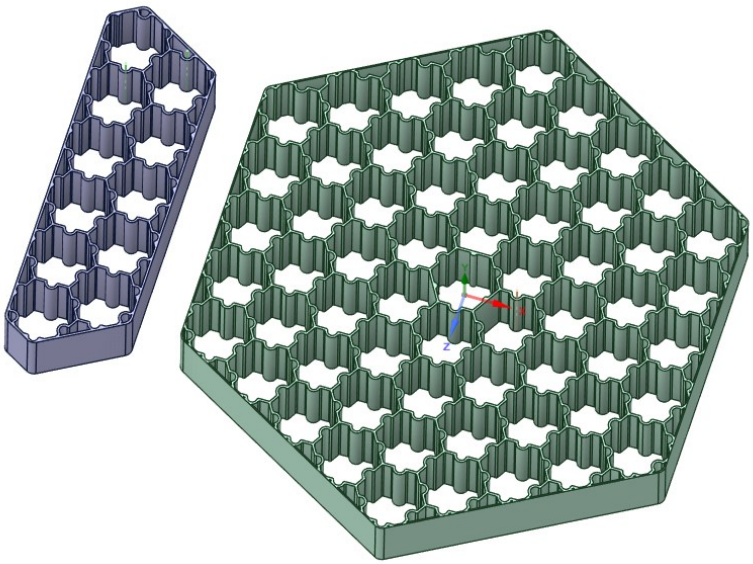


Figure 4.67 –Design of the spacer grids for the internal and external FAs.

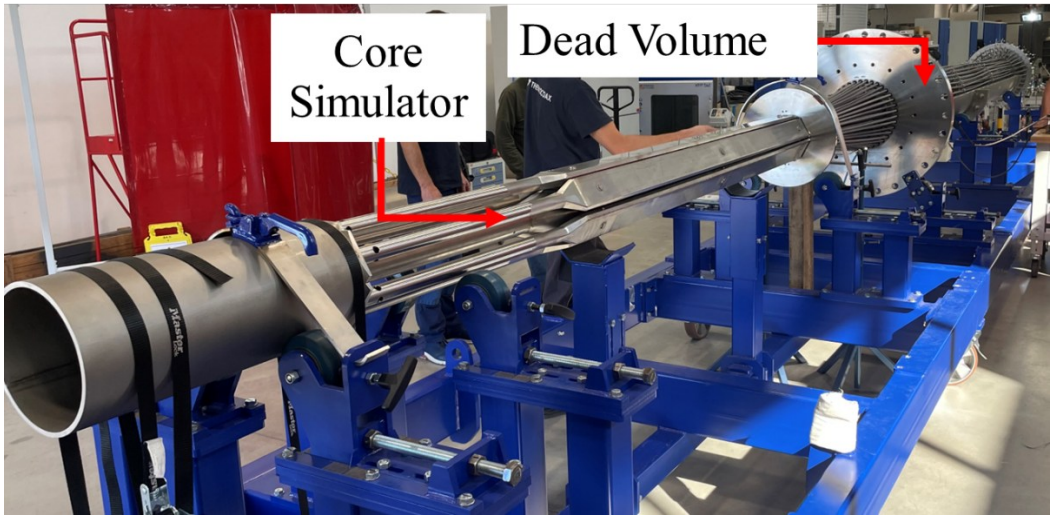


Figure 4.68 –Core Simulator and Dead Volume before the installation in the main vessel.

Table 4.16: Core Simulator geometry and operational parameters.

Parameter	Unit	Value
Pin diameter	mm	10.5
Central pin Diameter	mm	12.0
Pitch	mm	13.6
Pitch to Diameter ratio	----	1.29
Number of pins	----	126 (active)+1 (dummy)
Number of FAs	-	1 (61 pins) + 6 (11 pins)
Active length	mm	810.0
Pin total length	mm	8550.0
Wrapper thickness	mm	3.5
Central wrapper hexagonal key	mm	109.0
Shroud hexagonal key	mm	199.0
Gap between wrappers	mm	4.0
Total power	MW	2.21
Linear power	kW/m	21.65
Design mass flow percentage in the Central hexagonal Assembly	%	47.4
Design mass flow percentage in the External partial Assembly	%	8.5
Design mass flow percentage in the bypass	%	1.6

Main Heat Exchanger

The reference configuration of the MHX adopted in the ATHENA facility is based on the concept of Bayonet Tubes (BTs) and it is designed to remove from the lead pool a thermal power of 2210 kW (Figure 4.70). In this component, pressurized water is the secondary coolant, which enters the tubes side from a collector outside the main vessel at the top, then it flows downward through the slave tube that acts as a downcomer, reverses its direction at the bottom of the BTs, moves upward in the annular riser defined by the first and second tubes – where it exchanges power in counter current with respect to the Pb – and then exits into an outlet collector at the bottom of the inlet one. A dedicated secondary loop feeds the tubes of the MHX with pressurized water.

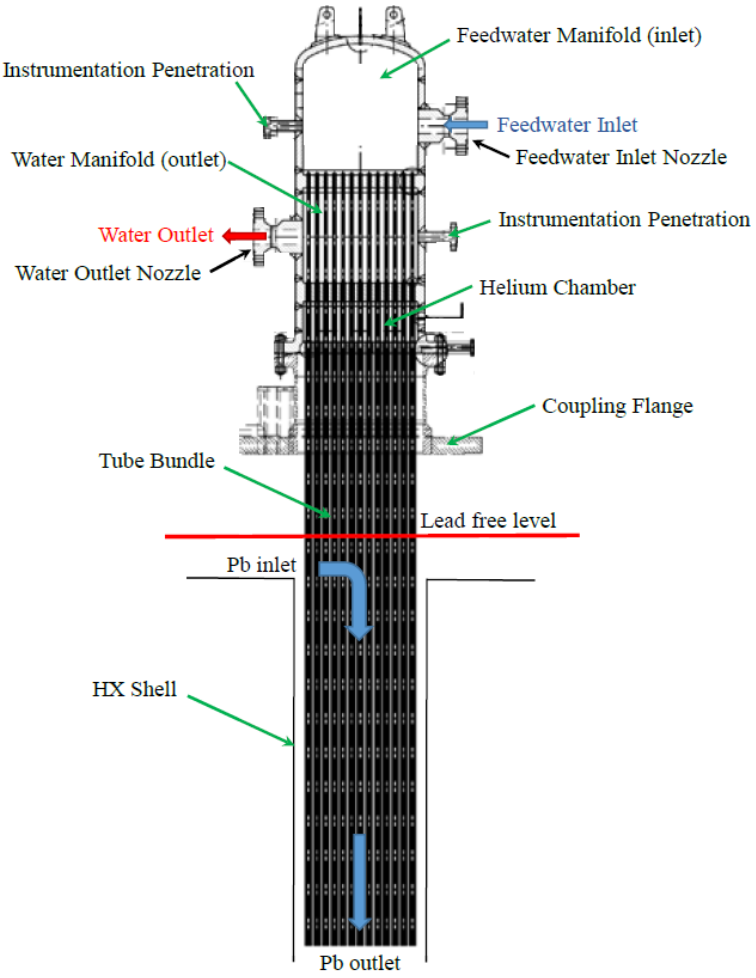


Figure 4.69 – Lateral view of the ATHENA Main Heat eXchanger.

The selected tube bundle active length is 3000 mm. It is composed of 91 BTs realized with 3 coaxial tubes, and it is arranged in a cylindrical geometry having a minimum pitch-to-diameter ratio of 1.3.

Table 4.17 summarizes the MHX main geometrical and operational parameters. The representation of the adopted configuration and the tube radial dimensions are reported in Figure 4.70.

Table 4.17: Main Heat eXchange geometrical and operational parameters.

Parameter	Unit	Value
Number of bayonet tubes	----	91
Tube bundle active length	mm	3000
p/D	----	1.3
Pitch geometry	----	Cylindrical
Bayonet tube geometry	----	3 coaxial tubes
Shell inner diameter	mm	499
Water pressure	MPa	2.50
Water temperature inlet	°C	110.0
Water temperature outlet	°C	200.0
Water mass flow rate	kg/s	5.67

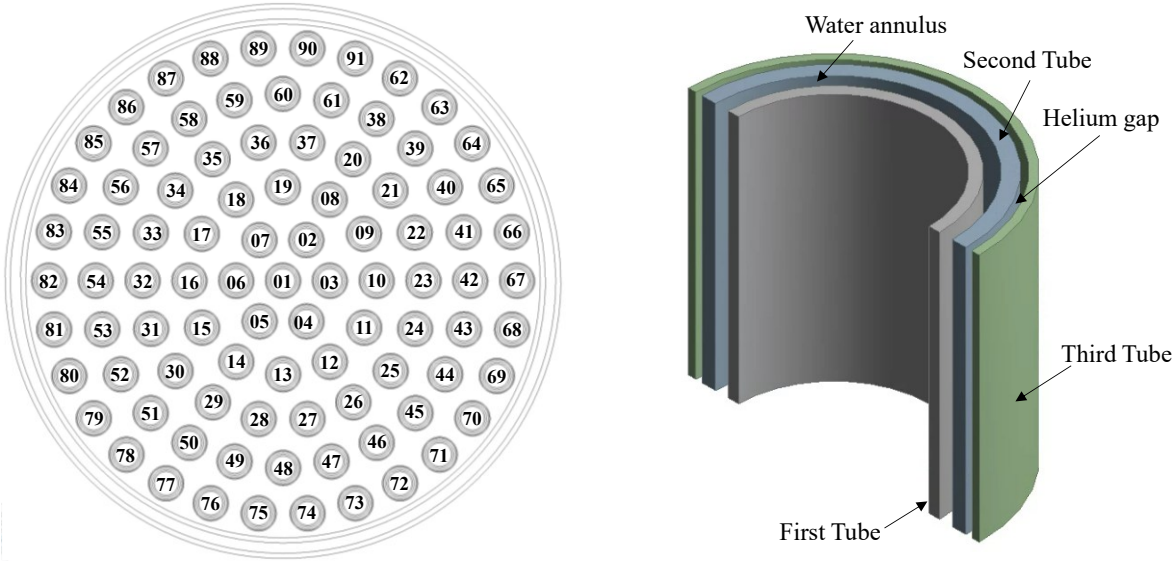


Figure 4.70 – Cross section view of the tube bundle (left) and of the bayonet tube structure (right).

4.3.2 Fitting Volume transient

The goal of the first ATHENA test case is to model the region where the lead coming from the eight channels of the CS (seven FAs and the inter-wrapper) is

collected, known as the Fitting Volume (FV). From this region, the mixed lead goes to the pump. The simulation domain for the test case corresponds to the FV integrated with the FC and the CS [52].

A transient simulation is performed by reducing flow while occluding 80% of the central channel's cross-sectional area. The 80% value is not representative of any specific real condition, but it is artificially selected to have a strong disturbance of the TH condition in the system. A constant pressure boundary condition is applied across the FC inlet and FV outlet. The change in mass flow rate causes a temperature rise at the channel exit. The generated hot fluid undergoes three-dimensional convection within the FV region, ultimately reaching the pump inlet.

To exploit the possible advantages of a CFD modelling, the coupled run foresees the FV simulated with CFX, including the solid structure reported in Figure 4.71. The CFX model receives mass flow rates and inlet temperatures from R5 for the three channels: the central FA, the external FAs integrated into a unified channel and the inter-wrapper channel. CFX then calculates the pressure variations at the three interfaces, which are subsequently imposed on the time-dependent volumes in the R5 model. In both coupled and standalone R5 simulations, the CS is represented by three pipes, one for each cannel (see Figure 4.72). A "fake" valve is inserted upstream of the active length in the central fuel assembly to initiate the transient at time 0 s by reducing the flow area. In the standalone RELAP5 model, the fluid exiting the CS is represented by a pipe connected to the FV, which is further modelled by two parallel pipes to enable potential recirculation within the volume. The average length of the fluid cell is 30 cm.

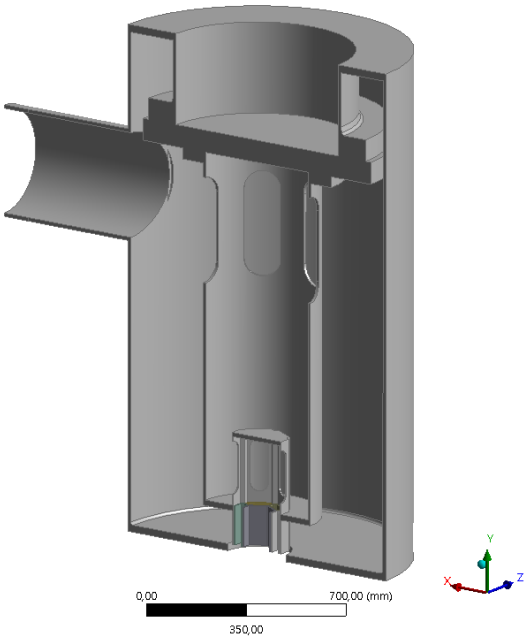


Figure 4.71 – Solid structures that define the ATHENA Fitting Volume CFD domain [52].

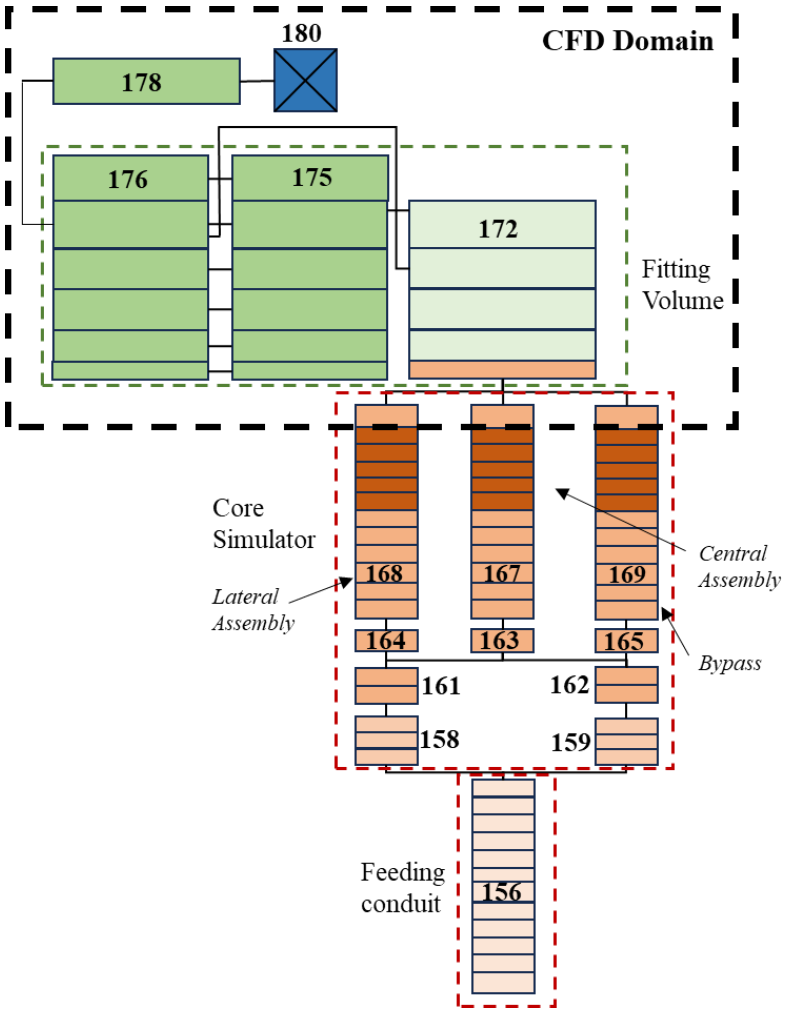


Figure 4.72 – RELAP5 nodalization of the Fitting Volume test case, with highlighted the part of the domain that in the coupled simulation are simulated in Ansys CFX [52].

In the CFD model, symmetry is exploited adopting only half of the 360° domain. Adiabatic conditions on the external walls are applied to simplify the problem: however, the assumption is justified by the fact that a double wall with air gap is foreseen in ATHENA to avoid heat transfer from the internals to the main pool. At the outlet section an opening boundary condition is imposed, with the fluid potentially re-entering with a temperature equal to 520°C. The adopted unstructured mesh consists of $5.64 \cdot 10^6$ cells. The decomposition domain approach and the semi-implicit numerical scheme are selected (see section 3).

The mass flow rate distribution (Figure 4.73) in the external and inter-wrapper (IW in the figures) channels is almost unchanged in both the initial and final steady

states, with a small increase, when the trigger of the transient is actuated, and it is almost identical among the two numerical models. The central channel mass flow rate shows a lower value for the coupled simulation with respect to the R5 standalone one during the entire analysis: this is due to a different evaluation of the pressure drops between the CFD and STH codes. Consequently, the temperature (Figure 4.74) increase in the CS shows lower values in the R5 standalone run, but with the same qualitative trend in time. The lead temperature exiting the inter-wrapper channel depends on the heat yield by the FAs to the bypass: after the transient the temperature is higher than the one exiting the external FAs due to the increase of the central FA value.

Even though the FV inlet conditions exhibit similar behaviour, the R5 standalone simulation shows a delay in the outlet temperature increase compared to the coupled simulation (Figure 4.75). While some possible discrepancies in representing the solid structure's heat capacity might influence the results, Figure 4.76 indicates that the intricate flow pattern within the FV also contributes to the transportation of hot fluid from the central channel's outlet to the FV outlet. In the domain, a thermal stratification is still visible after 1000 s from the start of the transient. At the outlet section a recirculation zone could be noticed at the bottom of the exiting conduit, where lead at 520 °C is introduced in the domain by the opening boundary condition. More realistic boundary condition at the outlet section could improve the reliability of the simulation (e.g. extending the conduit), but Figure 4.76 shows how the CFD code predicts the fluid re-entrance in the domain, phenomenon that could affect the temperature inside the FV and could not be represented by STH codes.

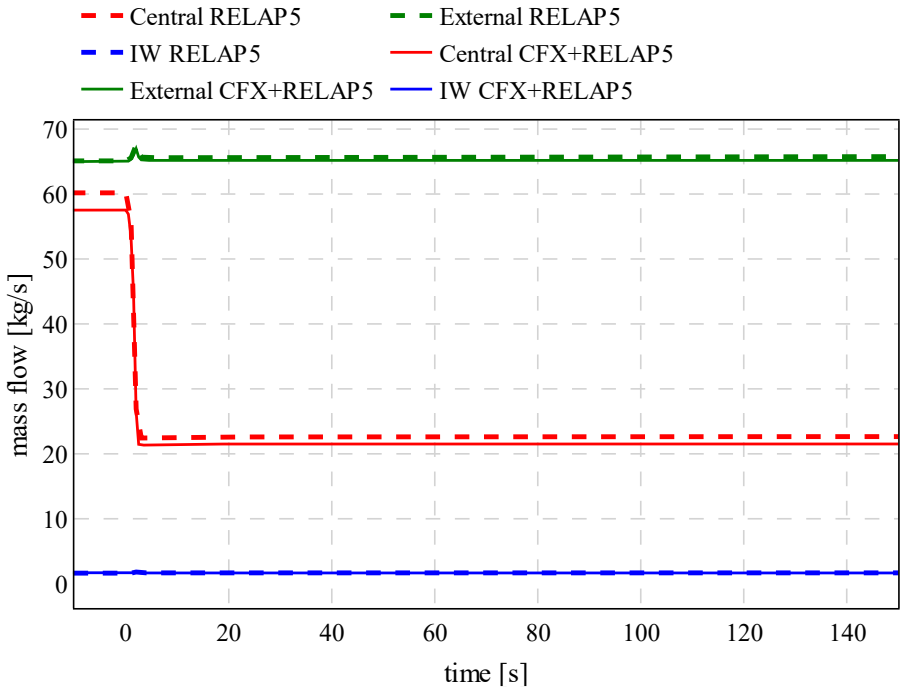


Figure 4.73 – Mass flow rate during the first 150s of the transient in the three channels and the global one [52].

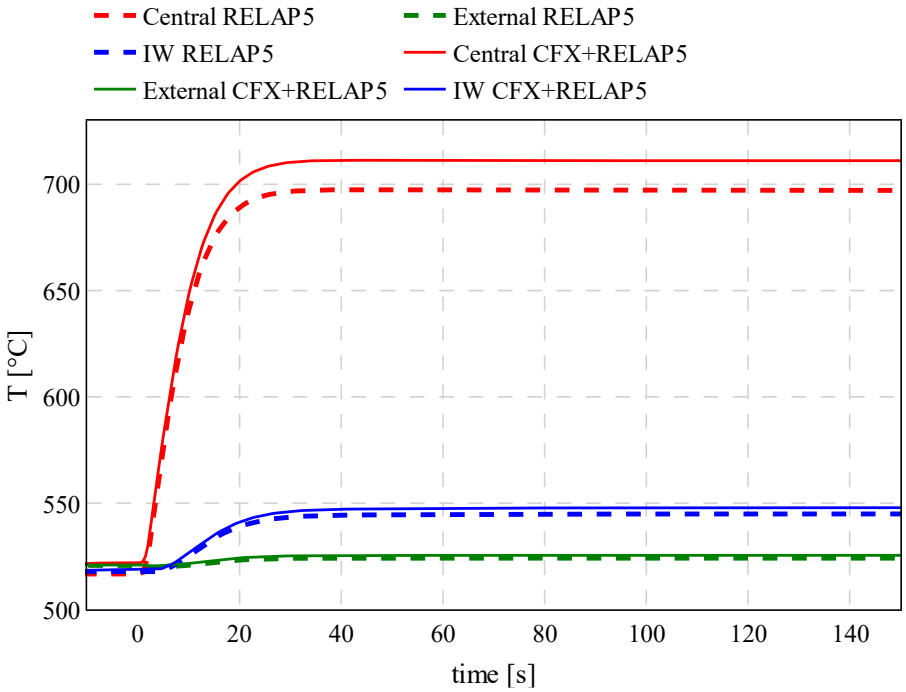


Figure 4.74 – Temperature at the inlet of the Fitting Volume during the first 150s of the transient in the three channels [52].

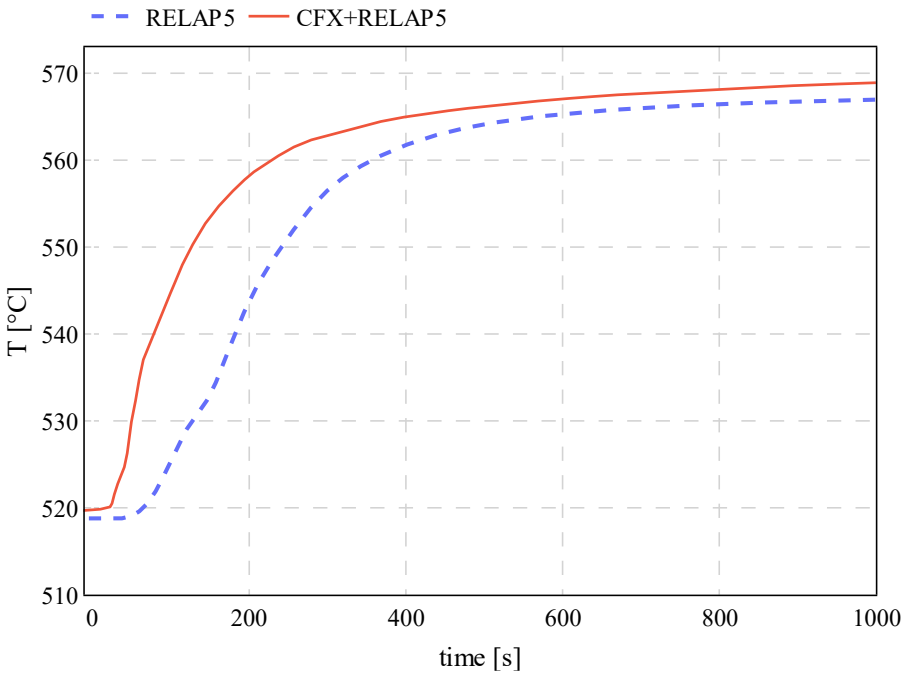


Figure 4.75 – Temperature at the outlet of the Fitting Volume [52].

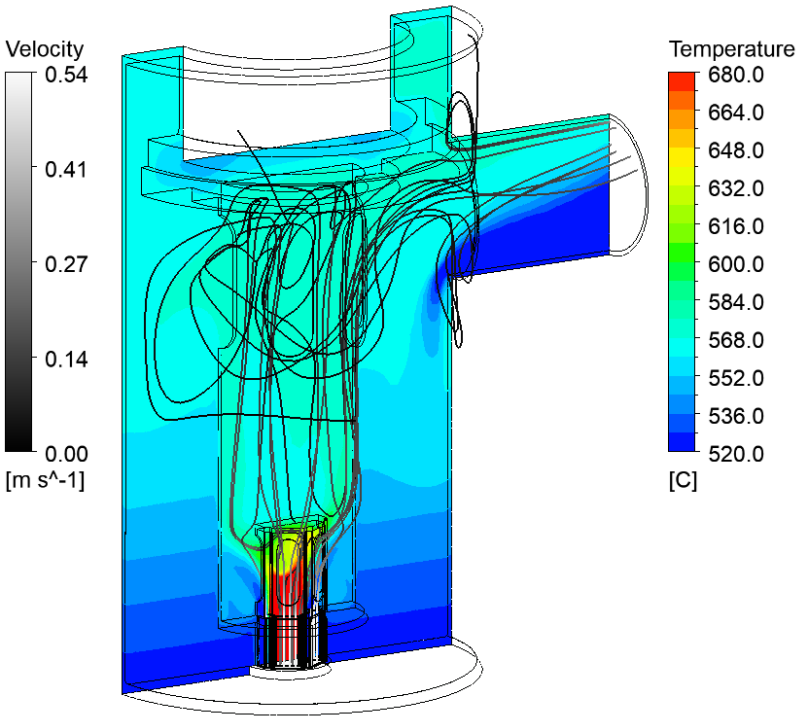


Figure 4.76 – Streamlines and temperature distribution in the symmetry plane, at the end of the transient (1000 s) [52].

This test case shows the potential of a multiscale approach through a possible application to components where three-dimensional phenomena are relevant. Even if the case is simplified by adiabatic conditions and imposing a fixed temperature for the fluid re-entering the domain, the coupled results have shown a faster increase of temperature with respect to the standalone case.

4.3.3 Pool thermal transient

The second ATHENA test case aims to test the differences in modelling the main pool between Ansys CFX and RELAP5 Mod3.3. The transient investigated consists of an initial steady state, characterized by an isothermal pool at 400°C and nominal conditions, perturbed by the instantaneous injection of hot lead from the MHX outlet at 600°C at a constant mass flow rate. The transient could be considered as a simplification of a Loss Of Heat Sink, but is not intended as the simulation of the entire system in representative condition.

The main quantity monitored is inlet flow rate and temperature to the Feeding Conduit, to understand how the two modelling approaches simulate the propagation of the MHX outlet perturbation to the inlet of the conduit leading to the CS. Further analyses are conducted on two monitoring planes (A and B, shown in Figure 4.77) to understand the discrepancies between the obtained results.

Since the focus of the test case is the behaviour of the main pool in itself, coupling has not been adopted for this test case; instead, a code-to-code comparison between the CFX and R5 models is carried out. In the following subsections, the model description and results are discussed.

Pool model

The pool model (Figure 4.77) encompasses the flow path from the MHX outlet to the Feeding Conduit inlet, passing through the volume inside the barrel where the lead is directed toward the cover gas region. It then flows radially through bottomholes to feed the downcomer located between the barrel and the main vessel.

The model includes the lead domain and the solid structure of the only the barrel. The boundaries of the lead domain facing the other solid component, both internally (e.g. CS, Separator, main pump, etc) and externally (i.e. Main Vessel) are adiabatic. Fluid to solid heat exchange occurs only through the AISI 316L solid barrel. This choice simplifies the problem and emphasizes the differences due to the modelling of the fluid domain. Heat transfer with other boundaries, especially

the internal ones, would only increase the three-dimensional complexity of the problem. In any case, such interactions are minimized as much as possible by design in ATHENA, foreseeing double walls where possible.

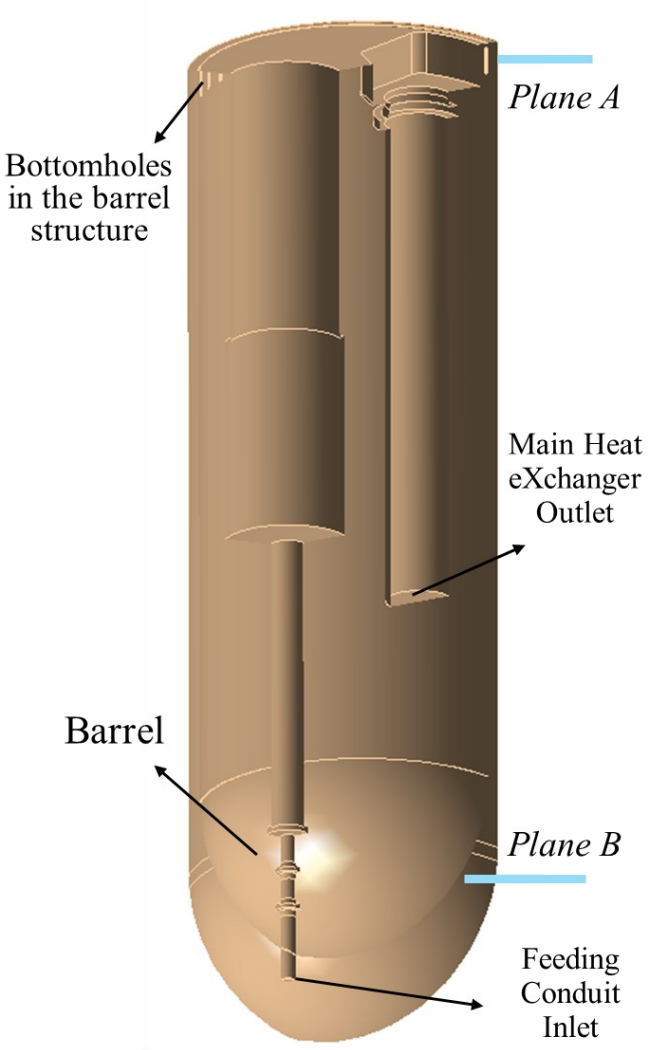


Figure 4.77 – Pool model domain.

The CFD model is discretized in an unstructured tetrahedral mesh, for a total of 5.7 M of nodes resulting in 30.5 M of elements. The SST k-ω [56] is selected as turbulence model with a turbulent Prandtl number of 2 [64]. Buoyancy is activated.

For what concern the STH model, the pool is discretized axially and azimuthally in 3x120° sectors. As shown in Figure 4.78, each sector contains one of the three main components of the ATHENA pool, i.e., CS, MCP, and MHX. Even in this case the sliced approach is adopted ([65], section 4.2.2).

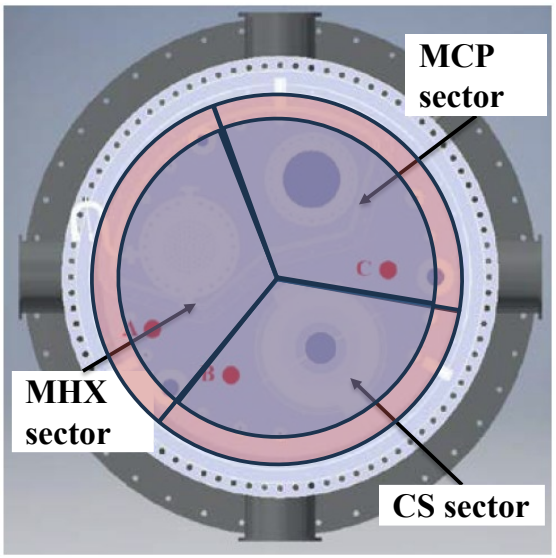


Figure 4.78 – Pool azimuthal nodalization.

The barrel solid structure is included as heat structure to model. The outlet of the MHX and the inlet of the Feeding Conduit are represented by time dependent volume plus time dependent junction and time dependent volume respectively. The mass flow rate is imposed as well as the temperature at the outlet of the MHX.

Simulation results

The simulation results reported in this section describe how the imposed temperature increase at the MHX outlet, occurring in the first seconds (from 0 s to 10 s) and varying from 400°C to 600°C, affects the Feeding Conduit inlet temperature. The mass flow rate is constant and imposed equal to 126 kg/s.

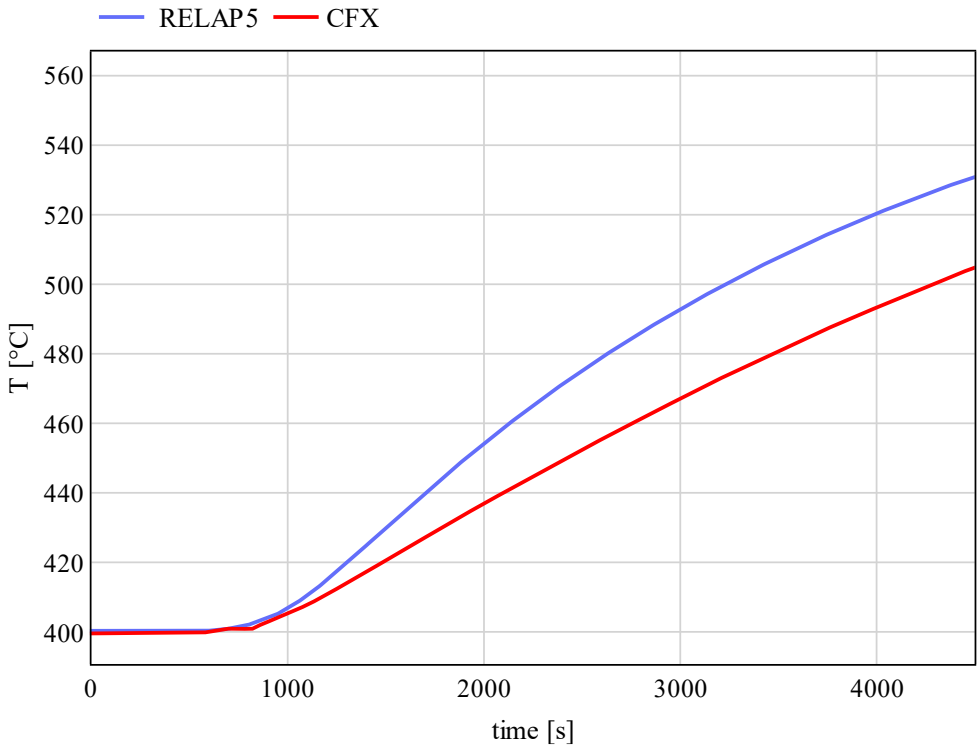


Figure 4.79 – Feeding Conduit temperature evolution during the pool thermal transient.

Figure 4.79 shows the first 4500 s of the transient. It is worthy to highlight that ATHENA is characterized by very high thermal inertia of the pool, especially if compared to the ALFRED one: while the ratio of the volumes is 5.5 (416 m^3/76 m^3), the ratio of the powers is 135 (300 MW/2.21 MW), meaning that the power over coolant volume ratio of ATHENA is much lower than the ALFRED one. For this reason, the R5 standalone code shows that more than 7 h are required to reach the new steady state with uniform 600 °C temperatures in the entire pool.

Even if a series of simplifications have been made in this test case (adiabatic vessel external surfaces, no heat exchange with the internals e. g. CS, etc.), at 4500 s the temperature at the Feeding Conduit inlet predicted by the R5 code is 26 °C higher than the CFX one.

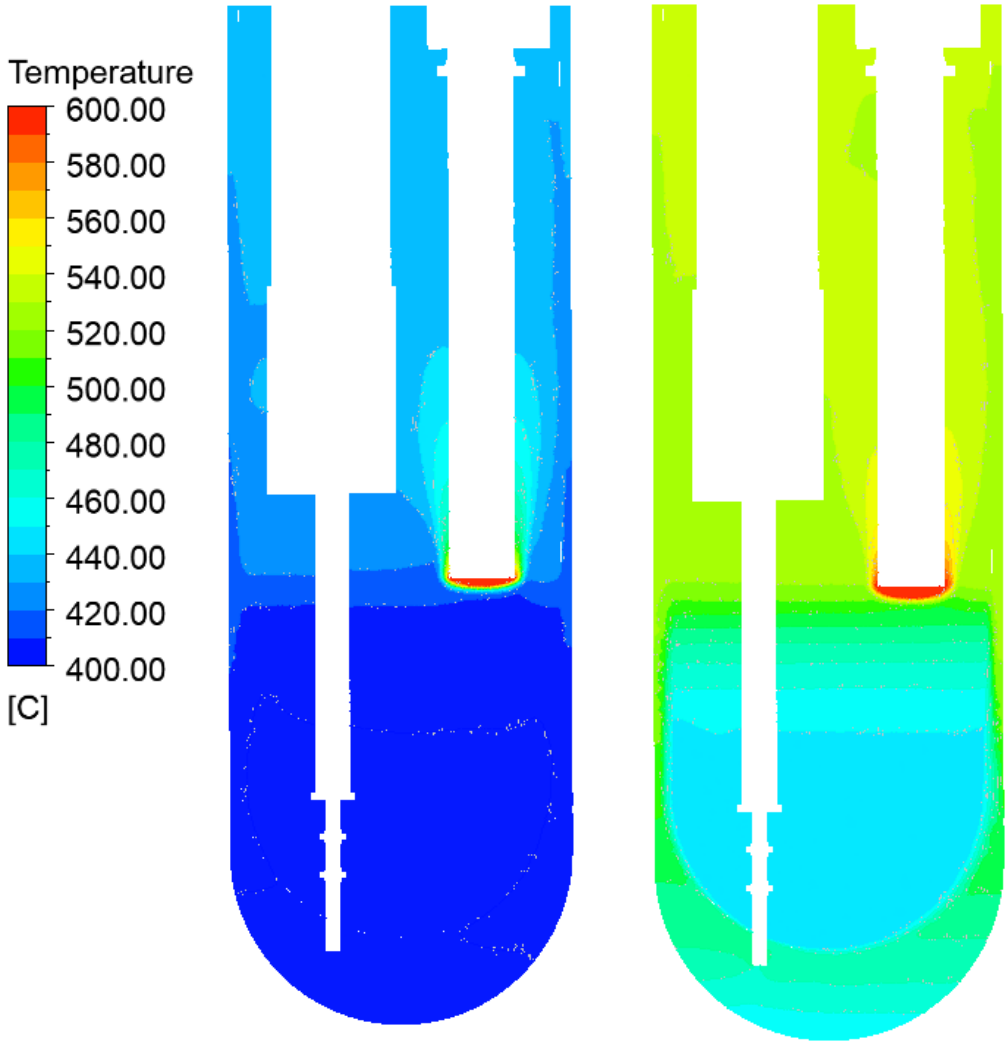


Figure 4.80 – Temperature distribution in the CFD model on a plan cutting the centres of the Main Heat eXchanger outlet and Feeding Conduit inlet at 500 s on the left and 3220 s on the right.

Figure 4.80 shows the temperature distribution in a plane cutting the centres of the MHX outlet and Feeding Conduit inlet at 500 s and 3220 s. The evolution of the thermal conditions in the pool demonstrates how hotspot propagation is driven by conduction and buoyancy forces, due to the very low velocity and the large volume of the facility. No coolant jet is visible at the MHX outlet, where the hot fluid almost immediately rises toward the top of the pool. The high thermal conductivity of lead causes rapid heat diffusion, primarily affecting the upper region of the facility where the hot lead accumulates.

Two monitoring planes (see Figure 4.77) are defined to explore the behaviour of the two models: Plane A, located at the middle of the bottomholes connecting the region inside and outside the vessel and Plane B located in the lower part of the barrel. In Figure 4.81 and Figure 4.82, the temperature distribution in those two planes is reported together with the temperature values of the corresponding R5 volumes of the three sectors inside and the three outside the barrel. The time selected for the comparison is 3220 s after the transient start. The comparison of the results between the codes describes qualitatively the behaviour of the models.

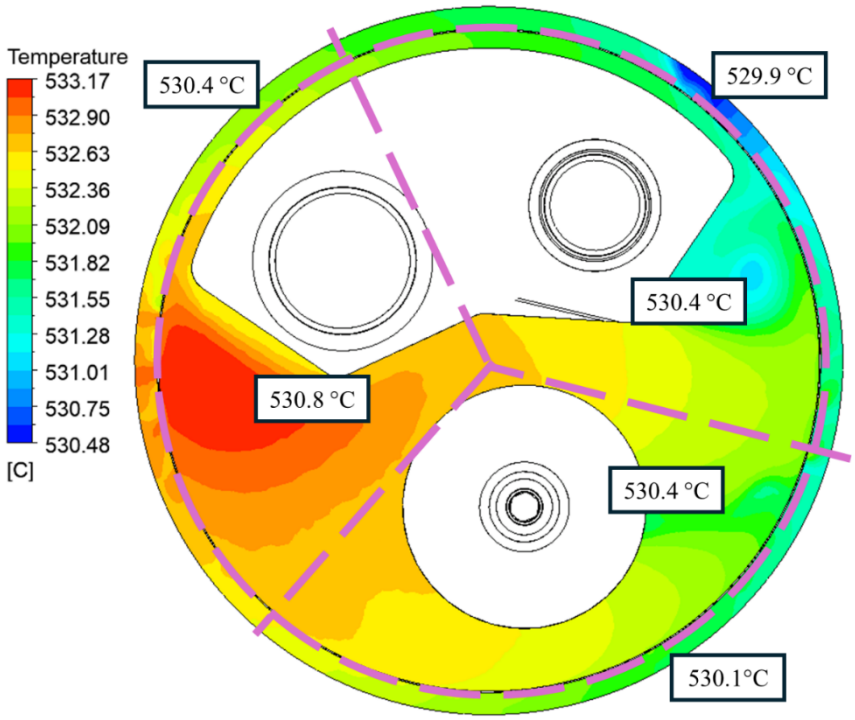


Figure 4.81 – Temperature at the Plane A location after 3220 s from the start of the transient. In the boxes, RELAP5 temperature of the corresponding volumes.

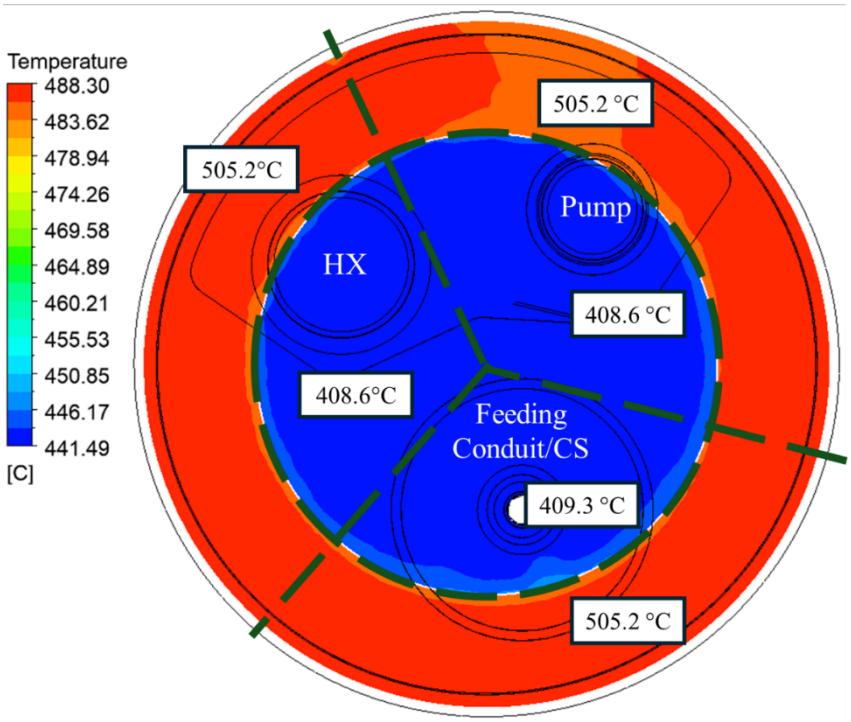


Figure 4.82 – Temperature at the Plane B location after 3220 s from the start of the transient. In the boxes, RELAP5 temperature of the corresponding volumes.

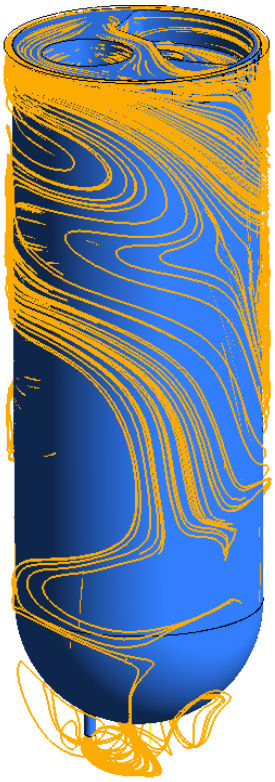
In Plane A, the temperature variation across the plane is very limited in both the CFD and STH code, with close values among the two. When the fluid reaches the upper part of the facility, the asymmetry due to the MHX location is almost imperceptible.

In Plane B, the CFD code predicts higher temperatures inside the barrel and lower temperatures in the downcomer, with the fluid inside the barrel that receives heat from outside. The STH code shows the same behaviour but with stronger gradients between the two regions.

The two models show similar global behaviour: the hot fluid is directed toward the top of the pool by buoyancy forces and releases part of the heat to the bottom region of the fluid inside the barrel while descending the downcomer. However, some important differences could be highlighted:

- the CFD code considers conduction in the fluid, heating the fluid below the MHX and reducing the gradient between the barrel and internal and external fluid region;

- the flow path in the CFD code is strongly three dimensional (Figure 4.83), having more space to exchange heat between inside and outside the barrel. This fact increases the temperature in the region inside the barrel below the MHX even further.



-

Figure 4.83 – Streamlines of the Ansys CFX model in the downcomer of the ATHENA facility at 3220 s.

The discretization into volumes within R5 and the absence of heat conduction within the fluid create important differences not only at the inlet of the Feeding Conduit, but also in the distribution inside the pool. While increasing the discretization and enhancing a modelling approach that approximates three-dimensionality may help, R5 still struggles to replicate the phenomena captured by CFX.

Assisted by the adiabatic conditions imposed as boundary conditions, the faster temperature increase measured by R5 and the different distribution inside the pool could be considered for some cases of limited impact on the overall performance of the model. However, it is crucial to verify the impact of these differences on the quantities of interest in the simulation.

ATHENA test case 2, described in this chapter, does not report an application of the coupled tool, but allows to analyse the impact of simulating the pool with a CFD code, retrieving important information on the possible deployment of coupled simulation for the TH analysis of pool systems.

4.3.4 Loss Of Flow Accident

The last test case presented in this thesis consists of the simulations of a Loss Of Flow accident, comparing the results of the STH stand-alone code and the coupled tool, in which the Core Simulator is simulated by the CFD code.

The simulated transient is composed of four phases:

1. steady state normal conditions corresponding to the one presented in chapter 4.3.1 (400 °C - 520°C thermal cycle, 126.5 kg/s, 2.21 MW);
2. closure of the MHX inlet and outlet secondary valves and opening of the discharge valve, initiating the vaporization of the fluid within the bayonet tubes. As the fluid transitions to steam, it exits through the discharge valve, leading to a decrease in the overall enthalpy within the tubes;
3. actuation of the pump trip when the enthalpy inside the MHX secondary side is equal to the one of the ALFRED reactor steam generators (SG) [79], scaled on the power, resulting in the target value of 1.01e7 J. This condition was selected to reach inside the ATHENA MHX a condition as representative as possible of the ALFRED SG cooling power;
4. CS shutdown, following the decay curve [80], when the outlet temperature of the central FA reaches 800 °C.

The described procedure, i.e., with a reduction in the efficacy of the secondary side to remove heat from the lead pool, has been selected to avoid the freezing of lead in the MHX during the PLOFA because of the very high temperature difference between the secondary fluid and the molten lead.

Core Simulator model

The Ansys CFX model of the CS consists of four different domains (Figure 4.84): the solid domain in the wrappers and the external steel casing; the fluid region in the inter-wrapper and two porous regions to represent the FA zone including the rods and the grids.

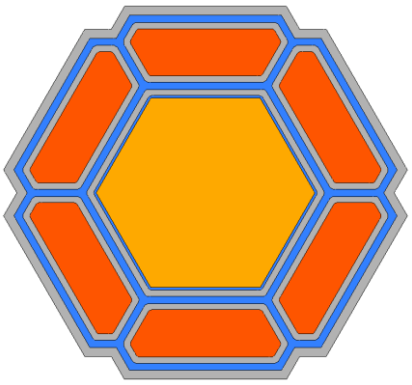


Figure 4.84 – Layout of the domain definition in the Ansys CFX code: steel (grey), liquid lead (blue), central porous medium (orange) and external porous media (red) [78].

Axially the investigated domain comprises: the active length (810 mm) from the upper surface of the lower spacer grid to the bottom surface of the top spacer grid, the development length of 187 mm upstream the active length and downstream an outlet region of 140 mm, for a total length of 1137 mm (Figure 4.85).

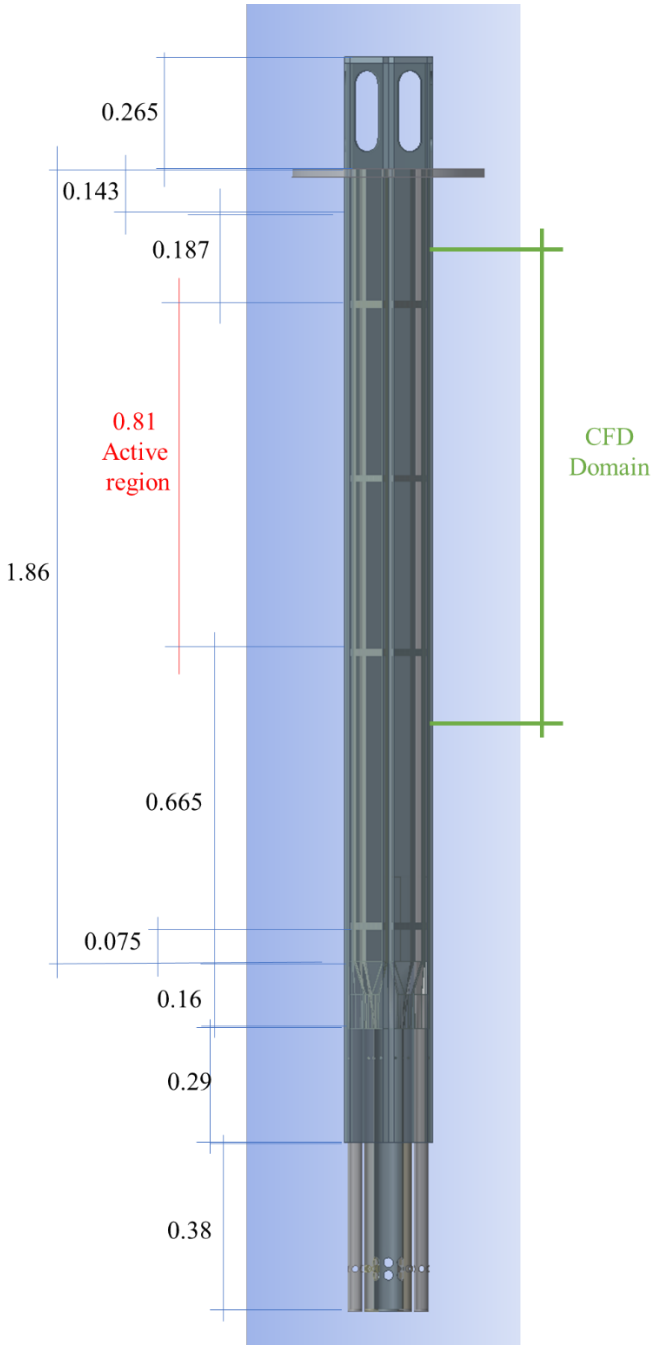


Figure 4.85 – Axial view of the ATHENA Core Simulator with dimension in meters [79].

As studied by the author in Ref. [81], for the representation of the seven FAs, two different approaches for defining the porous media parameters are identified:

- in the external FA a single porous medium;

- for the central hexagonal FA, the hybrid approach in which the domain is divided in an internal porous medium with hexagonal key of reduced dimension and the surrounding layer of fluid. The hexagonal key of the porous domain of the hybrid approach is computed such a way to have the same porosity as in the infinite lattice domain [82]:

$$1 - \frac{\sqrt{3}\,\pi D^2}{6P^2} = 1 - \frac{\sqrt{3}\,N\pi D^2}{6W^2} \tag{14}$$

reducing the equation to the following one:

$$W = \sqrt{N}\,P \tag{15}$$

where D and P are the pin diameter and pitch, and W is the across flat width of the central hexagon box and N is the number of electrically-heated pins.

The calibration of the porous media is conducted by a CFD analysis of the infinite lattice domain of the ATHENA CS (Figure 4.86), taking into account the effect of the grid by means of a concentrated loss coefficient also obtained by dedicated CFD simulation at different mass flow rates. Two different sets of parameters are retrieved as a function of the geometrical characteristics of the FAs and collected in Table 4.18.

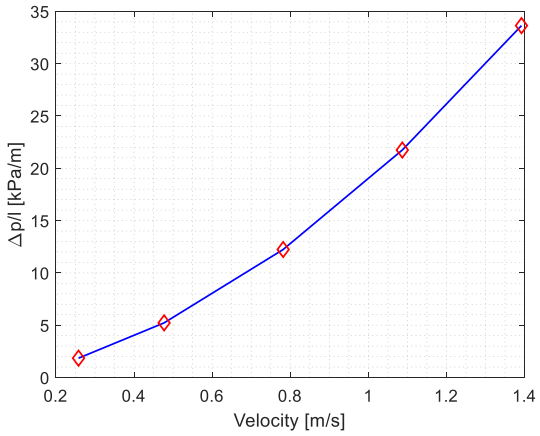


Figure 4.86 – Pressure per unit length for different velocities in the ATHENA infinite lattice model [81].

Table 4.18: Porous media parameters for the Core Simulator model [81].

	External FAs	Central FA
Porosity [-]	0.53	0.46
Volumetric heat source [MW/m^3]	118.6	133.0
Permeability [m^2]	3.26 e-07	3.26 e-07
Loss coefficient [m^{-1}]	2.83	2.83

The present CS porous media model definition has the goal to apply the best approach for the different geometries. As shown in Figure 4.87, the porous model is able to reproduce with good accuracy the temperature distribution on a section, reproducing the coldest spot located in the region where the external FA faces the central hexagon, and represents higher temperatures in the external corner of the polygonal FAs.

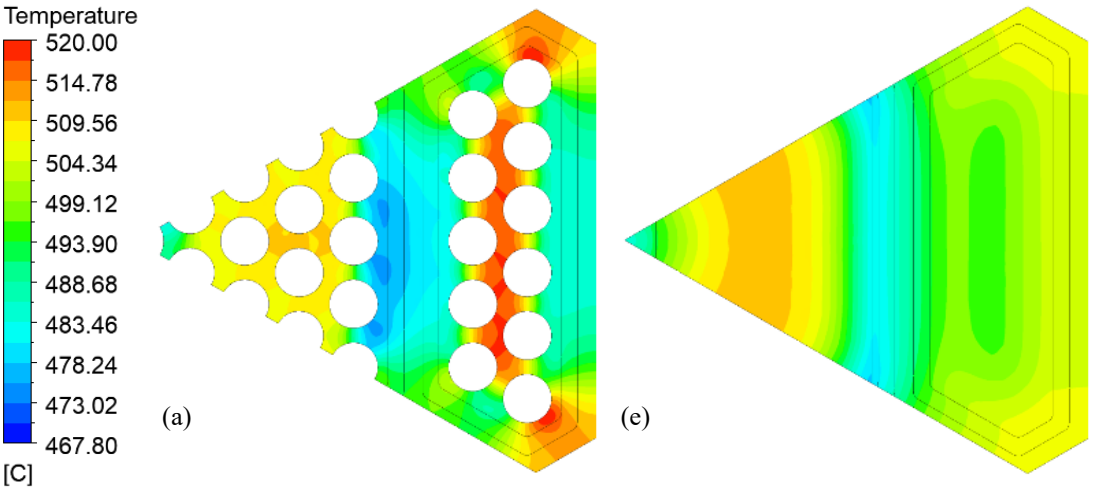


Figure 4.87 – Outlet temperature maps in detailed CFD model (on the left) and the porous media model (on the right) for the steady state condition studied in Ref. [81].

For the purposes of this study, porous media are employed as a compromise between the computationally expensive detailed representation of fuel assemblies and the simplified STH representation, which neglects three-dimensional flow behaviour and heat conduction in fluid. In future work, the CS representation could be enhanced to more accurately monitor local parameters, such as peak pin surface temperatures during transient events. Additionally, further evaluations of the performance of the proposed modelling strategies under abnormal conditions, such

as higher and lower Reynolds numbers than the nominal mass flow rate, will increase the confidence in adopting porous media approach for TH analysis.

The total number of cells in the structured mesh is ~3.13 M. The SST k-ω [56] is selected as turbulence model with a turbulent Prandtl number of 2 [64].The wall y^+ is higher than 30 in the porous region, while a y^+ lower than 1 is adopted in the fluid domain. On the external casing, adiabatic conditions are imposed. The properties of lead and the steel are taken from the handbook [55] and [83], respectively. The solid structure of the pins is taken into account in the definition of the porous models.

For the 8 channels (6 external FAs, central FA and inter-wrapper), at the inlet uniform temperature and velocity are imposed, while at the outlet zero relative pressure is set. Since the channels are independent, the pressure difference between parallel channels is not important, but only across them, i.e. the pressure drops.

System scale modelling

The ATHENA R5 model employs time dependent volumes and junctions as boundary conditions, such as cover gas pressure, pressurizer pressure, and air mass flow rate in the AC. Convective heat transfer to the environment is modelled using a constant heat transfer coefficient of 8 W/m²K and a constant external temperature of 10 °C.

The strategy adopted for the nodalization of the entire lead domain (including the MHX) is the sliced modelling approach ([65], section 4.2.2). Figure 4.88 shows the axial nodalization of the "1D" region only, i.e., the path from the Feeding Conduit to the MHX. The CS is modelled by three parallel pipes, representing the central FA, the polygonal FAs, and the inter-wrapper region.

The pool side of the main vessel of ATHENA is represented with the R5 model adopted in section 4.3.3, where it is azimuthally discretized in 3x120° sectors, each sector containing one among CS, MCP, and MHX.

The secondary loop (Figure 4.89) is discretized by fluid elements with a length of 15 cm in the active regions, i.e., MHX and air cooler, up to 25 cm in the piping sections and in the pressurizer, where the small gradients and the relatively large flow areas allow the adoption of larger axial volumes, following the general rule of maintaining a length-to-diameter ratio greater than 1 for each volume [84].

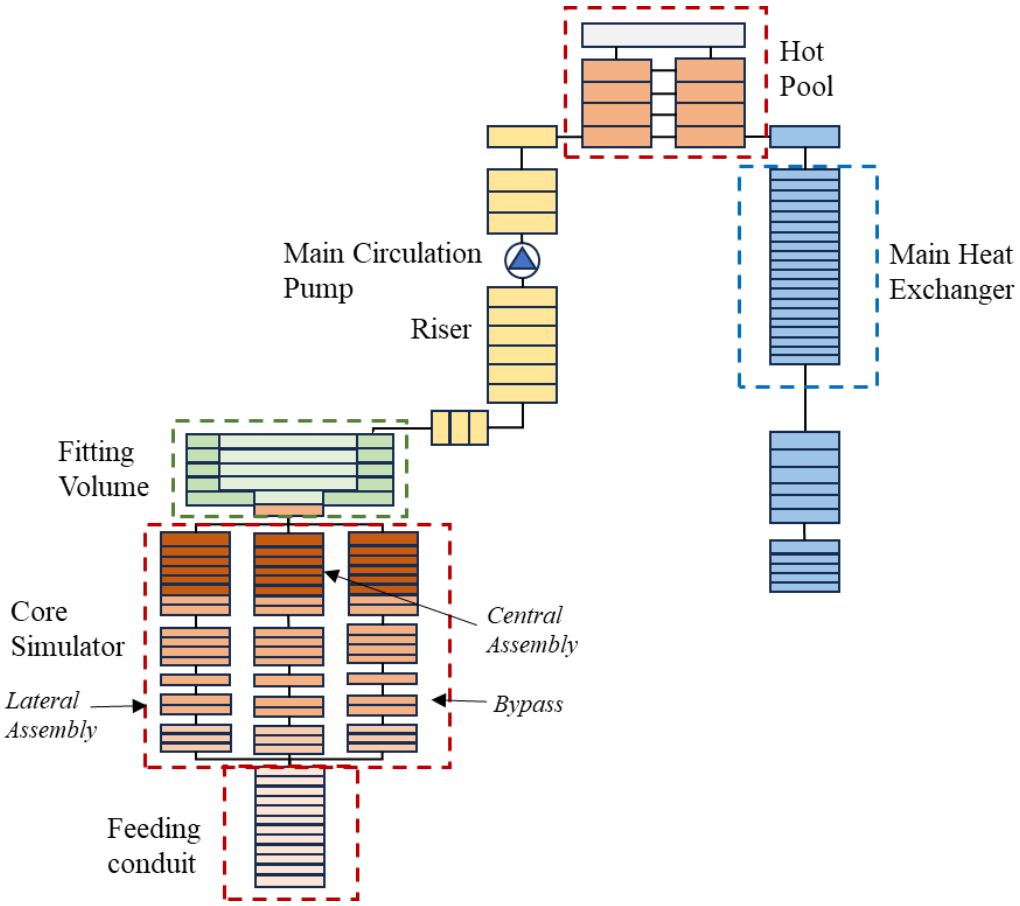


Figure 4.88 – “1D” region of the primary side axial nodalization [78].

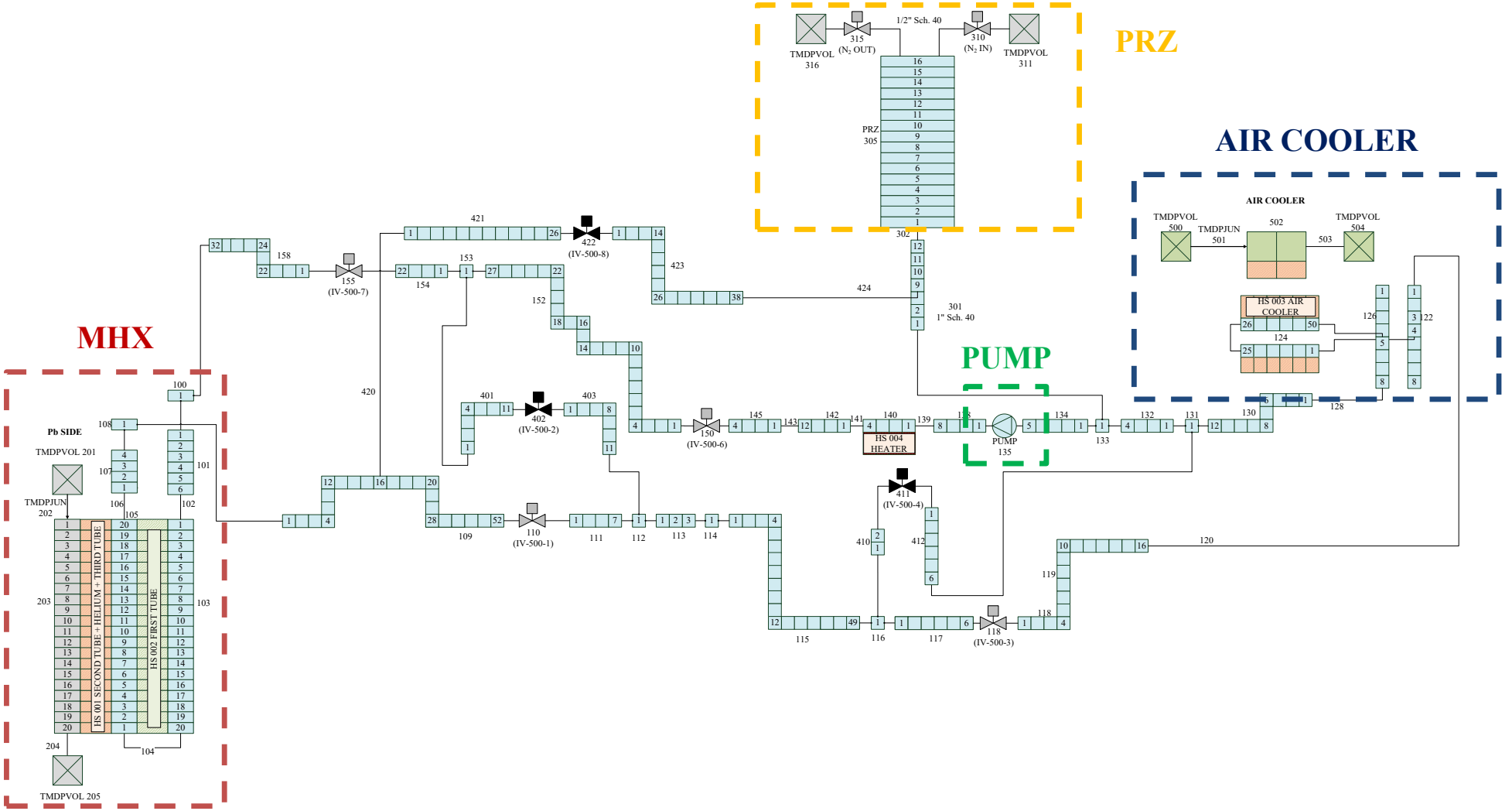


Figure 4.89 – Secondary loop nodalization.

For the coupled simulation, R5 simulates the entire primary and secondary system excepts the region of the CS CFX model, removed from the STH domain and replaced by three time-dependent volumes at the entrance of the Core Simulator and three time-dependent volume connected to three time-dependent junctions at the exit.

In this test case, the goal is to investigate possible discrepancies with respect to the R5 standalone code in the representation of the CS and its most relevant quantities.

The coupled simulation is preceded by R5 steady state calculation with the "open loop" model, together with the CS CFX steady state simulation: the values of the boundary conditions adopted in the steady states are those obtained with the R5 standalone model.

During the coupled run the two-way exchange of information regards:

- the CS outlet mass flow rates, temperatures and the pressure drop of the three channels (central and external FA and the inter-wrapper) are passed by Ansys CFX to R5;
- the CS inlet mass flow rates temperatures of the three channels from R5 to CFX, to be imposed at the inlet of the CFD model.

Coupled tool simulation results

The coupled simulation run is carried out with a semi-implicit time advancing scheme and a decomposition domain approach, with a coupled timestep of 5e-2 s and a CFX to R5 timestep ratio of 20. The coupling simulation starts when the second phase (closure of the MHX) begins (intended as time* = 0 s in the following figures). The trends in enthalpy reduction (Figure 4.90) are quite similar between the stand-alone model and the coupled model, with negligible differences. For both the simulation a new time is define with the zero value when the ALFRED enthalpy value is reached and the pump shut down (third phase of the transient, see first paragraph of section 4.3.4).

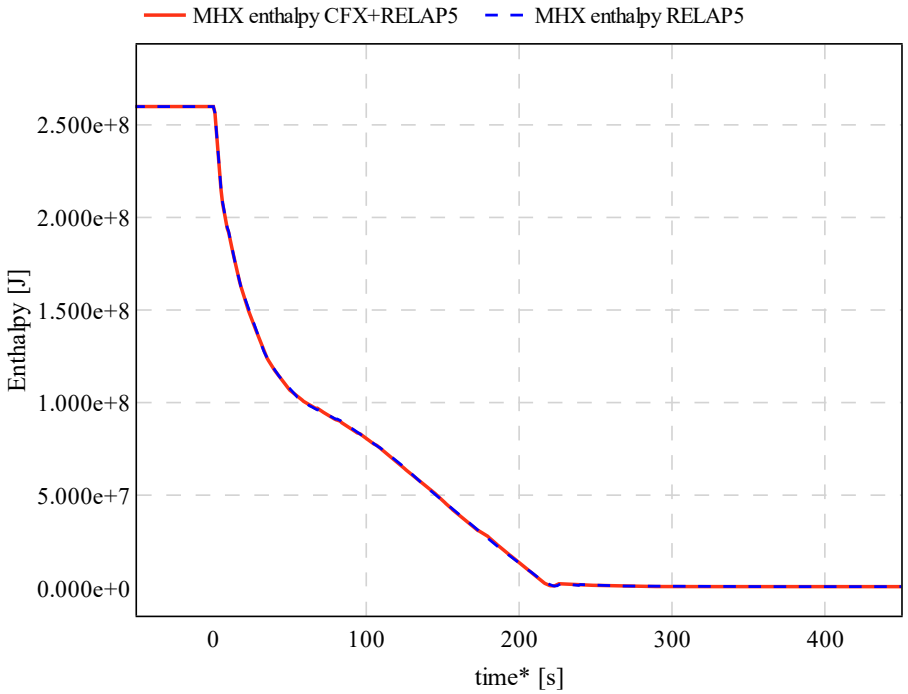


Figure 4.90 – Enthalpy inside the Main Heat eXchanger in function of the unmodified simulation time.

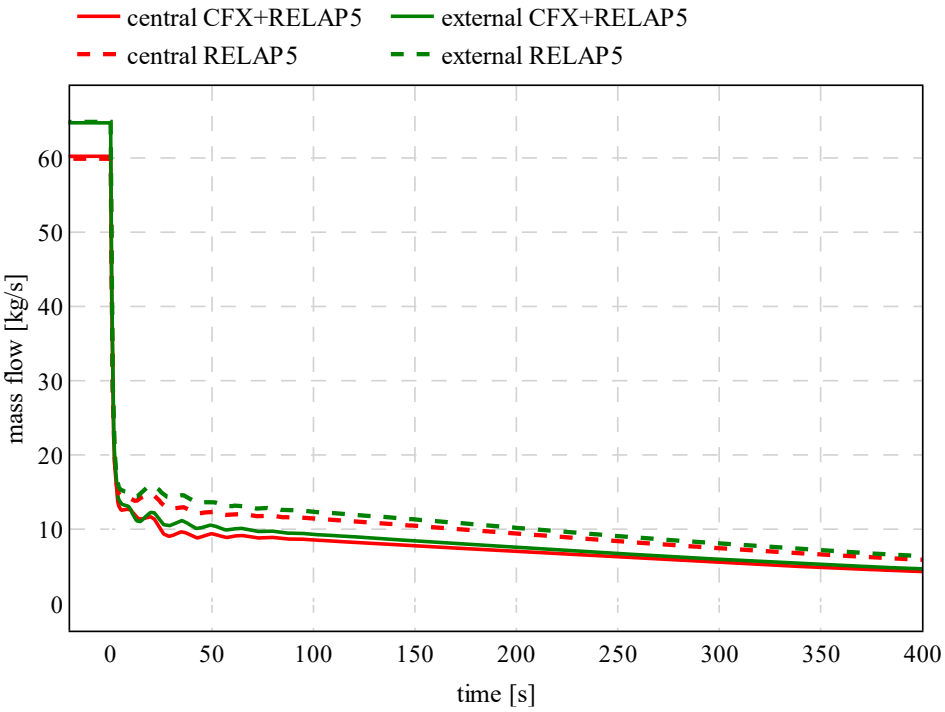


Figure 4.91 – Mass flow rate in the Core Simulator during the transient for the central Fuel Assembly and external Fuel Assemblies.

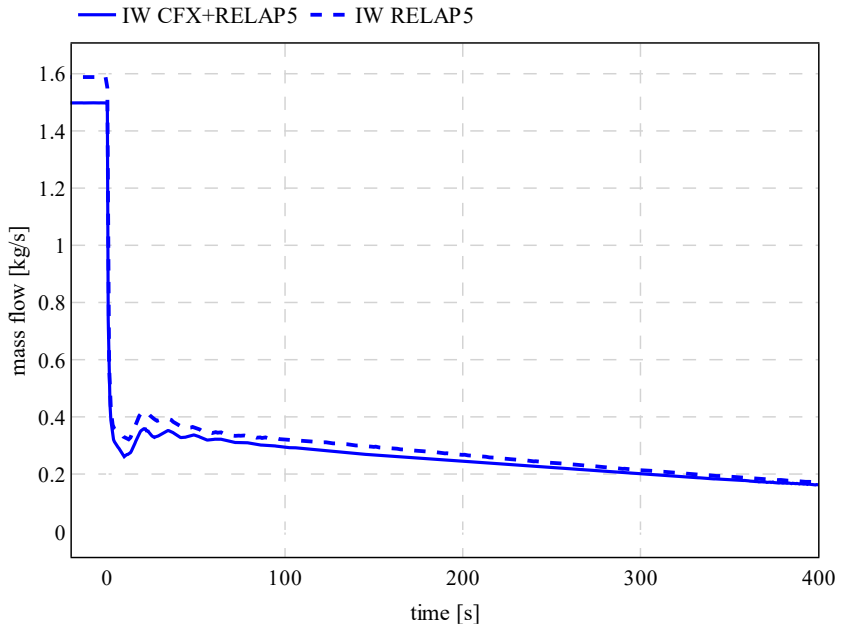


Figure 4.92 – Mass flow rate in the Core Simulator during the transient for the inter-wrapper channel.

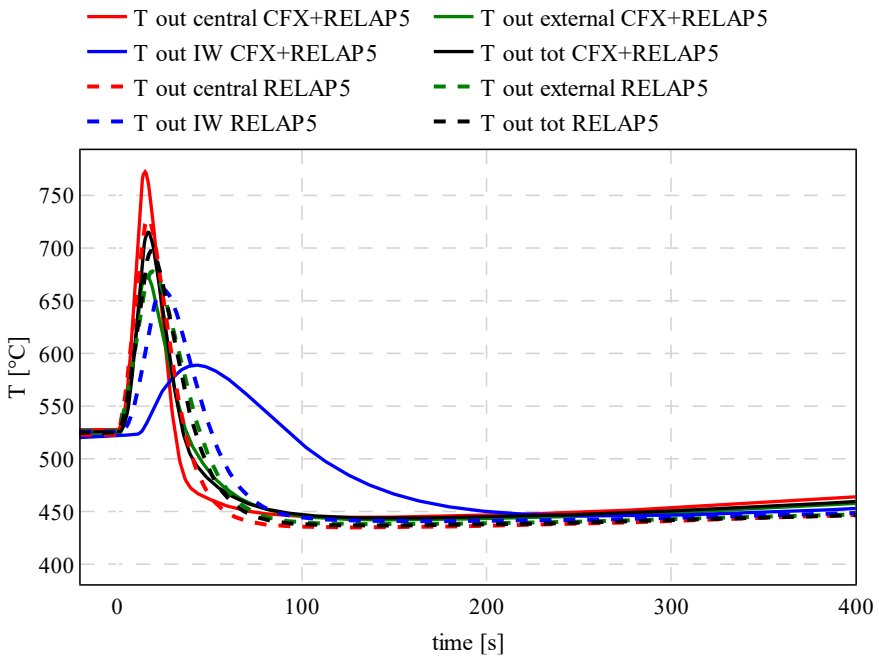


Figure 4.93 – Outlet temperatures of the Core Simulator during the transient for the central Fuel Assembly, external Fuel Assemblies and the inter-wrapper channels and the global value.

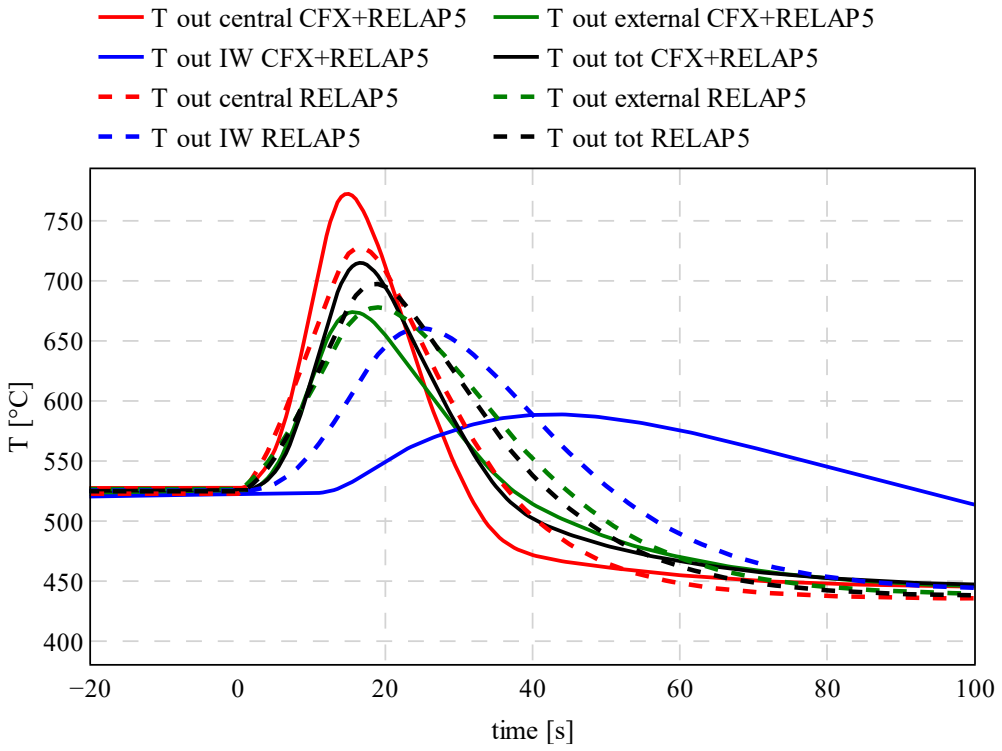


Figure 4.94 – Outlet temperatures of the Core Simulator during the transient for the central Fuel Assembly, external Fuel Assemblies and the inter-wrapper channels and the global value, first 100 s.

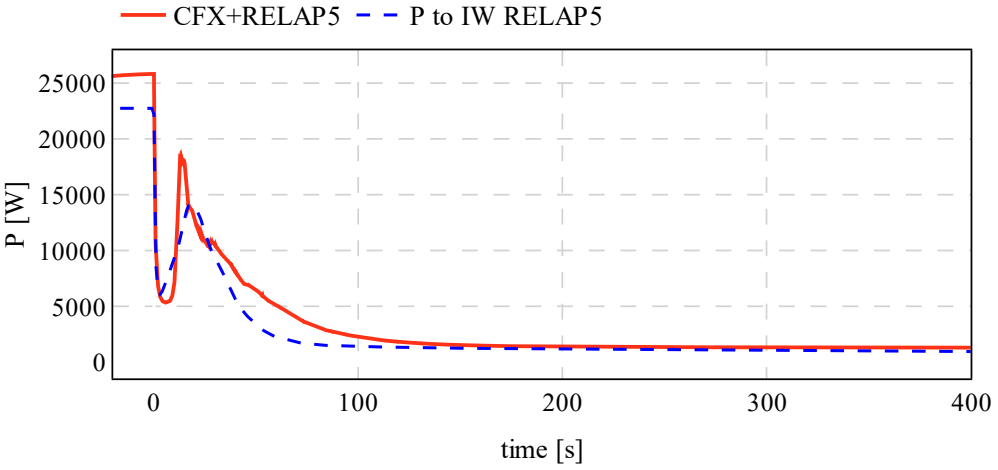


Figure 4.95 – Power transferred to the inter-wrapper region during the transient.

The mass flow rate reduction is reported in Figure 4.91 for the FAs channels and in Figure 4.92 for the inter-wrapper one, where it can be noticed that the initial steady state values are comparable between the two approaches with the coupled

simulation predicting slightly lower mass flow rate in the inter-wrapper. The transient is very similar, but the obtained mass flow rates with the standalone R5 model are slightly higher than the coupled ones due to the different pressure drops representation inside the CS.

The CS model outlet temperatures from the three fluid channels (Figure 4.93 and zoomed in Figure 4.94) present differences, some substantial, between the coupled and the STH standalone simulations, in particular:

- the central and external FAs temperatures start to increase more rapidly in the R5 model, but then the peak in the coupled simulation is higher and anticipated with respect to the R5 one;
- the coupled inter-wrapper temperature peak is around 70 °C lower and 20 s delayed in time with respect to the one predicted by the STH calculation. The trend is similar to the STH standalone calculation at the end of the simulation (after 250 s from the pump trip);
- the temperature difference between the three channels is slightly higher with the coupled approach, especially at the end of the simulation.

The last bullet is strictly related to the mass flow rate behaviour. Regarding the temperatures in the FAs, the model outlet temperature initial increase is delayed in the coupled model by heat conduction in the fluid, but the following behaviour is strictly correlated with the heat transfer conditions in the CS.

In the R5 model, a fraction of the heat generated within the fuel assembly is rapidly dissipated into the inter-wrapper region due to elevated temperatures within the channel volumes. As a single temperature is associated with the FA volumes directly impacted by the mass flow rate reduction, the resulting temperature profile within the inter-wrapper region exhibits a slower and smoother trend, albeit with similar characteristics to the FA temperature profile.

In the CFX model the temperature increase in the porous media has a delay time before being noticed at the wrapper boundaries, inducing a delay in the increase of power released from the FAs to the inter-wrapper. For this reason, the initial peak of the outlet temperature is higher.

The power transferred to the inter-wrapper region (Figure 4.95) is a consequence of heat transfer from the FA to the bypass fluid and is determined through an energy balance of the inter-wrapper channel. As previously discussed, the R5 model exhibits an immediate increase in power following the mass flow rate

reduction, whereas the coupled approach predicts a second peak due to the delayed propagation of heat transfer to the wrappers. The latter phenomenon is attributed to the earlier onset of the fourth phase (scram due to the attainment of an 800 °C outlet temperature) in the coupled approach.

The predicted core simulator behaviour is particularly significant for unprotected transients without SCRAM, such as loss-of-flow without scram. In these cases, heat and mass transport through the bypass can exercise a substantial influence on the fuel assembly temperature field, especially the pin temperature profile, potentially impacting reactor safety analyses. Validation of the models against experimental data is essential to verify the effectiveness of the porous media CFD model and the coupled approach.

Chapter 5

5 Conclusions and future work

The thesis consists of a series of activities aimed at presenting, verifying, and validating a novel Ansys CFX – RELAP5 Mod 3.3 coupled tool proposed for analysis for heavy liquid metal pool-type systems.

Various numerical activities have been conducted, starting from a simple but significative test on an isothermal single pipe transient, moving to loop type facility on which the tool is validated against experimental data, until the application to the ATHENA pool type facility, where different components are investigated to assess the impact and the differences obtained adopting a multiscale coupled approach.

In the following two sections, the conclusions are collected to highlight which are the achievements gained during the three years' work and the difficulties encountered. To follow, future works are presented to give an insight on the possible steps to advance the research program on the field.

5.1 Conclusions

Development of a novel CFD – STH coupling tool

A new CFD – STH coupling tool is successfully developed with the goal of applying it for LFR technology. Nevertheless, the developed computational tool has potential applications to any system that could benefit from a multiscale approach, including current nuclear power plants based on light water reactors. To implement the coupling technique, new software tools, e.g. Ansys CFX FORTRAN 77 subroutines and Python-written executables, are developed to drive the data exchange, manage code synchronization and compute numerical algorithms.

Validation of standalone Anys CFX and RELAP5 Mod 3.3 models

In this thesis, in addition to the coupled tool, different applications of the standalone codes are presented. In all the test cases RELAP5 Mod 3.3 code

are adopted with state-of the art methodologies (e.g. sliced approach, liquid metals properties, etc.). The comparison with experimental data is overall satisfactory for the NACIE and NACIE-UP applications. The TALL3D test highlights potential improvements achievable through a multiscale approach.

Anys CFX models are presented and discussed, comparing steady state and transient numerical results with experimental data, when available, to contribute to increase the maturity of the CFD code application. The CFD models generally performs well across all cases. Among all, the thermal representation in the non-uniformly heated bundle of the NACIE-UP test ADP06 is less accurate, with averaged and maximum error between CFD and experimental temperature equal to 5 and 17 °C respectively.

Computational time required for coupled simulations

The coupled tool is designed to achieve computational times acceptable for the design process and safety assessment, while providing enhanced performance compared to standalone STH codes in entire system representation during relevant transients. The applications of the coupled approach show how the adoption of a CFD code for the entire system representation can be avoided, adopting the CFD only for the components in which three dimensional phenomena are more relevant. This led to a time savings proportional to the ratio between the number of cells required for the part of the system actually simulated with CFD and those that would be required for simulating the entire system with CFD.

The impact of the choice of the coupling strategy among the ones available within the tool is investigated, assessing quantitatively the difference between an explicit and semi-implicit time advancing scheme. A relevant result, valid for the TALL-3D case, is that the explicit time advancing scheme runs 1.5 time faster than the semi-implicit one, when the same timestep is adopted. However, the user should be aware that the semi-implicit scheme could run at higher timestep. Negligible differences could be noticed between overlapping and decomposition domain approaches. The proposed coupled tool offers users various options to select the approach that best fits the analysed case.

Selection of the coupling approach

Among the coupling approaches discussed, the explicit decomposition approach demonstrates to be the easiest to be implemented, but the less robust, especially under rapid hydraulic changes. The overlapping approaches show potential, mainly the overlapping CA method, which appears promising for ensuring conservation and for demonstrating robustness even with the faster explicit time advancing scheme. The semi-implicit decomposition approach demonstrates to be the more mature, combining the simple implementation of the decomposition approach, even when multiple codes interfaces are required, and the robustness of the semi-implicit time advancing scheme, at the price of higher computational time. Overall, it is possible to simulate all the considered test cases with all the presented coupling approaches.

Verification and validation of the coupling tool

The process of verification and validation presented in this thesis assesses different transients, among which the rapid mass flow rate variation is of particular importance. The latter is studied in complex geometries during forced to natural circulation transition and even in PLOFA scenario, but also in the simple pipe case, where important aspects on the robustness of the different coupling approaches are highlighted. Furthermore, the pipe test is fundamental to discuss the methodology applied also in the following cases, with peculiar strategies as the adoption of a velocity map at the CFD model inlet.

The application of the Ansys CFX–RELAP5 Mod3.3 coupling tool to various loop-type facilities, such as NACIE, NACIE-UP, and TALL-3D, has enabled the demonstration of the tool's capabilities in representing complex thermal-hydraulic behaviours. The studies underline that loop-type facility experiments are essential for validating coupled CFD-STH tools before applying them to pool-type systems, but whenever all the components could be well approximated by the STH 1D representation, no relevant discrepancies between STH standalone and coupled models should be expected. Standalone STH simulations can be preferable, when possible, to obtain faster result whenever mono-dimensional representation could be considered sufficient. The TALL-3D test case is an example where the latter condition is not verified even in a loop, since the feedback of the 3D–TS pool

is better captured by the CFD code. The lessons learned are collected in a dedicated section (chapter 4.2.4).

ATHENA facility test cases

The last applications presented address the modelling of the ATHENA pool type facility. Since no experimental data are yet available, code to code comparisons are carried out, considering the application of the CFD code for three different components:

- the Fitting Volume analysis under CS flow blockage scenario shows faster temperature increase in the coupled simulation;
- the pool thermal transient investigates the fluid region from the MHX outlet to the Feeding Conduit inlet, showing how the complexity of the phenomena occurring inside and outside the barrel may require a three dimensional approach, where heat conduction within the fluid covers an important role;
- the PLOFA test case, where the CS is simulated by a CFX model implementing porous media to simulate the FAs, widely apply a multiscale approach, from the infinite lattice scale to set the porous media parameters, to the system scale to study the system behaviour. Even in this case some discrepancies are noticed, due to different heat transfer mechanisms within the CS and mainly involving the heat transferred to the inter-wrapper region.

In all ATHENA pool-type facility cases, the results differed from those of the R5 standalone model. If the differences between CFD and STH modelling of the component affect key quantities relevant to the study and significantly impact the entire system simulation, coupling should be considered.

Field of application of coupling CFD-STH tools

This thesis demonstrates that in LFRs, the analysis of components similar to the ATHENA Fitting Volume and, more importantly, large pools (hot as the ATHENA Separator or cold as the volume inside the Barrel) can be enhanced by the adoption of CFD models to represent behaviour during system transients. This is also the case for the inter-wrapper flow where the heat conduction within the fluid has higher importance, and where the three dimensional heat transfer could affect the heat removal capability of the

coolant during accidental scenarios. The coupling promises to improve the representation of transients involving thermal mixing and stratification and to enhance three-dimensional heat transfer phenomena. Improvement in the pressure drop representation of components for which reliable correlations are not available in literature seems not to be a priority of the coupling, since the problem could be solved with preliminary CFD standalone simulations and CFD-informed STH parameters.

Compared to the use of CFD for the entire primary system, the same level of performance is expected with properly design coupled simulations. However, this approach saves time and makes it easier to integrate the secondary system, which is difficult to include in CFD simulations due to the complexities of simulating two-phase flow.

5.2 Future work

Validation program

The development of this family of tools requires an extensive validation program in relevant conditions. This involves performing numerical activities, especially on pool type facilities, both for prediction (pre-test) and analysis (post-test) of experimental data, but also the design of experimental facilities and experimental campaigns capable of provide high quality data to carry out the validation.

The experimental results of the ATHENA facility will be important for the validation of the presented tool. Nevertheless, an example of application where the improvement of a multiscale approach promises to be relevant is the transition to reactor DHR operation in the main pool during accidental scenario. ATHENA is meant to study full scale components of ALFRED and demonstrate the operation of a large pool type facility, but it is not intended to carry out integral test. ELF for ALFRED (FALCON) and Precursor for LFR-AS-30 and LFR-AS-200 (newcleo) are two examples of facilities where the role of coupled simulation could be important, even for the design phase. ELF and Precursor will be designed with the goal to assess reactor performance and test safety procedures, including DHR operations.

Extending the number of applications on loop type facilities and simple test cases will increase the confidence of adopting the coupled tool for the more complex pool type applications. In addition to that, all the activities and

projects to increase the maturity of the STH, in particular RELAP5 Mod3.3, and CFD, in particular Ansys CFX, codes for LFR applications (e.g. ANSELMUS and LESTO) constitute an important contribution.

Uncertainty quantification

Another fundamental aspect that in the future should be addressed by the research community is the development of procedures for uncertainty quantification. Underestimation of the latter could strongly hinder the application of coupled tool for safety assessment and their acceptance by safety authorities.

Improvement of the coupled tool

- Future developments on the numerical aspect should focus on improve the overlapping CA approach: cases involving more than two boundaries, such as multiple inlets or outlets, should be addressed; improvements are needed in the representation of mass flow inversion when using the CA method; modification of the RELAP5 code to allow for the definition of the friction factor through a control variable will help in increasing the implicitness level of the methodology.
- The coupling tool will benefit from investigation on the implementation of more accurate boundary conditions at hydraulic coupling interfaces in the CFD domain, involving velocity and temperature maps, together with the estimation of the turbulence quantities.
- Furthermore, tests with thermal boundaries conditions need to be addressed and the management of R5 data during restart file generation and data extraction, including the use of double precision, should be further investigated.
- Eventually, future effort could be dedicated at the optimization of the CFX FORTRAN 77 subroutines and the Python executables to reduce the computational time of the simulations, and a user-friendly interface can be developed to facilitate the tool application.

Acronyms

ALFRED	Advance Lead-cooled Fast Reactor European Demonstrator
ANSELMUS	Advanced Nuclear Safety Evaluation of Liquid Metal Using Systems
AS	Anphora Shaped
ASIV	Anphora Shaped Inner Vessel
ATHENA	Advanced Thermal-Hydraulics Experiment for Nuclear Application
BoT	Beginning of the Transient
BREST	Bystryj Reaktor so Svincovym Teplonositelem
BT	Bayonet Tubes
BWR	Boiling Water Reactor
CA	CAlculation
CEL	CFX Expression Language
CFD	Computational Fluid Dynamics
CFX	Ansys CFX
CIRCE	CIRColazione Eutettoidico
CLEAR-I	China LEAd-based Research Reactor
CRP	Coordinate Researcg Project
CU	Continuos Update
DC	Dip-Cooler
DHR	Decay Heat Removal
DNS	Direct Numerical Simulation
ELF	Electric Long running Facility
ENEA	Agenzia nazionale per le nuove tecnologie, l'energia e lo sviluppo economico sostenibile
EoT	End of the Transient
EPM	Electric Permanent Magnet
FA	Fuel Assembly
FALCON	Fostering ALfred CONsortium
FC	Forced Circulation
GEN IV	Generation four
HLM	Heavy Liquid Metal
HS	Heat Source

HX	Heat eXchanger
IAEA	International Atomic Energy Agency
ICN	Institutul de Cercetari Nucleare
INEL	Idaho National Engineering Laboratories
KAERI	Korean Atomic Energy Research Institute
LFR	Lead-cooled Fast Reactor
LES	Large-Eddy Simulation
LESTO	LEad fast reactor Safety design and TOols
PLOFA	Protected Loss Of Flow Accident
LWR	Light Water Reactor
MH	Main Heater
MHX	Main Heat eXchanger
MYRRHA	Multi-purpose Hybrid Research Reactor for High-tech Applications
NACIE	NAtural CIrculation Experiment
NC	Natural Circulation
NRC	Nuclear Regulatory Commission
PWR	Pressurized Water Reactor
R&D	Research and Development
RANS	Reynolds-averaged Navier-Stokes
R5	RELAP5 Mod3.3
SEALER	Swedish Advanced Lead Reactor
SESAME	Simulations and Experiments for the Safety Assessment of MEtal cooled reactors
SG	Steam Generator
SIMPLE	Semi-Implicit Method for Pressure-Linked Equations
STH	System Thermal Hydraulics
STSG	Spiral Tube Steam Generator
TH	Thermal Hydraulics
THINS	Thermal-Hydraulics of Innovative Nuclear Systems
TC	Thermo-Couple
TS	Test Section

References

[1] Lamarsh, J. R. (1966). *Introduction to nuclear reactor theory*. Addison-Wesley.

[2] International Atomic Energy Agency. (2002). *Accident analysis for nuclear power plants* (IAEA Safety Reports Series No. 23). Vienna, Austria: International Atomic Energy Agency. https://www.iaea.org/publications/6610

[3] Merzari, E., Obabko, A., & Fischer, P. (2017). Spectral element methods for liquid metal reactors applications. *arXiv*. https://doi.org/10.48550/ARXIV.1711.09307

[4] Versteeg, H. K., & Malalasekera, W. (2007). *An introduction to computational fluid dynamics* (2nd ed.). Pearson.

[5] Roelofs, F., Di Piazza, I., Merzari, E., 6.2.3 - Core thermal hydraulics, Editor(s): Ferry Roelofs, Thermal Hydraulics Aspects of Liquid Metal Cooled Nuclear Reactors, Woodhead Publishing, 2019, Pages 311-340, ISBN 9780081019801. https://doi.org/10.1016/B978-0-08-101980-1.00020-X.

[6] D'Auria, F., & Rohatgi, U. S. (2017). A historical perspective of nuclear thermal hydraulics. In *Advances in Thermal Hydraulics* (pp. 5-28). Elsevier. https://doi.org/10.1016/B978-0-08-100662-7.00002-6

[7] Song, C. H. (2016). Some issues and challenges in advanced thermal-hydraulic safety research. *Nuclear Technology*, 196(3), 421–445. https://doi.org/10.13182/NT16-91

[8] U.S. Department of Energy & Generation IV International Forum. (2014). *Technology roadmap update for Generation IV nuclear energy systems*. https://www.gen-4.org/gif/upload/docs/application/pdf/2014-03/gif-tru2014.pdf

[9] International Atomic Energy Agency. (n.d.). Lead fast reactors. *Nucleus LMFR*. https://nucleus.iaea.org/sites/lmfns/Pages/overviewlfr.aspx

[10] Alemberti, A., Caramello, M., Frignani, M., Grasso, G., Merli, F., Morresi, G., & Tarantino, M. (2020). ALFRED reactor coolant system design. *Nuclear Engineering and Design*, 370, 110884. https://doi.org/10.1016/j.nucengdes.2020.110884

[11] Newcleo. (n.d.). *Our mission*. https://www.newcleo.com/

[12] Lorusso, P., Bassini, S., Del Nevo, A., Di Piazza, I., Giannetti, F., Tarantino, M., & Utili, M. (2018). GEN-IV LFR development: Status & perspectives. *Progress in Nuclear Energy*, 105, 40-51. https://doi.org/10.1016/j.pnucene.2018.02.005

[13] Frignani, M., Alemberti, A., & Tarantino, M. (2019). ALFRED: A revised concept to improve pool-related thermal-hydraulics. *Nuclear Engineering*

and Design, 355, 110359. https://doi.org/10.1016/j.nucengdes.2019.110359

[14] Liao, J., Stansbury, C. A., Durse, M. E., Wise, D. L., Tatli, E., Loebig, T. G., Wright, R. F., Ferroni, P., Lee, S. J., Epstein, M., Caramello, M., Frignani, M., Tarantino, M., Grasso, G., Di Piazza, I., Bassini, S., Lorusso, P., Antonelli, A., Martelli, D., Wimshurst, A., Watkins, R., Macpherson, G., Wilson, D., Iacovides, H., Cioncolini, A., Francis, J., Buckley, J. (2024). Lead fast reactor thermal-hydraulic testing facilities in support of the UK advanced modular reactor program. *Nuclear Technology*, 1–11. https://doi.org/10.1080/00295450.2024.2361187

[15] Agbevanu, K. T., Debrah, S. K., Arthur, E. M., & Shitsi, E. (2023). Liquid metal cooled fast reactor thermal hydraulic research development: A review. Review Article, 9(6), e16580. https://doi.org/10.1016/j.heliyon.2023.e16580

[16] Pacio, J., Van Tichelen, K., Eckert, S., Wondrak, T., Di Piazza, I., Lorusso, P., Tarantino, M., Daubner, M., Litfin, K., Ariyoshi, G., Obayashi, H., & Sasa, T. (2022). Advanced thermal-hydraulic experiments and instrumentation for heavy liquid metal reactors. *Nuclear Engineering and Design*, 399, 112010. https://doi.org/10.1016/j.nucengdes.2022.112010

[17] Bestion, D. (2017). System thermal-hydraulics for design basis accident analysis and simulation: Status of tools and methods and direction for future R&D. *Nuclear Engineering and Design*, 312, 12-20. https://doi.org/10.1016/j.nucengdes.2016.10.009

[18] NEA-OECD. (2018). *Benchmarking of thermal-hydraulic loop models for lead-alloy-cooled advanced nuclear energy systems - Phase II Natural Convection* (NEA/NSC/R(2018)1). Nuclear Science Committee.

[19] Information Systems Laboratories. (2003). *RELAP5/Mod3.3 code manual volume I: Code structure, system models, and solution methods*.

[20] Information Systems Laboratories. (2001b). *RELAP5/Mod3.3 code manual volume VII: Summaries and reviews of independent code assessment reports*.

[21] Information Systems Laboratories. (2001a). *RELAP5/Mod3.3 code manual volume IV: Models and correlations*.

[22] Balestra, P., Giannetti, F., Caruso, G., & Alfonsi, A. (2016). New RELAP5-3D lead and LBE thermophysical properties implementation for safety analysis of Gen IV reactors. Science and Technology of Nuclear Installations, 2016, Article 1687946. https://doi.org/10.1155/2016/1687946

[23] Forgione, N., Martelli, D., Barone, G., Giannetti, F., Lorusso, P., Hollands, T., Papukchiev, A., Polidori, M., Cervone, A., & Di Piazza, I. (2019). Post-test simulations for the NACIE-UP benchmark by STH codes. *Nuclear Engineering and Design*, 353, 110279. https://doi.org/10.1016/j.nucengdes.2019.110279

[24] Lorusso, P., Del Nevo, A., Narcisi, V., Giannetti, F., Caruso, G., Zwijsen, K., Breijder, P. A., Hamidouche, T., Castelliti, D., Rozzia, D., & Tarantino, M. (2021). Total loss of flow benchmark in CIRCE-HERO integral test facility. *Nuclear Engineering and Design*, 376, 111086. https://doi.org/10.1016/j.nucengdes.2021.111086

[25] Giannetti, F., Vitale Di Maio, D., Naviglio, A., & Caruso, G. (2016). Thermal-hydraulic analysis of an innovative decay heat removal system for lead-cooled fast reactors. *Nuclear Engineering and Design*, 305, 168-178. https://doi.org/10.1016/j.nucengdes.2016.05.005

[26] Narcisi, V., Giannetti, F., Del Nevo, A., Tarantino, M., & Caruso, G. (2018). Pre-test analysis of accidental transients for ALFRED SGBT mock-up characterization. *Nuclear Engineering and Design*, 333, 181-195. https://doi.org/10.1016/j.nucengdes.2018.04.015

[27] Smith, B. L., Bieder, U., Graffard, E., Heitsch, M., Henriksson, M., Höhne, T., Komen, E., Mahaffy, J., Moretti, F., Morii, T., Muhlbauer, T., Rohde, U., Scheuerer, M., Song, C. H., Zigh, G., Andreani, M., Bestion, D., Ducros, F., Houkema, M., Lucas, D., Menter, F., & Watanabe, T. (2008). Assessment of computational fluid dynamics (CFD) for nuclear reactor safety problems. *Nuclear Engineering and Design*, NEA/CSNI/R(2007)13.

[28] Papukchiev, A., Roelofs, F., Shams, A., & Lecrivain, G. (2015). Development and application of computational fluid dynamics approaches within the European project THINS for the simulation of next generation nuclear power systems. *Nuclear Engineering and Design*, 290, 13-26. https://doi.org/10.1016/j.nucengdes.2014.12.003

[29] Roelofs, F., Shams, A., Otic, I., Böttcher, M., Duponcheel, M., Bartosiewicz, Y., Lakehal, D., Baglietto, E., Lardeau, S., & Cheng, X. (2015). Status and perspective of turbulence heat transfer modelling for the industrial application of liquid metal flows. *Nuclear Engineering and Design*, 290, 99-106. https://doi.org/10.1016/j.nucengdes.2014.11.006

[30] Cheng, X., Batta, A., Bandini, G., Roelofs, F., Van Tichelen, K., Gerschenfeld, A., Prasser, M., Papukchiev, A., Hampel, U., & Ma, W. M. (2015). European activities on crosscutting thermal-hydraulic phenomena for innovative nuclear systems. *Nuclear Engineering and Design*, 290, 2-12. https://doi.org/10.1016/j.nucengdes.2014.11.007

[31] Tarantino, M., Roelofs, F., Shams, A., Batta, A., Moreau, V., Di Piazza, I., Gershenfeld, A., & Planquart, P. (2020). SESAME project: Advancements in liquid metal thermal hydraulics experiments and simulations. *EPJ Nuclear Science & Technology*, 6, 18. https://doi.org/10.1051/epjn/2019046

[32] Roelofs, F., Gerschenfeld, A. & Van Tichelen, K. Liquid metal thermal hydraulics R&D at European scale: achievements and prospects. *Front. Energy* **15**, 842–853 (2021). https://doi.org/10.1007/s11708-021-0743-2

[33] Anselmus. (n.d.). *Anselmus – Your Nuclear Consulting*. https://www.anselmus.eu/en
[34] ANSYS. (2011). *CFX – Introduction guide*.
[35] Papukchiev, A., & Buchholz, S. (2017). Validation of ANSYS CFX for gas and liquid metal flows with conjugate heat transfer within the European project THINS. *Nuclear Engineering and Design*, 312, 338-350. https://doi.org/10.1016/j.nucengdes.2016.07.028
[36] Di Piazza, I., Magugliani, F., Tarantino, M., & Alemberti, A. (2014). A CFD analysis of flow blockage phenomena in ALFRED LFR demo fuel assembly. *Nuclear Engineering and Design*, 276, 202-215. https://doi.org/10.1016/j.nucengdes.2014.05.033
[37] Ferrini, M., Borreani, W., Lomonaco, G., & Magugliani, F. (2016). Design by theoretical and CFD analyses of a multi-blade screw pump evolving liquid lead for a Generation IV LFR. *Nuclear Engineering and Design*, 297, 276-290. https://doi.org/10.1016/j.nucengdes.2015.12.006
[38] Boumaza, M., Höhne, T., Mohammedi, B., & Dizene, R. (2019). The capability of Ansys CFX to predict the mixing phenomena in ROCOM test facility. *SN Applied Sciences*, 1(1644), 1-10. https://doi.org/10.1007/s42452-019-1574-1
[39] Papukchiev, A. (2018). Experimental validation of ANSYS CFX for transient flows with heat transfer in a tubular heat exchanger. *Proceedings of the 26th International Conference on Nuclear Engineering (ICONE26)*, London, England. https://doi.org/10.1115/ICONE26-81104
[40] ANSYS. (2011). *CFX – Solver theory guide*.
[41] R. Martineau, D. Andrs, R. Carlsen, D. Gaston, J. Hansel, F. Kong, A. Lindsay, C. Permann, A. Slaughter, E. Merzari, Rui Hu, A. Novak, R. Slaybaugh, Multiphysics for nuclear energy applications using a cohesive computational framework, Nuclear Engineering and Design, Volume 367, 2020, 110751, ISSN 0029-5493. https://doi.org/10.1016/j.nucengdes.2020.110751.
[42] Zanino, R., Bonifetto, R., Chiampichetti, A., Di Piazza, I., Savoldi, L., & Tarantino, M. (2012), First validation of the FRENETIC code thermal-hydraulic model against the ENEA integral circulation experiment, *Transactions of the American Nuclear Society*, volume 107, pp. 1395–1398.
[43] Zanino, R.; Bonifetto, R.; Hoa, C.; Savoldi, L. (2013), AIP CONFERENCE PROCEEDINGS, In: *Advances in Cryogenic Engineering Cryogenic Engineering Conference* (Anchorage (AK)), Vol.1573 pp.8 (pp.1586-1593) ISSN:0094-243X ISBN:9780735412033 DOI:10.1063/1.4860896.
[44] Aumiller, D. L., Tomlinson, E. T., & Bauer, R. C. (2001). A coupled RELAP5-3D/CFD methodology with a proof-of-principle calculation. *Nuclear Engineering and Design, 205,* 83-90. https://doi.org/10.1016/S0029-5493(00)00370-8

[45] Bertolotto, D., Manera, A., Frey, S., Prasser, H.-M., & Chawla, R. (2009). Single-phase mixing studies by means of a directly coupled CFD/system-code tool. Annals of Nuclear Energy. https://doi.org/10.1016/j.anucene.2008.11.027
[46] Grunloh, T. P., & Manera, A. (2016). A novel domain overlapping strategy for the multiscale coupling of CFD with 1D system codes with applications to transient flows. Annals of Nuclear Energy. https://doi.org/10.1016/j.anucene.2015.12.027
[47] Forgione, N., Angelucci, M., Ulissi, C., Martelli, D., Barone, G., Ciolini, R., & Tarantino, M. (2019). Application of RELAP5/Mod3.3 – Fluent coupling codes to CIRCE-HERO. Journal of Physics: Conference Series, 1224, 012032. DOI: 10.1088/1742-6596/1224/1/012032
[48] J. J. Jeong, S. Sim, C. Ban, and C. Park, "Assessment of the COBRA/RELAP5 code using the LOFT L2–3 large-break loss-of coolant experiment," Annals of Nuclear Energy 24, 1171 (1997).
[49] Toti, A. (2018). Development and Validation of a System Thermal-Hydraulic/CFD Codes Coupling Methodology for Multi-Scale Transient Simulations of Pool-Type Reactors (PhD thesis). Ghent University.
[50] Pucciarelli, A. (2020). Coupled system thermal Hydraulics/CFD models: General guidelines and applications to heavy liquid metals. Annals of Nuclear Energy. https://doi.org/10.1016/j.anucene.2020.107990
[51] ANSYS. (2011). *CFX – Solver modelling guide*.
[52] Cioli Puviani, P., Del Moro, T., Gonfiotti, B., Martelli, D., Giannetti, F., Zanino, R., Tarantino, M., 2025. A novel Ansys CFX – RELAP5 coupling tool for the transient thermal-hydraulic analysis of liquid metal systems. Prog. Nucl. Energy 180, 105590. ISSN 0149-1970. https://doi.org/10.1016/j.pnucene.2024.105590.
[53] Martelli, D. (2015). Experimental and Numerical Thermal-Hydraulic Analyses in support of GEN-IV Lead-cooled Fast Reactor Design (PhD thesis). University of Pisa.
[54] Huxford, A., Coppo Leite, V., Merzari, E., Zou, L., Petrov, V., & Manera, A. (2023). A hybrid domain overlapping method for coupling system thermal hydraulics and CFD codes. *Annals of Nuclear Energy*, *189*, 109842. https://doi.org/10.1016/j.anucene.2023.109842.
[55] OECD/NEA Nuclear Science Committee. (2015). Handbook on Lead-bismuth Eutectic Alloy and Lead Properties, Materials Compatibility, edition, Thermal-hydraulics and Technologies.
[56] Menter, F. R. (1994). Two-equation eddy-viscosity turbulence models for engineering applications. AIAA Journal, 32(8), 1598–1605.
[57] Coccoluto, G., Gaggini, P., Labanti, V., Tarantino, M., Ambrosini, W., Forgione, N., Napoli, A., & Oriolo, F. (2011). Heavy liquid metal natural circulation in a one-dimensional loop. Nuclear Engineering and Design, 24, 1301-1309.

[58] Martelli, D., Forgione, N., Barone, G., Del Nevo, A., Di Piazza, I., & Tarantino, M. (2014). Coupled simulations of natural and forced circulation tests in NACIE facility using RELAP5 and ANSYS Fluent codes. In Proceedings of the 22nd International Conference on Nuclear Engineering (ICONE22).

[59] Di Piazza, I., Hassan, H., Lorusso, P., & Martelli, D. (2022). Benchmark Specifications For NACIE-UP Facility: Non-Uniform Power Distribution Tests. ENEA Report ID: NA-I-R-542, CR Brasimone.

[60] Cioli Puviani, P., Venturini, A., Di Piazza, I., Sermenghi, V., Del Moro, T., Papa, F., Martelli, D., Zanino, R., & Tarantino, M. (2024). Development of a thermal mass flow meter for heavy liquid metal applications. *Nuclear Engineering and Design, 427*, 113427. https://doi.org/10.1016/j.nucengdes.2024.113427

[61] Di Piazza, I., Angelucci, M., Marinari, R., Tarantino, M., & Martelli, D. (2019). Thermo-fluid dynamic transients in the NACIE-UP facility. Nuclear Engineering and Design, 352, 110182. https://doi.org/10.1016/j.nucengdes.2019.110182

[62] Del Moro, T., Cioli Puviani, P., Gonfiotti, B., Di Piazza, I., Martelli, D., Ciurluini, C., Giannetti, F., Zanino, R., & Tarantino, M. Analysis of the experimental tests performed at NACIE-UP facility through a novel CFX-RELAP5 codes coupling. *Nuclear Engineering and Design*. Volume 429, 2024, 113676, ISSN 0029-5493, https://doi.org/10.1016/j.nucengdes.2024.113676.

[63] Marinari, R., Di Piazza, I., Tarantino, M., Angelucci, M., & Martelli, D. (2019). Experimental tests and post-test analysis of non-uniformly heated 19-pins fuel bundle cooled by heavy liquid metal. *Nuclear Engineering and Design, 343*, 166-177.

[64] Martelli, D., Marinari, R., Barone, G., Di Piazza, I., & Tarantino, M. (2017). CFD thermo-hydraulic analysis of the CIRCE fuel bundle. Annals of Nuclear Energy, 103, 294-305. https://doi.org/10.1016/j.anucene.2017.01.031

[65] Narcisi, V., Giannetti, F., & Caruso, G. (2019). Investigation on RELAP5-3D© capability to predict thermal stratification in liquid metal pool-type system and comparison with experimental data. Nuclear Engineering and Design, 352, 110152. https://doi.org/10.1016/j.nucengdes.2019.110152

[66] Mascari, F., Vella, G., Woods, B.G., Welter, K., Pottorf, J., Young, E., Adorni, M., D'Auria, F., 2011. Sensitivity analysis of the MASLWR helical coil steam generator using TRACE. Nucl. Eng. Des. 241 (4), 1137–1144. https://doi.org/10.1016/j. nucengdes.2010.05.002.

[67] Idelchik, I. E. (2003). *Handbook of hydraulic resistance* (3rd ed.). Jaico Publishing House.

[68] Chen, S. K., Petroski, R., & Todreas, N. E. (2013). Numerical implementation of the Cheng and Todreas correlation for wire wrapped bundle friction factors—Desirable improvements in the transition flow region. *Nuclear Engineering and Design, 263*, 406-410. https://doi.org/10.1016/j.nucengdes.2013.06.012

[69] Cheng, S. K., & Todreas, N. E. (1986). Hydrodynamic models and correlations for bare and wire-wrapped hexagonal rod bundles: Bundle friction factors, subchannel friction factors and mixing parameters. *Nuclear Engineering and Design, 92*(2), 227-251. https://doi.org/10.1016/0029-5493(86)90249-9

[70] Cioli Puviani, P., Zanino, R., Del Moro, T., Giannetti, F., Gonfiotti, B., Di Piazza, I., Martelli, D., & Tarantino, M. (2023, August 20–25). *CFD–STH code coupling for the thermal-hydraulic analysis of NACIE-UP experimental facility*. Paper presented at the 20th International Topical Meeting on Nuclear Reactor Thermal Hydraulics (NURETH-20), Washington, D.C., USA.

[71] Grishchenko, D., Mickus, I., Kööp, K., Jeltsov, M., & Karbojian, A. (2015). TALL-3D experimental setup description for the first test series. *SESAME Project, Deliverable N° D4.3.1_M09*.

[72] Grishchenko, D., Jeltsov, M., Kööp, K., Karbojian, A., Villanueva, W., & Kudinov, P. (2015). The TALL-3D facility design and commissioning tests for validation of coupled STH and CFD codes. *Nuclear Engineering and Design*, *290*, 144–153. https://doi.org/10.1016/j.nucengdes.2014.11.045

[73] Moreau, V., Profir, M., Alemberti, A., Frignani, M., Merli, F., Belka, M., Frybort, O., Melichar, T., Tarantino, M., Franke, S., Eckert, S., Class, A., Yanez, J., Grishchenko, D., Jeltsov, M., Kudinov, P., Roelofs, F., Zwijsen, K., Visser, D. C., Badillo, A., Niceno, B., & Martelli, D. (2019). Pool CFD modelling: Lessons from the SESAME project. *Nuclear Engineering and Design*, *355*, 110343. https://doi.org/10.1016/j.nucengdes.2019.110343

[74] Cioli Puviani, P., Del Moro, T., Gonfiotti, B., Martelli, D., Ciurluini, C., Giannetti, F., Zanino, R., & Tarantino, M. (2025). Performance evaluation of a coupled CFX-RELAP5 tool adopting experimental data from the TALL-3D facility. *Nuclear Engineering and Design, 432*, 113818. https://doi.org/10.1016/j.nucengdes.2024.113818

[75] Kim, C. S. (1975). Thermophysical properties of stainless steels (ANL-75-55).

[76] Caramello, M., Frignani, M., Grasso, G., Tarantino, M., Martelli, D., Lorusso, P., & Di Piazza, I. (2023). Improvement of ALFRED thermal hydraulics through experiments and numerical studies. *Nuclear*

Engineering and Design, 409, 112365. https://doi.org/10.1016/j.nucengdes.2023.112365

[77] ENEA, Banca Dati PROGETTI UE, DETTAGLI PROGETTO LESTO. https://progettiue.enea.it/proWEB.php?id=2197

[78] Cioli Puviani, P., Zanino, R., Del Moro, T., Giannetti, F., Gonfiotti, B., Di Piazza, I., Martelli, D., & Tarantino, M. (2023, August 20–25). *CFD–STH code coupling for the thermal-hydraulic analysis of NACIE-UP experimental facility*. Paper presented at the 20th International Topical Meeting on Nuclear Reactor Thermal Hydraulics (NURETH-20), Washington, D.C., USA.

[79] Del Moro, T., Giannetti, F., Puviani, P. C., Di Piazza, I., Diamanti, D., & Tarantino, M. (2025). Loss-of-heat-sink transient simulation with RELAP5/Mod3.3 code for the ATHENA facility. *Annals of Nuclear Energy*, 211, 110948. https://doi.org/10.1016/j.anucene.2024.110948

[80] Del Moro, T., Giannetti, F., Khalil Youssef, G., Lorusso, P., Caramello, M., Cauzzi, M. T., & Tarantino, M. (2023). Post-Test Analysis of SIRIO Facility Data by System Thermal-Hydraulic Codes for LFR Application. In Proceedings of the 20th International Topical Meeting on Nuclear Reactor Thermal Hydraulics (NURETH-20), Washington, D.C.

[81] Cioli Puviani, P., Di Piazza, I., Marinari, R., Zanino, R., & Tarantino, M. (2023). Multiscale thermal-hydraulic analysis of the ATHENA core simulator. Nuclear Technology, 210(4), 692-712. https://doi.org/10.1080/00295450.2023.2215682

[82] Wang, X. A., Zhang, D., Wang, M. J., Song, P., Wang, S. B., Liang, Y., Zhang, Y., Tian, W., Qiu, S., & Su, G. H. (2009). Hybrid medium model for conjugate heat transfer modeling in the core of sodium-cooled fast reactor. Nuclear Engineering and Technology, 52(4), 708-720. https://doi.org/10.1016/j.net.2019.09.009

[83] Bentz, D. P., & Prasad, K. R. (2007). Thermal performance of fire resistive materials I: Characterization with respect to thermal performance models (NISTIR 7401). National Institute of Standards and Technology.

[84] Information Sytem Laboratories, RELAP5/Mod3.3 Code Manual Volume V: User's Guidelines.